SCUOLA NORMALE SUPERIORE

New Fluorescent Tools For The Development of Advanced Vapochromic Films Based on Themoplastic Polymers

Supervisor: Prof. Andrea Pucci

Candidate: Muzaffer Ahmad

Co-supervisor: Dr. Giuseppe Brancato

Acknowledgements

The work was carried out at the Department of Chemistry and Industrial chemistry at the University of Pisa. I would like to begin with my sincere thanks to my supervisor Prof. Andrea Pucci for granting me an opportunity to work in his laboratory. He has been always highly supportive and encouraging throughout my research work. I would also like to thank my co-supervisor Dr. Giuseppe Brancato for his kindness and support.

I must thank all the people here in the department of chemistry particularly who have been around me during this entire period. I would like to thank to Pierpaolo, who is not working here now, for his support particularly at the initial stages in the department. I would always remember his support to learn the new techniques during my research work. I would also like to mention the other people who have been equally supportive and my friends including Giuseppe, Francesco, Serani, Mirko and Matteo. I never thought that I am far away from my home in their company. I would consider myself lucky to have such wonderful people around me. I would also like to pay my thanks to all other master students who have been with me throughout my stay in the department particularly Francesca, George, Guada, Irene, Matteo and Jonathan. I am sorry if I missed to mention the name of some people.

I wish to thank the people from other laboratories particularly Dario, Sabrina, Guazelli and Sara for allowing me to perform the DSC measurements. I would also like to thank to Dr. Elisa Passaglia and Roberto from CNR for allowing me to make DSC analysis in their laboratory. I am also grateful to the people of NEST for performing some analysis of my research work, especially, my co-supervisor Dr. Giuseppe Brancato for computational calculations and Antonella Battisti for the confocal imaging.

I would also like to thank my friends from Scuola Normale Superiore who have also been a wonderful part of my stay here in Pisa, particularly for having the food together in the canteen. I am also thankful to all other people in the administrative service of the scoula for being always available.

I must thank my parents who allowed me to choose my carrier without any interference. I know it was not so easy for them to let me stay far away from them. They never let me feel that I was far away from them. I am also thankful to my two elder brothers for their support and encouragement.

Finally, I wish to thank the Scuola Normale Superiore for the grant of PhD scholarship and department of chemistry of the University of Pisa for giving me an opportunity to work in the department.

Abstract

The harmful effects of Volatile Organic Compounds (VOCs) demand simple sensitive, selective and cost effective sensors for their detection. Considering this fact, the sensing ability of the fluorescent molecules for the detection of VOCs is demonstrated in this work. In particular, here in we investigated the vapochromic behaviour of special fluorescent molecules known as fluorescent molecular rotors (FMRs), sensitive to both viscosity and polarity of the environment. The higher sensitivity of FMRs in determining the microviscosity changes inspired their application as sensors for VOCs. The sensor system was prepared by the dispersion of a very small amount (0.05-0.1 wt. %) of 4-(diphenylamino)phthalonitrile (DPAP) within poly(methyl methacrylate) (PMMA) and polycarbonate (PC). DPAP/PMMA films show a good and reversible vapochromism when exposed to the VOCs with high polarity index and favourable interaction with the polymer matrix such as tetrahydrofuran (THF), chloroform ($CHCl_3$) and acetonitrile. Analogously, DPAP/PC films exposed to polar and highly polymer-interacting solvents, that is, toluene, THF, and $CHCl_3$ show a gradual decrease and red-shift of the emission. Contrary to DPAP/PMMA films, an unexpected increase and further red-shift of fluorescence is observed at longer exposure times after the initial decrease as a consequence of an irreversible, solvent-induced crystallization process of PC. The vapochromism of DPAP-doped polymer films is rationalized on the basis of alterations of the rotor intramolecular motion and polarity effects stemming from the environment, which, in concert, influence the deactivation pathways of the DPAP intramolecular charge transfer state. The present results support the use of DPAP-enriched plastic films as a new chromogenic material suitable for the detection of VOCs.

We also investigated, in some detail, the effect of the polymer film thickness on the vapochromic response of a new FMR namely 4-(triphenylamino) phthalonitrile (TPAP) in PC films. The results were discussed in terms of both the spectral signal features and the kinetics of its response. PC films of variable thickness (from 20 to 80 μm) containing small amount of TPAP were exposed to the saturated atmosphere of different VOCs. Interestingly, the fluorescence behaviour of the TPAP/PC films shows a non-trival tuneable dependence of film thickness during the second solvent exposure stage. The latter effect is attributed to the variable extent of the crystallization process occurring in PC films based on their thickness. This

observation suggests an effective procedure to modulate the spectroscopic response in such functionalized polymeric materials through a precise control of the film thickness.

The vapochromic properties of a solvatochromic dye 3-[2-(4-nitrophenyl) ethenyl]-1-(2-ethylhexyl)-2-methylindole (NPEMI-E) characterized by intramolecular charge transfer (ICT) character, dispersed in polycarbonate (PC) films is also reported. NPEMI-E solvatochromism is investigated by means of experimental and computational methods. NPEMI-E/PC films show remarkable and reversible vapochromism when exposed to VOCs with high polarity index and favourable interaction with PC matrix such as $CHCl_3$. Only minor variations of the emission wavelength are actually recorded for all other classes of VOCs investigated. The hue parameter is also used for the effective extraction of spectral information from digital colour images without the need for wavelength discriminators. Overall, the present results support the use of NPEMI-E/PC films for the cost-effective detection of $CHCl_3$ vapours.

Finally, we investigated the effect of polymer glass transition temperature (T_g) on the vapochromic behaviour of highly viscosity sensitive FMR, 2-(methylbutyl)-2-cyano-3-julolidine acrylate (MBCJA). Mixing of poly(methyl methacrylate) (PMMA) and poly(butyl methacrylate) (PBMA) in different compositions with the fluorophore resulted in new compatible polymer blends with different T_g. The vapochromic response of the dye containing pure PMMA and PBMA films indicated a better variation in the emission intensity contrary to blends. Based on the strong compatibility and single T_g of the blends, strong intermolecular interactions are supposed to play a significant role in hampering the solvent interaction with blends. These interactions along with T_g must probably play the role in the solvent interaction with blends and accordingly changed the fluorescence response of the fluorophore mixed in polymer matrices.

Table of contents

Chapter 1

1. Introduction

1.1. Volatile Organic Compounds

Volatile Organic Compounds (VOCs) are the organic chemicals that form vapours at normal temperature and pressure. According to the World Health Organization (WHO), VOCs are considered to be the organic compounds having boiling point in the range of 50–260 °C. On the basis of the degree of volatility and the boiling point, VOCs are classified into three types (Table 1). VOCs are also classified on the ozone forming potential, polarity and their effects on ecosystems.[1,2]

Table 1 Classification of VOCs on the strength of volatility and boiling point range.

Name	Boiling point range (°C)	Examples
Very Volatile Organic Compounds (VVOCs)	<0-100	Propane, butane, methyl chloride
Volatile Organic Compounds (VOCs)	50-100 to 240-260	Aldehydes, toluene, acetone, alcohols
Semi-Volatile Organic Compounds (SVOCs)	240-260 to 380-400	pesticides including DDT, chlordane etc.

The uncontrolled release of chemicals containing VOCs into the environment can cause the generic health problems thereby effecting the population, particularly, in urban and industrial areas.[3–6] The harmful effects of VOCs on human health mostly include acute and chronic respiratory effects, eye and throat infection etc.[6–9] The effect on human health depends on the total concentration of the VOCs as well as the exposure time. It is reported that below 0.20 mg/m^3 no effects are evident and above this level of exposure, the effects start to multiply. The toxic exposure range is believed to occur at concentration above 25 mg/m^3.[10] The effect of exposure time on the intensity of combined eye, nose and throat irritation was reported by Molhave et al.[11] Accordingly, the irritation was recorded after the 75 min exposure to VOCs and reached the significant value after 2.75 h compared to the exposure to clean air.[11] The other effects including headache, drowsiness etc. were also realized. The study also indicated

that both olfactory and trigeminal systems are activated by the exposure to VOCs and the perception of odour intensity decreases with exposure time.[11]

Solvents like benzene have proven to be to carcinogenic and account for about 40% of the risks for each category of indoor environment.[12] Life time risk associated with exposure to benzene in smoking areas is much higher than non-smoking homes. Exposure to higher concentration of benzene could lead to the circulatory and immunological dysfunctions. VOCs including 1,1,-dichloroethane, methylene chloride, chloroform and trichloroethane used as solvents, detergents and insectsides are also associated with higher lifetime risks.[12] Rumchev et al. investigated the association of VOCs and asthma and concluded that most of the VOCs appeared to contribute significantly to the risk of asthma.[13] Benzene followed by ethyl benzene and toluene were considered to be significant risk factors for asthma. They also reported that for every 10 unit increase in benzene ($\mu g/m^3$), the probability of asthma increased to three times.

The potential effects of chlorinated VOCs (Cl-VOCs) including polychloromethanes, polychloromethanes and polychloroethylene on human health is one of the growing concern of VOCs.[4] These compounds have high volatility and resistance to degradation thereby can enter our body easily through inhalation. The source for such Cl-VOCs include metal degreasing, dry cleaning, manufacture of pesticides, adhesives etc. Chloroform, one of the Cl-VOCs, is highly volatile and unreactive and slightly dissolves in water. Due to its broader applications, the total global annual production of chloroform in the late 1990 was about 520000 tonnes.[14] Exposure to chloroform may cause severe health related problems including mutagenesis, cytotoxicity etc.[15] The other Cl-VOCs including carbon tetrachloride, dichloromethane etc. are also reported to pose serious effects on health and needs to be monitored regularly.

VOCs also influence the atmosphere by forming ozone on reacting with OH radicals in presence of light in troposphere.[2,16] 1,3-butadiene and 1,3,5-trimethylbenzene are reported to have higher potential for ozone formation.[2] Tropospheric ozone has harmful effects on both plants and human beings. Contrary, halogen containing VOCs react with ozone in stratosphere thereby enhancing the depletion of ozone, which in turn allows the harmful UV radiations to pass through it easily. The reaction of VOCs with natural constituents of air also leads to their partial degradation. The formation of secondary pollutants of higher toxicity can occur during the photo-degradation of VOCs in the atmosphere. The photo-degradation of

trichloroethylene to phosgene gas illustrates this effect very well.[16] The life time of VOCs in the atmosphere depends on the oxidation by tropospheric hydroxyl radicals.[17] Alkanes generally have life time of about 2-30 days while methane and ethane have 10 years and 120 days respectively.[17] On the other hand alkenes have shortest life time among the organic compounds (0.4-4 days), almost similar to aromatic hydrocarbons.

1.1.1. Sources of VOCs

VOCs enter into the environment from different sources including industrial process, transportation, agriculture etc.[8,18–21] For example, non-methane hydrocarbons enter into the environment by burning of fossil fuels, vegetation, transportation, geochemical changes etc. The oxidation of these compounds leads to the formation of ketones, aldehydes, alcohols, and phenols etc., which are considered harmful for human health. The anthropogenic contribution usually comes from the exploitation of fossil fuels. Methane is released from the coal production. Many gases usually hydrocarbons including methane, ethane, propane, butane etc. are released during crude oil production.[22] Emission from vehicles contributes to the highest increase of VOCs in the form of non-methane hydrocarbons (NMHCs) in the public environment. In particular, the emission from the gasoline and diesel combustions results in the production of paraffins (C_1-C_5) and methane respectively. The other VOCs formed involve olefins, aromatic hydrocarbons, aldehydes, ketones and other higher molecular weight paraffins.[22]

The presence of VOCs in indoor environment is also a growing concern since some studies indicate higher level of VOCs concentration in indoor environment than outdoor environment.[23] The indoor VOCs mostly include aromatics, aldehydes and halocarbons. Many sources are involved for the release of indoor VOCs, however, the building materials are considered as main sources.[23] The release of several VOCs including ethyl benzene, 1,1,1, trichloroethane, xylenes etc. from the new buildings decrease over the time indicating that sources are related to materials or finishing. [24]

Photocopy centres are also considered potential sources of many VOCs including benzene, toluene, ethyl benzene, xylene and styrenes (BTEXS).[25] The toner powder that contains the organic components is believed to the source of VOCS in photocopy centres.[26] In general, there is wide variation of VOCs identified in different photocopy centres however, toluene and 1,2,4-trimethylbenzene were found in all the centres investigated.[26]

Natural resources of VOCs include marine and terrestrial environments. Plants release VOCs in the form of isoprenes and trepenes, which are actually reduced forms of the carbon, during photosynthesis and are among the most abundant sources of biogenic VOCs.[22] Biogenic emissions also contain other kinds of VOCs including alcohols, esters, aldehydes, ketones, alkenes and alkenes. Some studies reported that alkanes and aromatics contribute significantly to the VOC emission from plants, however, most of the findings contradict this report. Biogenic VOCs are also involved in the production of organic acids, organic nitrates and organic aerosols.[27] The harvesting and grazing practices are also responsible for the emission of NMVOC to some extent. Drying of vegetation is also reported to play a significant role in the NMVOC emission. Consequently, the emission of VOCs from plants is becoming an interesting research area. The measurement of biogenic VOCs in Europe have been carried out by Biogenic emissions in the Mediterranean area (BEMA) and Biogenic VOC emissions and photochemistry in boreal regions of Europe (BIPHOREP).[27] Some soil microorganisms are also reported to release some VOCs into the atmosphere.[28] A relatively small amount of organic compounds in the form of alkanes and alkenes are also emitted from the ocean. The contribution of volcanic eruptions, combustion of organic matter and biomass and forest fires has to be taken into account as well.[2,28,29]

1.1.2. Methods for the detection of VOCs

The growing concern of VOC emission has forced the many countries around the globe to limit and monitor the use of VOCs. In Europe, VOC Solvent Emissions Directive (council directive 1999/13/EC of 11 March 1999) was issued by the council of European Union for the reduction of industrial emissions of VOCs in Europe. In Unites States the VOCs are regulated by the United States Environmental Protection Agency (USEPA). In China the Ministry of Environmental Protection of China has classified VOCs as major pollutant.[30] According to Wang et al. China produced more than 6.5 million tons of VOCs in 2010 and the level is going to rise further in future due the industrial growth.[31] The Atmospheric Pollution Prevention Law in China manages and monitors VOCs from the pollution sources. In India the Central Pollution Control Board has regulated Benzene and Benzo(a)pyrene by including them in National Ambient Air Quality Standard to control their release into the environment.[32] The Global Emissions Inventories Activity (GEIA), a part of the International Global Atmospheric project (IGAC) has also recognized VOC as a part of their programme.[19]

All these issues with VOCs demand suitable sensors for their detection with higher sensitivity and selectivity. Accordingly, different sensors have already been developed for monitoring the presence of VOCs.[33–36] Li et al. reported the porous SnO_2 as sensors for VOCs with higher gas sensing performance up to ppb level.[37] They demonstrated the dependence of temperature on the response of the sensor with maximum performance at 260°C for 2-chloroethanol and formaldehyde. On increasing temperature, oxygen molecules are adsorbed on the SnO_2 surface forming ionized oxygen species due to the electrons from conducting band of the semiconductor. Hence, the resistance increase due to space-charge region. On exposure to VOCs, oxygen species react with gas molecules allowing the release of electrons to the SnO_2 surface, eventually increasing the conductivity of the system. The device displays higher sensitivity, however, there are many issues that can limit the application of the sensor. The preparation of SnO_2 nanospheres needs acidic solvents for etching which needs to be handled with very high care. At the same time, maximum response at higher temperature (260 °C) restricts the application of the sensor at room temperature for detection of VOCs. Also, the selectivity issue with such kind of sensors needs to be addressed for the desired applications.

Penza et al. used carbon nanotubes as sensing material into three different sensory systems using complementary transducing principles for sensing VOCs in wide range of vapour pressure[38]. The three transducers with complementary principles of operation were surface acoustic waves (SAWs), quartz crystal microbalance (QCM), and standard silica optical fibre (SOF) The idea of integration of the three sensor systems was simultaneous use of different chemical sensing elements for efficiently increasing the information. The sensitivity of the sensors for the detection of VOCs on the basis of vapour pressure at the room temperature was reported. However, the complexity and the time consuming of the method limits the real application of such systems. The sensor response also diminishes due to mass loading of vapour molecules accumulated into the sensing material. The vapour molecules have to be removed every time by purging nitrogen.

Recently the application of weight-detectable quartz crystal microbalance (QCM) and silicon based microcantilever coated with crystalline metal-organic framework (MOF) thin films as sensors for VOCs was demonstrated.[39] Notably, the function of MOF as VOC concentrator and the adsorption/desorption was detected by frequency changes of the weight detectable sensors. Furthermore, the selectivity of the sensor was enhanced due to the size –selective adsorption of VOCs within nanospheres of MOF. Certain limitations associated with such

sensors involves the loss of resonance propagation in the sensing layer in QCM, ascribed to the viscoelasticity of sensing layers, resulting in the unstable oscillation. The higher working temperature and the temperature sensitive frequency changes of such sensors also restrict their application under normal conditions.

Many other sensors reported also demonstrate VOC sensing ability but some of the issues related with these sensors are not favourable for the desired applications. In general, the sensors based on chromatography/spectrometry are selective but not suitable for in-situ applications. Electrochemical sensors are sensitive but lack selectivity while mass sensors are sensitive but it depends on high-frequency excitation.[40] Besides, these problems, they consume too much power adding their cost.[41] Metal oxide semiconductors (MOS) sensors have been successfully developed for arrays of VOC sensing, however they require heating at very high temperature for sensing VOCs.[39] The differential optical absorption spectroscopy (DOAS) is reported to have high resolution without the chemical interference. On the other hand, the technique is costly and is limited due to the interference of oxygen and hydrocarbons with similar spectra.

To address all the aforementioned issues with the already existing sensors, there is a strong need for the development of the simple and cost effective sensors for the detection of VOCs. This has driven the attention of the researchers to look for other alternatives with better features.

One of the interesting and promising methods to develop sensors for VOCs is the application of fluorescence molecules. There is a growing interest of researchers for developing sensors based on fluorescent materials for the detection of VOCs considering their higher sensitivity, selectivity, low cost, fast response non-destructibility of the sample etc.[42,43] Fluorescence is considered as one of the most powerful tool to detect the chemical recognition event.[44] Over the past few years a number of fluorescence and spectroscopy techniques have been developed based on different sensing mechanisms.[45] The application of fluorescence in chemical sensors dates back to 1980s for development of fluorescent calcium indicators.[46,47] A lot of work has been done since then to improve the sensing ability of the fluorescent chemical sensors.

1.2. Fluorescence methods for VOCs detection

1.2.1. Mechanism of Fluorescence

Before discussing the application of fluorescent sensors for the detection of VOCs, it is necessary to understand the mechanism of fluorescence. Generally, the interaction of light with matter can result in scattering or absorption of the light. In case of absorption, the electrons are excited to the higher energy level and deactivate through different pathways. Accordingly, the deactivation can occur by radiative pathways including fluorescence and phosphorescence or non-radiative pathways involving internal conversion (IC) intramolecular charge transfer (ICT), conformational changes, and interaction in the excited state with other molecules (quenching).

All these possible deactivation pathways of the fluorescent molecule on photo-excitation are best represented by a well known Jablonski diagram (Figure 1). In this diagram, the singlet electronic ground state is depicted by S_0, singlet excited states by $S_{1,}S_{2.....,}$ triplet excited states by T_1, T_2,……Accordingly, the absorption occurs very fast 10^{-15}s so there is no displacement of nuclei as stated by *Franck-Condon* principle.[48]

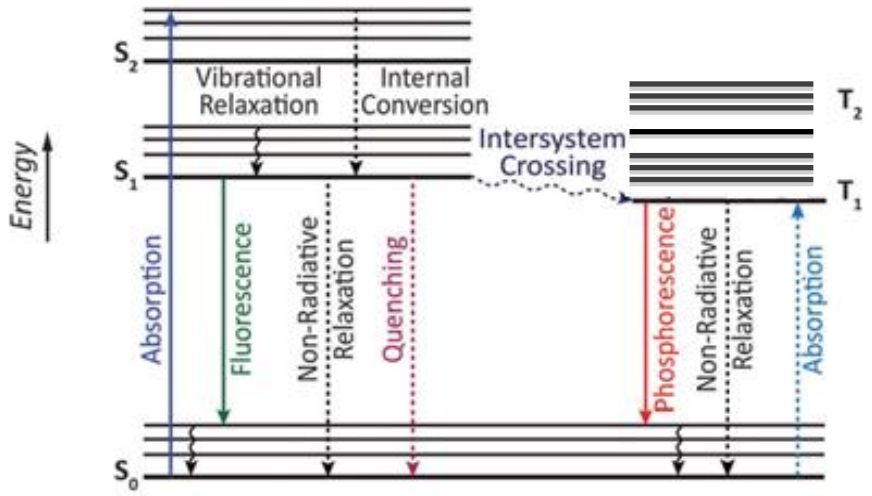

Figure 1 Jablonski diagram showing the radiative and non radiative processes in the electronic system of molecules during photoexcitation. [48]

Fluorescence occurs during the transition of electron from the singlet excited state to the ground state of the opposite spin. The process is very fast and occurs in 10^{-8} s^{-1} since, the

transition is spin allowed. Fluorescence is independent of the excitation wavelength and is located at higher wavelengths than the absorption due to some loss of energy during vibration. The difference in the maximum of the absorption and emission is described as Stokes shift. Due to the different electronic distribution in the excitation state, the dipole moment of the fluorophore changes accordingly. Solvent effected excited state reactions and the complex formation can also alter the Stokes shift. Stokes shift can explain the behaviour of the excited states, higher the Stokes shift, better the detection of fluorescent species.

The fluorescence of a molecule is determined by quantum yield (ϕ_F). ϕ_F of the fluorescence can provide the essential information about the interactions of the excited state molecule with the surrounding medium. ϕ_F represents the fraction of excited molecules responsible for the fluorescence, since all excited molecules do not necessarily deactivate through fluorescence. Because of the Stokes shift, ϕ_F cannot be equal to unity but close to unity if the non-radiative decay is much smaller e.g. rhodamines

Mathematically, ϕ_F can be calculated using the following equation

$$\phi_F = \frac{k_r^s}{k_r^s + k_{nr}^s} = k_r^s \, \tau s = \frac{\tau}{\tau + K_{nr}} \qquad (1)$$

Where ϕ_F is the fluorescence quantum yield, k_r^s and k_{nr}^s are the rate constants of the radiative and non-radiative deactivation from S_1 to S_0, τs is the lifetime of the excited state and τ is the emissive rate.

The lifetime (τs) of the fluorophore is one of key characteristic of the fluorescence. It depends on the average time which the molecule spends in the excited state and is given by

$$\tau s = \frac{1}{k_r^s} + \frac{1}{k_{nr}^s} \qquad (2)$$

Where τs is the life time of the excited state, k_r^s and k_{nr}^s are the rate constants of the radiative and non-radiative transitions respectively.

The lifetime is generally independent of the excitation wavelength and lasts tens to picoseconds to hundreds of nanoseconds. However, the life time of the triplet excited state is larger than the singlet excited state. The temperature can affect both the quantum yield and the life time of a fluorophore. Accordingly, ϕ and τs decreases on increasing the temperature due to the thermal collisions and vibrations which favour the non-radiative deactivation.[49]

1.2.1.1. Fluorescence quenching

The quenching of fluorescence results in the decrease of the emission intensity. Quenching occurs through different mechanisms including collision, formation of non-fluorescent probes on interaction with quenchers, self quenching (excimer) etc. Collisional quenching occurs during the interaction of the excited state with the external molecule known as quencher. The decrease in the intensity due to quenching is given by a well known Stern-Volmer equation [49]

$$\frac{F_0}{F} = \frac{I_0}{I} = 1 + K[Q] = 1 + k_q \tau_0 [Q] \qquad (3)$$

Where F_0 and F represent the fluorescence in absence and presence of the quencher respectively, K is the Stern-Volmer constant, k_q is the quenching rate constant, τ_0 is the lifetime of the non-quenched deactivation and [Q] is the concentration of the quencher.

The Stern-Volmer constant K is given by the slope of the I_0/I as a function of the quencher concentration [Q]. The constant K defines the sensitivity of the fluorophore towards the quencher. The quencher can be in the form of different molecules like oxygen, halogens, amines etc.[49]

The formation of excimer (excited state dimer) at higher concentration changes the fluorescence band to the higher wavelength than the monomer. The excimer is formed between the excited molecule and the unexcited molecule of the same fluorophore and the process is very rapid. Furthermore, the emission spectra band can be differentiated from the excimer band since, the latter is without the vibronic peaks (Figure 2).[50]

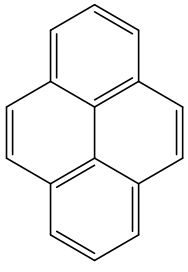

(a)

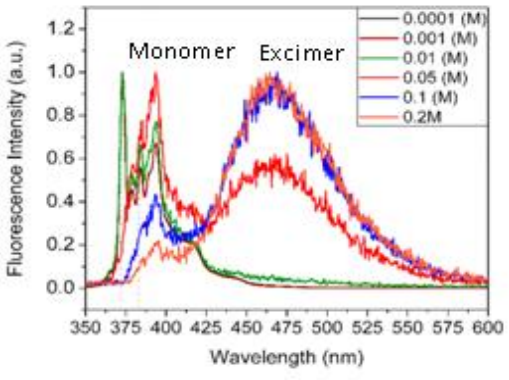

(b)

Figure 2 (a) Structure of pyrene and (b) fluorescence of the pyrene showing increase in excimer intensity on increasing the pyrene concentration in acetone solution.

1.2.1.2. Phosphorescence

Phosphorescence occurs when the excited electron in the triplet excited state returns to the singlet state with same spin. Such transition is spin forbidden and hence takes due to spin-orbital coupling, making it a slower process (10^3-10^0 s^{-1}).[51] At room temperature, phosphorescence is absent in solutions since there are many deactivation processes that compete with the phosphorescence. Phosphorescence is bathochromically shifted than the fluorescence and the rate constant for such emission is higher than the latter. The phosphorescence can be enhanced by the incorporation of heavy atoms including bromine, iodine etc. since they favour the intersystem crossing.[52]

1.2.1.3. Non-Radiative pathways of deactivation

Many non-radiative processes including internal conversion, intersystem crossing can compete with the fluorescence of the molecule.[48] Internal conversion occurs during the transition of an electron from the higher vibrational level of excited state to lower vibrational level of the S_1 state of same spin multiplicity at the rate of 10^{-13} s to 10^{-11} s.

The other non-radiative pathway that competes with the fluorescence is the inter system crossing. Such transition occurs from the first excited state, S_1 to the triplet state T_1, having isoenergetic vibrational energy levels. The process is faster (10^{-7}-10^{-9} s) than fluorescence and internal conversion and is favoured by the spin-orbit coupling, since, it is spin forbidden.

In addition to these processes, sometimes other undesirable processes similar to fluorescence results at higher time scale, described as delayed fluorescence.[51] During this process the transition occurs from T_1 –S_1. This is possible only if the energies of these two states are comparable or when the life time of triplet state is higher. This process is rare or completely absent in the aromatic hydrocarbons due to large energy difference between T_1 and S_1.

1.2.1.4. Types of fluorescent molecules

Fluorescent compounds can be organic (aromatic hydrocarbons, fluorescein, rhodamines, coumarins etc.) (Figure 4), inorganic luminescent compounds (uranyl ions, crystals of ZnS, CdS etc.) or organometallic complexes particularly based on platinum, ruthenium etc. The most common fluorophores are typically aromatic in nature including 1-4, bis(5-phenyloxazol-2-yl)benzene (POPOP), quinine sulphate, fluorescein, acridine orange,

rhodamine B, pyridine 1 etc. (Figure 3). The significant applications of these fluorophores have been intensively investigated and reported.[53–56] For example pyridine 1 and rhodamine are function as laser dyes, solutions of quinine sulphate work as standard for quantum yield calculations.[57,58] The other kinds of fluorophores that are intensively investigated belong to polynuclear aromatic hydrocarbons like anthracene, perylene etc. These fluorophores have potential ability for the application of sensors for oil pollution and other areas.

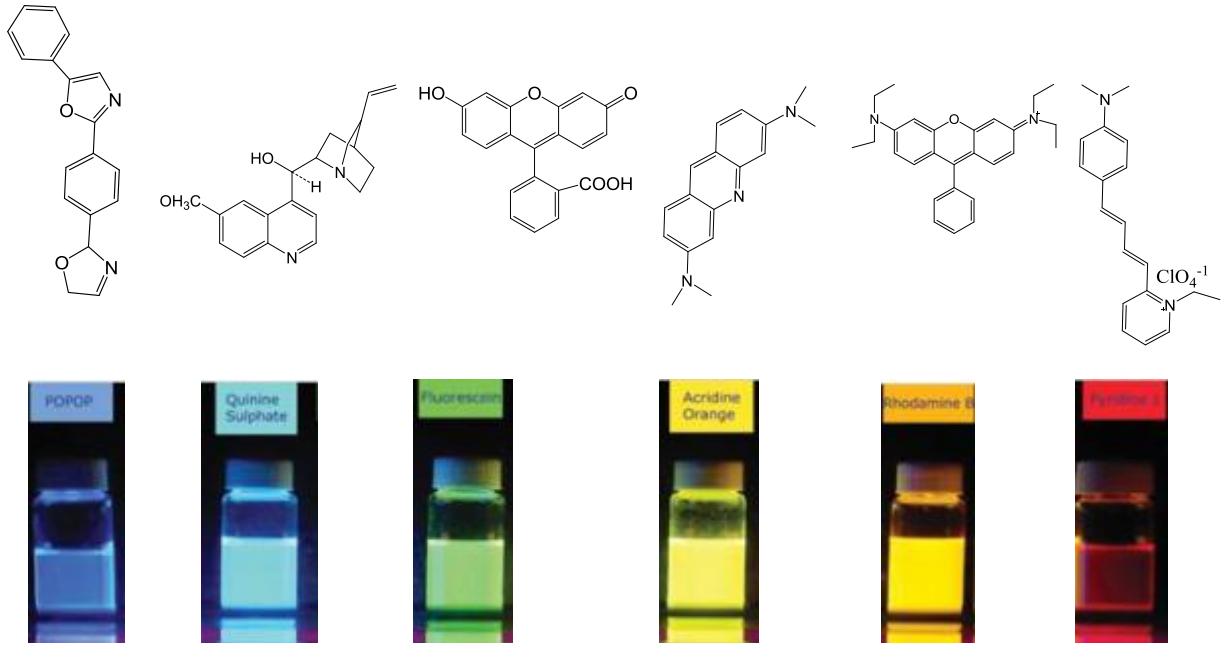

Figure 3 Structures and the fluorescence of some typical aromatic fluorescent molecules under the illumination of UV light.[49]

1.3. Fluorescent Molecular Rotors

Fluorescence of some fluorophores depends on the structure and flexibility of their molecules. Among these molecules are well known special type of fluorophores whose fluorescence is highly dependent on their structure and flexibility and are known as Fluorescent molecular rotors (FMRs). Typically, FMRs undergo intramolecular twisting in the excited state.[59] FMR typically consist of than electron donor moiety, and an electron acceptor moiety joined together by conjugated electron rich unit.[59] Accordingly, the electrons are transferred from the donor to the acceptor through the conjugated system during photoexcitation. During the charge transfer from donor to acceptor moiety, the intramolecular twisting of the side groups occurs due to electrostatic forces described as twisted

intramolecular charge transfer (TICT) (Figure 4).[60] The FMR thus assumes a non-planar configuration in the excited state from planar configuration in the ground state. The twisted ground state has higher energy and always has natural tendency to return to the less energetic planar ground state. The energy of TICT state is lower than the locally excited (LE) state and hence the energy barrier to change from LE to TICT needs to overcome. The energy barrier between the locally excited state (LE) and TICT is strongly influenced by the surrounding medium including viscosity and polarity. The deactivation process of excited molecules from TICT conformation results in the decrease of emission intensity or complete nonradiative transition depending on the energy gap between the twisted excited state (S_1) and ground state (S_0), which in turn depends on the molecular structure and the surrounding medium.[61,62] It must be noted that there are two types of deactivation processes in FMRs depending on the structure of the molecular rotor. Accordingly some FMRs exhibit dual emission related to LE and TICT conformations. For molecular rotors with emission from the twisted state with bathochromic shift, steric hindrance of TICT formation results in the emission from LE state.[63] However, the molecular rotors with non radiative deactivation from twisted state, steric hindrance only increases the fluorescence without altering the shift.[64]

Polarity of the medium can also influence the deactivation process in some FMRs by favouring stabilization of TICT state.[65] The formation of TICT actually results in the unbalanced increase of dipole moment during photoexcitation. Alternatively, the dipole moment of polar solvent molecules reorients with that of the FMR molecules and is described as solvent relaxation. Consequently, this results in the decrease in energy of the excited state confirmed by the red-shifted fluorescence.

The Jablonski diagram depicting the photophysics of FMRs is modified by altering the energy gap between the excited and ground states (Figure 5). The degree of the intramolecular rotation determines the ground and excited state energy levels. Notably, the ground state is associated with the planar conformation while as twisted conformation is preferred for the excited state.

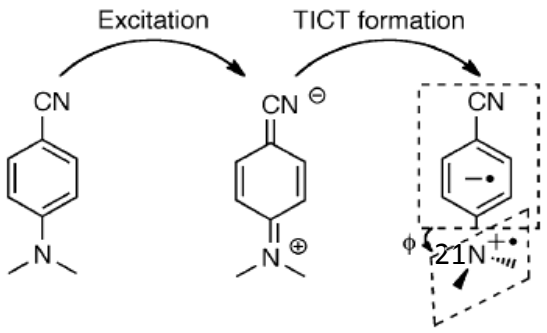

Figure4 Representation of Twisted intramolecular charge transfer (TICT) in p-N,N–dimethylaminobenzonitrile (DMABN)[52]

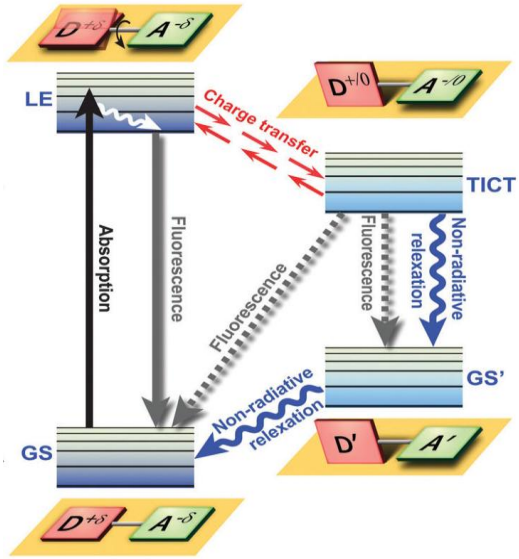

Figure 5 Jablonski diagram for FMRs showing TICT dynamics. (D and A represent donor and acceptor moieties respectively)[66]

Most commonly known FMRs are based on nitriles such as 1,4 dimethylamino benzonitrile (DMABN), Julolidine derivatives such as 9-dicyanovinyl julolidine (DCVJ) and stilbenes such as *p*-(dimethylamino) stilbazolium (*p*-DASMPI, D) (Figure 6). The significant importance of these FMRs is indicated by their potential application in detecting microviscosity in biological systems [59]. It is noted that DMABN allows emissive relaxation due to higher energy gap between the ground and first excited state. Furthermore, the molecule also emits from the LE state with red-shifted fluorescence. The relative intensity of the two emission bands is determined by the formation of TICT state. On the other hand the twisted state of DCVJ is specified by much smaller S_1-S_0 energy gap thereby favouring nonradiative relaxation of the molecule in non-viscous solvents.[62] Such types of FMRs do not display second emission band.

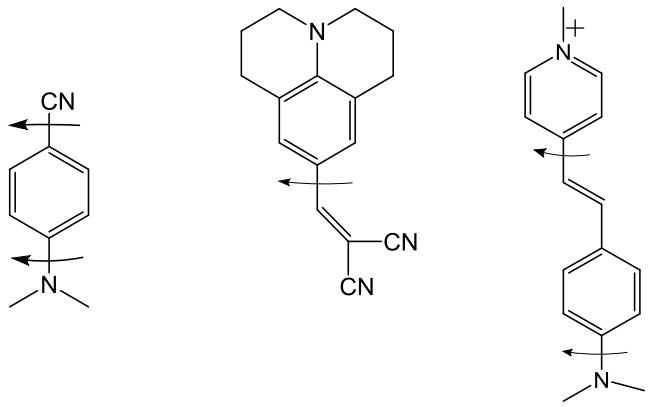

(c)

Figure 6 Typical structure of some FMRs (a) 1,4 dimethylamino benzonitrile (DMABN), (b) 9-dicyanovinyl julolidine (DCVJ) (c) *p*-(dimethylamino) stilbazolium (*p*-DASMPD) The arrows represent the rotating moieties of the molecule.[59]

1.3.1. FMRs based on julolidine

Julolidine derived FMRs are among the highly investigated FMRs reported to have significant biological applications for measuring the viscosity dependent changes.[52,67,68] Some common Julolidine derived FMRs reported to display the microviscosity changes in the biological systems include 9-[(2-cyano-2-hydroxy carbonyl) vinyl] julolidine (CCVJ), 9-(dicyanovinyl) julolidine (DCVJ), 2-carboxy-2-cyanovinyl julolidine farnesyl ester (FCVJ) etc. (Figure 8).[69,70]

Typically they belong to the group of benzylidene malonitriles and charge transfer usually takes place from the nitrogen atom to electron acceptor nitrile group through the benzylidene moiety (Figure 7). The presence of nitrogen atom within the fused ring system hinders the rotation of C-N bond and increases the energy gap between LE and TICT. It is noteworthy that on excitation, the C=C vinyl bond exhibits single bond character and is responsible for the nonradiative deactivation in julolidine based FMRs. The quantum mechanical calculations also supported the view that the excited state rotation across the C–C is not favoured energetically compared to the rotation in the ground state. Contrary, the rotation of C=C is hindered in the ground state and is favoured in the excited conformation. The rotation around the vinyl double bond could result in the isomerisation of the molecule and thereby compete with the deactivation process of the FMR.[62]

The possibility of introduction of different functional groups by replacing one of the nitrile

moiety with carboxylic group allowing addition of different hydrocarbon chains (R) was reported by Haidekker et al.[52] Different water soluble julolidine derivatives were synthesized from non-soluble DCVJ with promising application in aqueous colloidal solutions and biofluids.[71] On one hand, the incorporation of side chains enhance the solubility in polar and non polar solvents while the replacement of the functional groups can wider the application without interfering the viscosity sensitivity of the molecular rotor.[69,72]

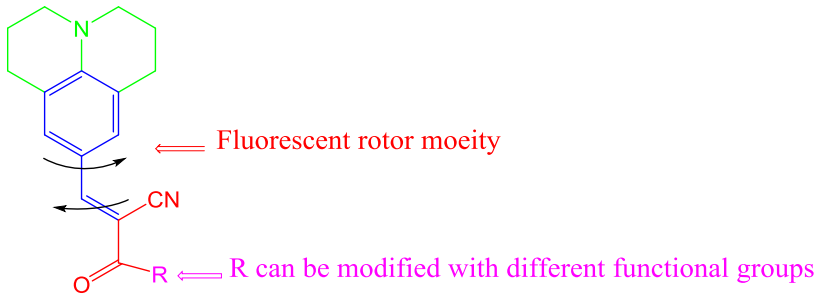

Figure 7 General Structure of the julolidine based FMR showing rotor part and the variable group .The colours represent different functions of FMR (green represent electron donor, blue conjugated part and red electron acceptor.

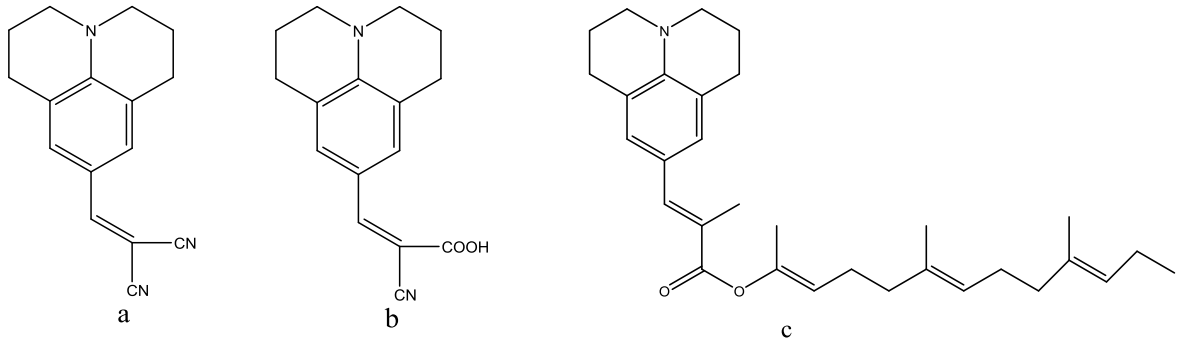

Figure 8 Structure of julolidine FMRs used to detect microviscosity in biological systems. (a) DCVJ, (b) CCVJ, and (c) FCVJ[70]

1.3.2. Applications of FMRs

The effect of viscosity and polarity on the formation of TICT in FMRs has attracted the attention of researchers for the wide range of applications particularly in determining the local microviscosity. The effect of viscosity on DCVJ can be realised in the solution using the mixtures of solvents with much different viscosities. For example the mixture of ethylene glycol and glycerol when mixed in different proportions result in the solutions with wide range of viscosities. Accordingly, DCVJ experienced higher fluorescence in the mixtures with higher viscosity and vice versa (Figure 9).

The dynamics of FMRs in sterically restricted environment has been reported to be useful for the fluorescence imaging in biological systems. The research interest of studying viscosity changes in biological systems is very useful, for example, the changes in the cellular membrane microviscosity can directly affect the cellular functioning resulting in some diseases.[70,72]

The application of fluorescent based molecules for measuring the local viscosity is favoured by the higher spatial resolution time and the fast response. Fluorescence anisotropy and fluorescence recovery after photobleaching (FRAP) methods have been already used for the estimation of viscosity changes.[73,74] However, their application is limited due to the requirement of the specific equipment and the lower resolution.

FMRs based on julolidine derivatives are reported to serve as smart tools for the detection of microviscosity changes in biological systems, thanks to their higher sensitivity, better resolution etc. The fluorescent properties of these molecular rotors is strongly enhanced by small changes in viscosity.[66] Furthermore, the stability of FMRs against photo bleaching also support their application in measuring the precise viscosity changes.[72] FMRs are considered as a better alternative to mechanical rheometer to detect the viscosity in biological systems, as the latter is time consuming and limited to bulk volumes.[59] Besides, after using the mechanical viscometer, complex cleaning process becomes another limitation as proteins adhere to the walls of the instrument.[69] On the other hand the amount of sample required for determination of viscosity by FMRs is very less (micro litre) and also allows the real time monitoring of the micro viscosity changes. Furthermore, the viscosity measurement by FMRs can meet the precision and accuracy to that of the mechanical viscometers.[69]

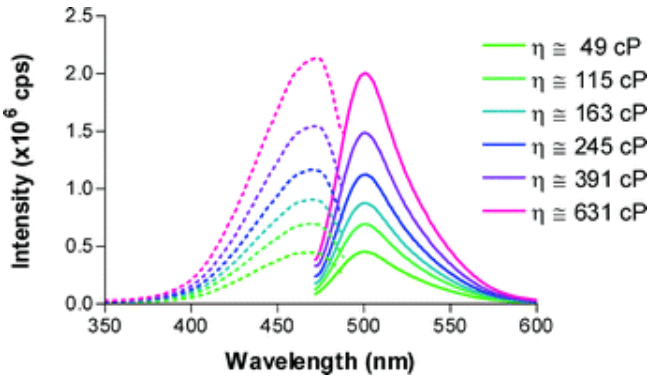

Figure 9 Emission spectra (solid lines) of DCVJ in different mixtures of ethylene glycol and glycerol. The dashed lines indicate the excitation spectra.[69]

The quantum yield of the FMRs depends on the molecular structure of the molecule. For example, the viscosity sensitivity of CCVJ is higher than DCVJ in the same viscous

medium[52] and thus the fluorescence of the former is higher than the latter (Figure 10). Accordingly the quantum yield of CCVJ is reportedly higher than DCVJ.

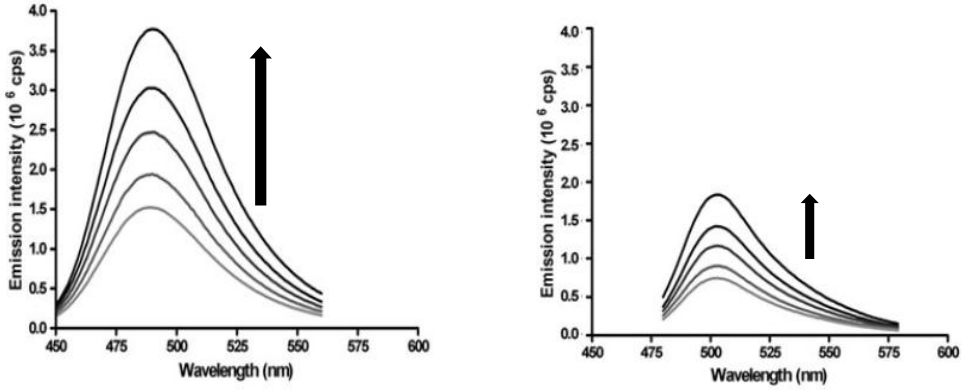

(a) (b)

Figure 10 Emission spectra of (a) CCVJ (b) DCVJ in mixture of ethylene glycol with different fractions. Arrows represent the increase in fluorescence in similar viscous solvents.[52]

The relation between the viscosity and the quantum yield is given by the Forster –Hofmann equation[69]

$$log\phi = C + x\,.\,log\eta \qquad (4)$$

Where C is the temperature dependent constant, the constant x depends on the dye, η is the viscosity and ϕ is the quantum yield.

The emission intensity and the quantum yield are directly and proportionally related as

$I_{em}\ \alpha\ I_{ab}\phi$,

Where I_{em} and I_{ab} represent the emission and absorption intensities respectively and ϕ is the quantum yield.

The viscosity sensitivity of FMRs has also been explored for the determination of the molecular weight and tacticity of the polymers.[75] Actually, the free volume of the polymer depends on the molecular weight and can therefore directly influence on the quantum yield of the FMRs. This suggests the possible application of FMR for the determination of the polymerization process. Fluorescent molecules can also work as real time monitoring of the polymer dynamics.[76] The other applications of FMRs in polymers include determination of degradation, thermal transitions, crystallization, swelling etc.[77]

1.3.3. Effect of polarity on FMRs

The effect of polarity on the fluorescence of FMR is a complex issue and is still under investigation. It was believed primarily that FMR cannot be sensitive to both viscosity and polarity since the role of intramolecular charge transfer (ICT) is hardly evident in their excited state. Accordingly, if a FMR is sensitive to viscosity, polarity changes will not affect the fluorescence behaviour and vice versa.[69,78] However, contrary to this, it was reported that by tuning the electron donating ability of the substituents in fluorophore, the effect of ICT can be induced. Zhaou et al. designed many new FMR, 2-(4-(diphenylamino) benzylidene) malonitrile, a derivative of triphenyl amine (TPA), displayed sensitivity to both viscosity and polarity thereby depicting the role of ICT (Figure 11).[78] This behaviour is ascribed to the configurational transformation of TPA as well as the larger size of the rotor molecule. After photoexcitation, the solvent molecules reorient themselves around the FMR and interact by van der walls or hydrogen bonding depending on the solvent. Consequently, there is some energy transfer from the excited state of the molecule to the polar solvent molecules resulting in the red-shift of the emission spectra.[68] Also, the formation of TICT is favoured in higher polar solvents and vice versa. Unlike many fluorescent probes, like coumarin derivatives, julolidine derived FMRs are less sensitive to the polarity changes (Figure 12). Notably, this is the result of less favourable intermolecular charge transfer in the julolidine based FMRs.

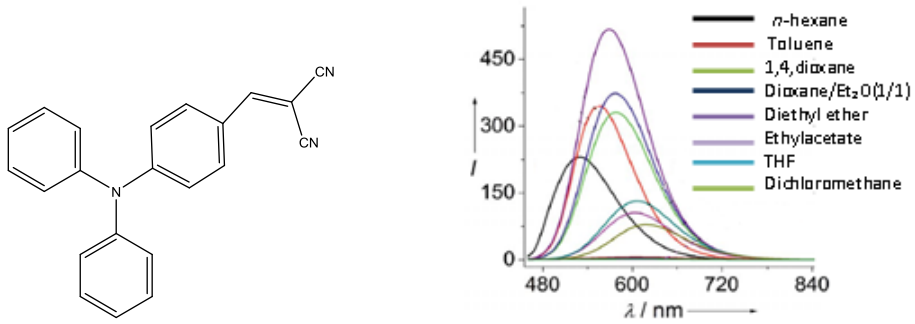

(a) (b)

Figure11 (a) Structure of 2-(4(diphenylamino)benzylidene) malonitrile and (b) its emission spectra in solvents of different polarity.

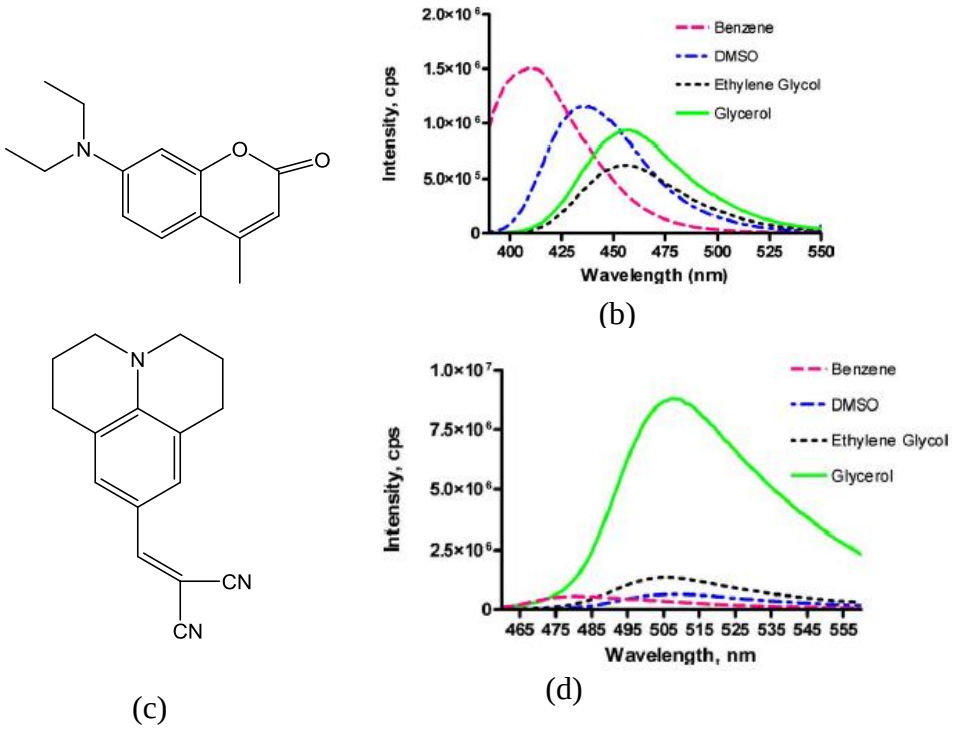

Figure 12 (a) Structure and (b) fluorecsence of coumarin 1 in different solvents, (c) structure and (d) fluorescence of DCVJ in the similar solvents.[68]

1.3.4. Fluorescent molecules as vapochromic sensors

The spectroscopic change that occurs due to interaction of vapochromic material with VOC is termed as "vapochromism". Vapochromic materials change colour on interaction with volatile organic compounds (VOCs), making it possible to detect their presence by naked eye.[79] Considering the harmful effects of the VOCs, the researchers are actively involved in the development of vapochromic sensors for their easy and simple detection (Fig. 13).

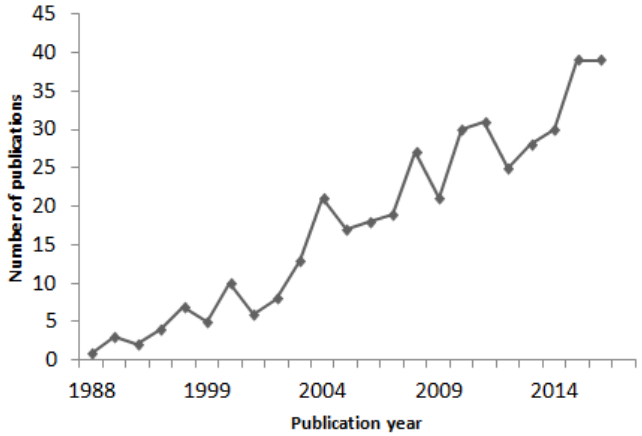

Figure 13 Number of increasing publications in each year on vapochromism. (Scifinder® January 2017)

Different classes of fluorescent materials have been developed as vapochromic sensors. These materials can either belong to organometallic complexes or organic dyes. Vapochromic organometallic compounds belong to platinum (II), palladium (II), gold (I), zn (II) etc. Among these organometallic complexes, vapochromism of platinum(II) compounds have been highly investigated.[79,80] Lu et al. reported the vapoluminescent materials of [pt-^{t}Bu$_2$bpy)arylacetylide)$_2$ complexes (Figure 14a) with different acetylide groups as 4-pyridyl, 3-pyridyl , 2-pyridyl, 4-ethynylpyridyl, 2-thienyl and pentafluoro. The solid state emission was reportedly dependent on the crystalline structure of the complexes. Films of each complex responded differently when exposed to similar solvents.[81] On exposure to dichloromethane, fluorescence intensity increased drastically. In the crystal structure with acetylide as 4-pyridyl, it was noted that dichloromethane molecules interact with bis(acetylide) moiety through C-H….π(C≡C) interactions . On evaporation of the solvent, the intensity decreased gradually confirming the reversible vapochromic response of the fluorophore (Figure 14b).

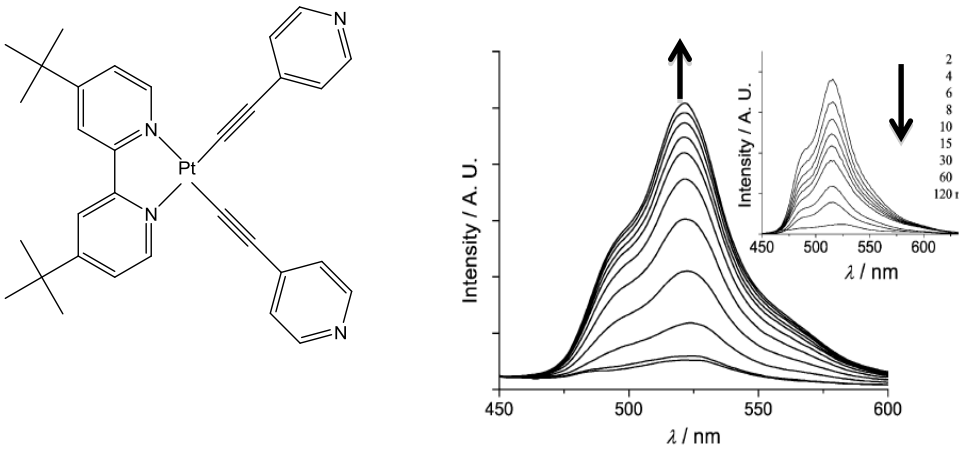

(a) (b)

Figure 14 (a) Structure of [pt- *t*Bu$_2$bpy)aryl 4-pyridyl)$_2$ and (b) fluorescence of the film of this complex on exposure to saturated dichlomethane vapours (Inset b) shows the emission spectra of the film on the removal of the dichloromethane from the film.[81]

Wang and co-workers reported the reversible vapochromism of platinum (II) complex Pt (dbbpy) (C≡CC$_6$H$_4$bMes$_2$)$_2$ upon exposure to different VOCs.[82] The system exhibited complex fluorescence shifts based on interaction with solvents of different polarity. Solvents including dichloromethane chloroform, acetonitrile, THF, acetone induce a shift from yellow to green while benzene, 1,4-dioxane result in the red-shift emission (Figure 15).[82]

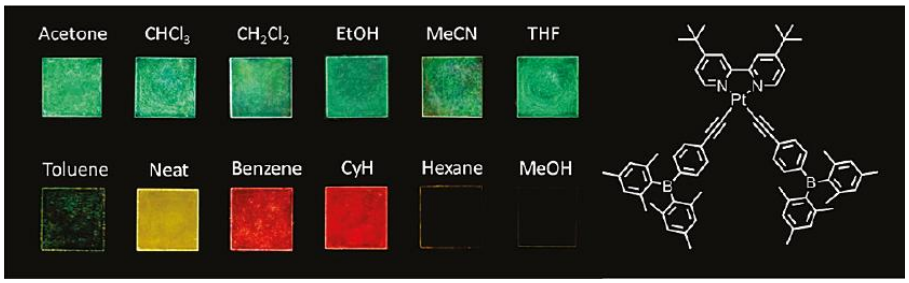

Figure15 Vapochromic behaviour of Pt (dbbpy) $(C{\equiv}CC_6H_4bMes_2)_2$ films on exposure to different solvents (Left). Molecular structure of Pt (dbbpy) $(C{\equiv}CC_6H_4bMes_2)_2$. (Right)[82]

The vapochromic behaviour of many fluorophores has been investigated in different polymer matrices. An interesting vapochromic behaviour was reported on exposure of the PMMA films containing square-planar Pt(II) complexes of 4-dodecycloxy-2,6-bis(N-methylbenze imidizole-2'-yl) pyridine (1), to the vapours of acetonitrile (Figure 16a).[83] Notably, the colour of the film changed from yellow to orange red before and after exposure respectively (Figure 16b (inset). The emission intensity of the dye/polymer system increased drastically on exposure to acetonitrile thus making it suitable sensor for the detection of the solvent (Fig 16 b).

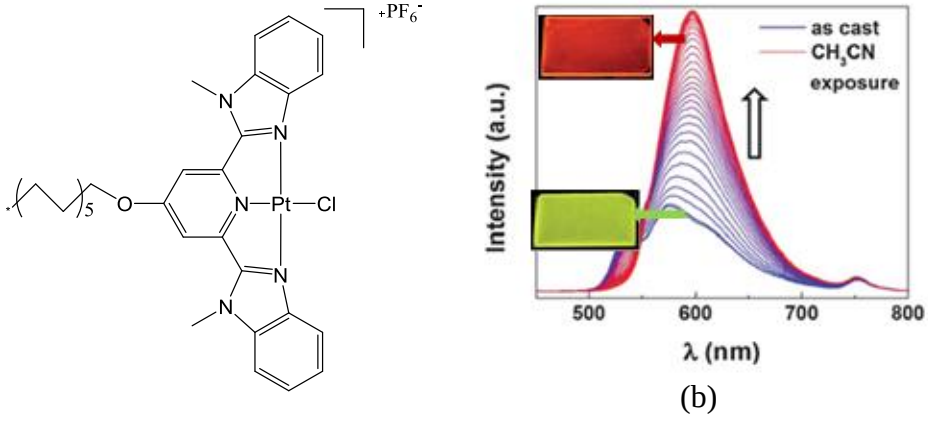

(b)

Figure 16 (a) Molecular structure of the $[Pt(1)Cl](PF_6)$ (b) Vapochromism of 10wt% $[Pt(1)Cl](PF_6)$ in PMMA on exposure to acetonitrile for 900s under the UV lamp excitation at 377nm. (Inset b) Images of the dye/polymer films before exposure (yellow) and after exposure to CH_3CN (orange red) after 900s.[83]

Recently the vapochromic behaviour of the Zn(II)-bisthienylethynylbipyridine complex (Figure 17a) in poly(methyl methacrylate) (PMMA) films was reported by Irina et al.[84] The presence of thienylethylene moieties maintain the π electronic conjugation and the heteroatomic rings are supposed to hinder the intermolecular interactions based on π-π stacking. The complex on exposure to VOCs indicated sensitivity to both polarity and the viscosity (Figure 17b). The polarity sensitivity was addressed to the ICT character of the complex favouring the reorganization energy of transition on increasing the polarity. The decrease in viscosity inside PMMA matrix was attributed to the diffusion and swelling on exposure to dichloromethane favouring the better salvation of the Zn(II) complex. The solvation of the complex also decreases the energy gap of the different electronic states and thus speedup the electron transfer rate which in turn accelerated the relaxation to non emissive state. The simplicity and cost effectiveness of the method opens new ways to detect the VOCs by fluorescent molecules using polymers as supporting materials.

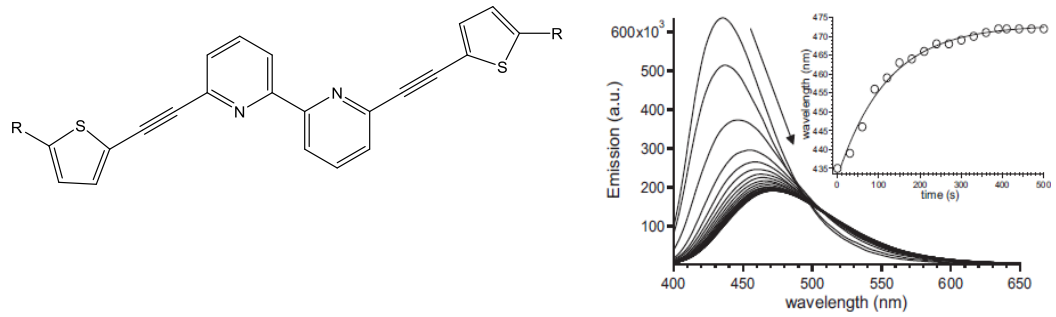

(a) (b)

Figure 17 (a) Structure of 6,6'-(Bis 5-methylthiophen-2-yl)ethynyl)-2,2'-bipyridine (b) Fluorescence of 0.5wt.% of a:Zn/PMMA on exposure to dichloromethane indicating vapochromic behaviour of the dye.(Inset b) Change in the maximum emission wavelength as a function of exposure time depicting the bathochromic shift.[84]

1.3.5. FMRs as vapochromic sensors

The better sensitivity of FMRs towards viscosity and polarity as explained before is explored for the application of vapochromism. The dynamic features of these moleculecular rotors render them potential candidates for the VOCs sensing ability. The vapochromic behaviour of few FMRs has been already investigated successfully. Martini et al. explored the vapochromic application of viscosity sensitivity julolidine derived FMRs including DCVJ, CCVJ and 9-(2-(1H,1H,2H,2H-perfluorodecyloxycarbonyl)-2-cyanovinyl) julolidine (F8CVJ) dispersed in polystyrene (PS) films (Figure 18a).[85] Different FMR/polystyrene films were

prepared by solution casting with 0.1wt. % of the fluorescent dyes in each film. The FMR/PS films on exposure to well polymer interacting solvents (chloroform and toluene) favoured the TICT of FMRs resulting in diminishing of intensity (Figure 18b). Eventually, the formation of TICT is supported by the relaxation of macromolecular chains due to solvent molecules, resulting in greater mobility with increase in free volume. Consequently, this leads to the decrease in viscosity inside the polymer matrix. It was noted that F8CVJ performed better than DCVJ and CCVJ and was attributed to the preferential molecule concentration in outer layer of polymer film (Figure 18c). This effect is caused by the selective segregation of fluorinated fluorophore thereby enabling F8CVJ to interact more easily with vapours. The solvents which were unable to interact with PS displayed no vapochromic response.

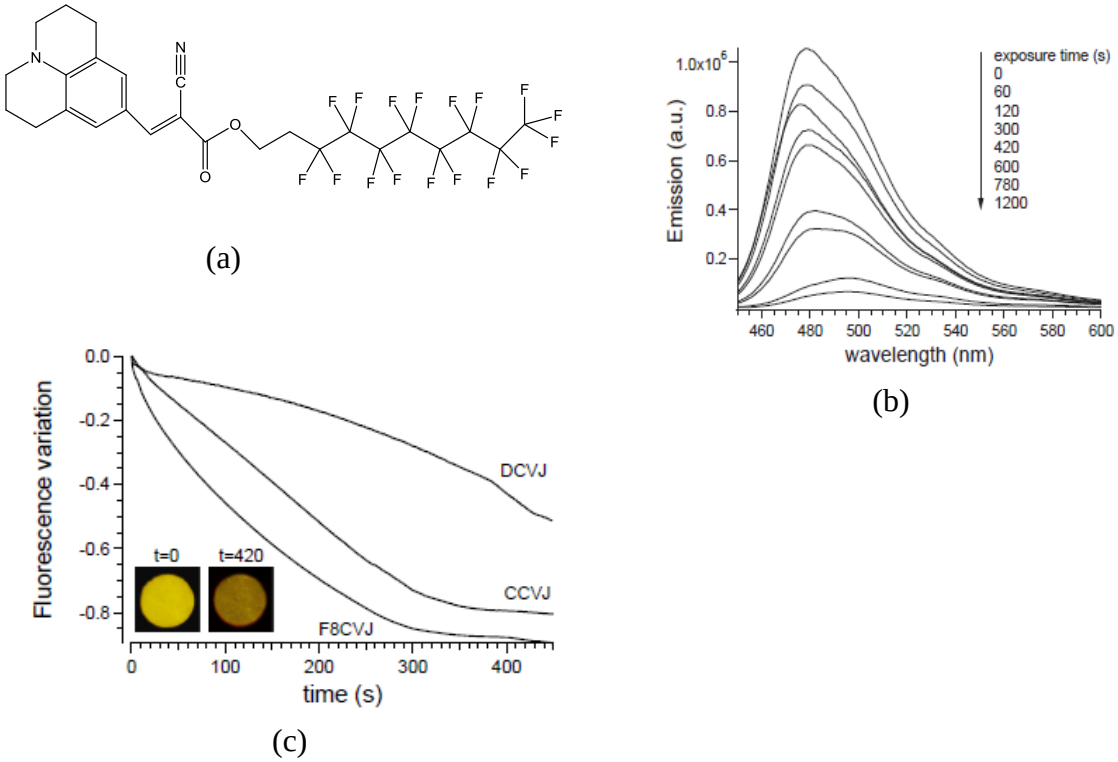

Figure 18 (a) Molecular structure of F8CVJ (b) Change in Fluorescence of 0.05%wt of F8CVJ/PS films on exposure to chloroform (c) variation of fluorescence maximum intensity as a function of time of 0.05wt% DCVJ,CCV,F8CVJ in PS on exposure to chloroform, inset (c) Images of F8CV/PS films with 0.05wt% FMR before and after exposure to $CHCl_3$ under UV lamp excitation.[85]

Recently, the vapochromic behaviour of jolulidine–containing styrene copolymer was reported by some workers in our group with significantly faster response.[86] Accordingly, poly(styrene-co-hydroxyethylmethacrylate) copolymers were functionalized with cyanovinyl-julolidine to prepare (polystyrene-co-2-methylacryloxy) ethyl-2-cyano-3-julolidin-acrylate (P(STY-co-JCAEM) (Figure 19a) and their vapochromic behaviour was investigated.

Interestingly during exposure to VOCs, the fluorescence decrease was much faster (Figure19b) reasonably due to the homogeneous JCAEM moieties distribution favoured by covalent bonding between the FMR and the polymer.

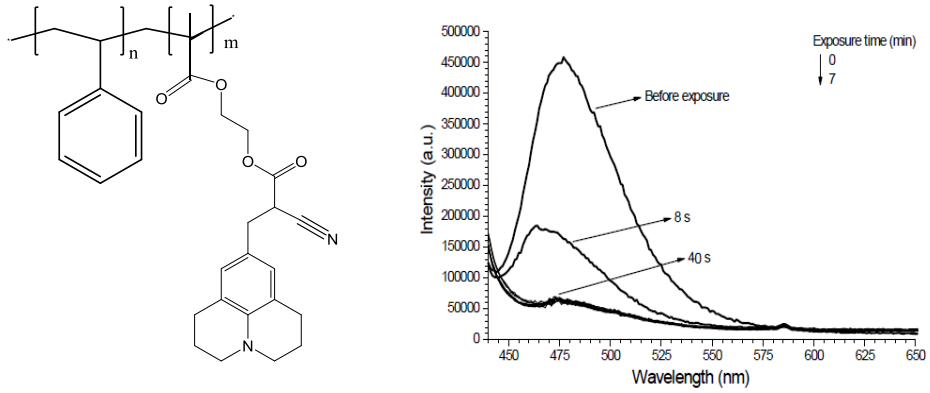

(a) (b)

Figure 19 (a) Structure of P(STY-co-JCAEM) and (b) Fluorescence of P(STY-co-JCAEM) film on exposure to chloroform, indicating fast vapochromic response. [86]

1.4. Aggregation induced emission (AIE) in fluorophores

Aggregation of most of the fluorophores results in quenching of the fluorescence and is known as aggregation caused quenching (ACQ). When fluorophores aggregate together, there is the possibility of the intermolecular π-π interaction which results in quenching of fluorescence.[87] For example, fluorescein is a typical ACQ fluorophore and is insoluble in many organic solvents but dissolved in water. Consequently, in organic solvents like acetone, the fluorophore aggregates and becomes non-emissive in contrary to highly emissive in water (Figure 20a). Accordingly, the planar polycyclic aromatic structure of the fluorescein favours the aggregate formation due to the π-π stacking resulting in excimer formation and thereby causing ACQ. The non-emissive deactivation of such fluorophores limits their application in real-world technology. For example, ACQ effect limits the application of fluorescent materials in the fabrication of optoelectronic devices like organic-light emitting diodes and other practical applications.[87,88] However, the aggregation cannot always result in the fluorescence quenching. Some fluorophores become highly emissive on aggregation and such phenomenon is known as aggregation induced emission (AIE) and the molecules depicting such behaviour are termed as AIEgens. AIEgens are actually special type of FMRs and were first reported by Ben Zhong Tang and co-workers.[88] They reported a series of silole

derivatives which were non-fluorescent in dilute solutions and highly emissive in aggregate form. The AIE effect was first discovered in Hexaphenylsilole (HPS), a propeller and non-planar molecule. The phenyl rotors in HPS undergo intramolecular rotations in dilute solution resulting in the non-emissive deactivation transition on photoexcitation (Figure 20b). However, on aggregation in poorly soluble solvents, the π-π interaction is avoided due to the non-planar structure and propeller shape.[89] On the other hand, the intramolecular rotation of the aryl groups is restricted and such process is known as restricted intramolecular rotations (RIR) (Figure 21a). It is this RIR phenomenon that is supposed to be responsible for the AIE in HPS and other such luminogens. This fact was further supported by measuring the fluorescence of HPS in viscous solvents at lower temperature and higher pressure.[90–92] A large numbers of AIEgens have been synthesized and their potential application in different areas has been highly investigated. For example tetraphenylethylene (TPE) is one such highly investigated AIEgen with broad range of applications reported.[87,93] TPE display typical structural features with four phenyl rings attached to the central ethylene rod through single bond makes. In dilute solution the phenyl rings freely rotate against the ethane rod serving as the non-radiative path for deactivation. Contrary, in the aggregated form, RIR of the phenyl rings favour the highly emissive behaviour of TPE. (Figure 21b).[94]

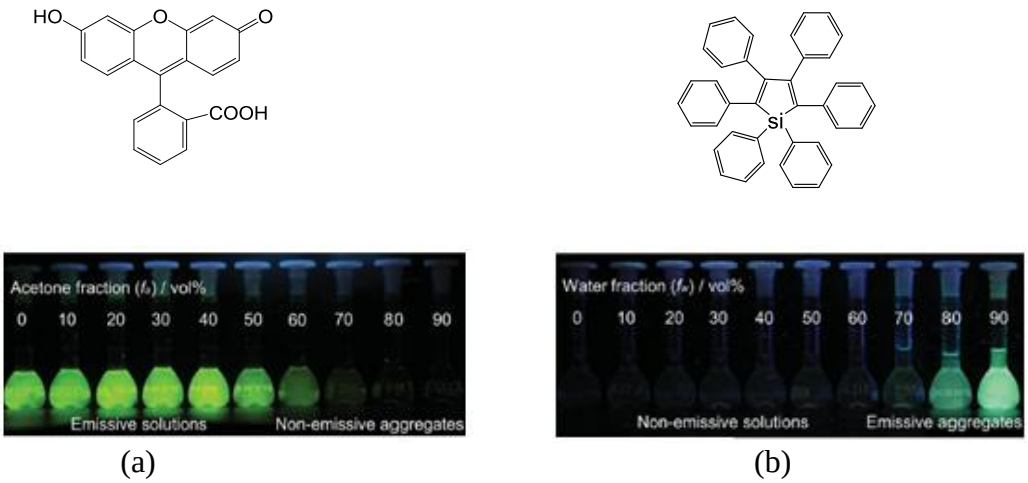

(a) (b)

Figure 20 (a) Structure and fluorescence of fluorescein different water/acetone mixtures with variable fractions and (b) structure and fluorescence of hexaphenylsilole (HPS) in water/THF mixtures of different fractions.[87]

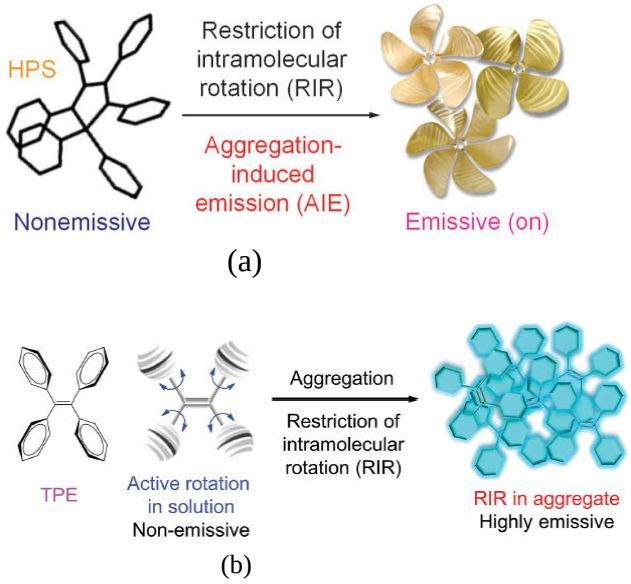

Figure 21 Representation of the restricted intramolecular rotation (RIR) aggregation in (a) hexaphenylsilole (HPS) [93] and (b) tetraphenylethylene (TPE).[95]

1.4.1. Application of AIEgens

The effect of concentration quenching restricts the application of fluorophores for desired purposes. On the other hand quantum dots are considered as better alternative to overcome such restrictions, however, the difficult synthesis, limited variety and toxicity makes them unsuitable for the desired applications.[96,97]AIEgens are reported to overcome all such limitations since there is no concentration quenching or toxicity effects related to these luminogens. The AIE effect is suitable to work where the ACQ effect fails. Soon after the discovery of AIE in 2001, interest for developing new AIEgens with fascinating applications has gone up too rapidly. AIEgens with large scale applications in biological imaging, photodynamic therapy, chemical detection, optoelectronic device fabrication etc. have been successfully developed and investigated (Figure 22).[98–105]

Certain luminogens like HPS are reported to display interesting features for sensing applications including viscochromism, piezochromism, and thermochromism.[106] Viscochromism effect is due to enhancement of RIR in higher viscous solvents and hence increasing the fluorescence. Pressure sensitivity of HPS is assumed due to the compression, bringing molecules together resulting in hindrance of the rotation of the phenyl rings. However at much higher pressure the formation of excimer can decrease the emission. Temperature sensitivity of HPS recorded in THF indicated the potential application of

AIEgens for thermochromism. Since, cooling hinder the thermally allowed intramolecular rotations, the HPS solution in THF resulted in intensified emission on cooling.

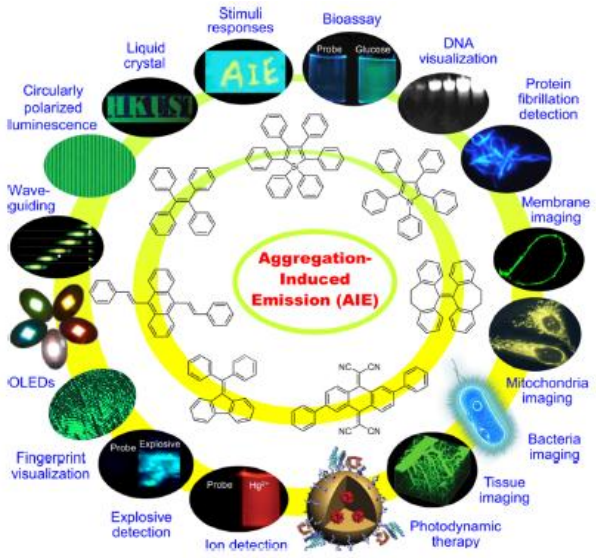

Figure 22 Structure and real-world applications of some AIEgens.[95]

1.4.2. AIEgens as VOCs sensors

TPE derived AIEgens also demonstrate exhibit solvatochromic behaviour enabling their application for measuring polarity changes. Tang et al. reported the solvatochromic behaviour of the 1,3 indandione–modified TPE (IND-TPE) (Figure 23a,b).[87] 1,3-indadione acts as an electron acceptor and its attachment with TPE core results in a push-pull chromophore due to ICT phenomenon. On changing the solvent from toluene to acetonitrile, a bathochromic shift from 543 to 597 nm was recorded (Figure 23c). Such kind of application allows measuring the AIE and polarity changes without affecting the photophysical properties of AIEgen.

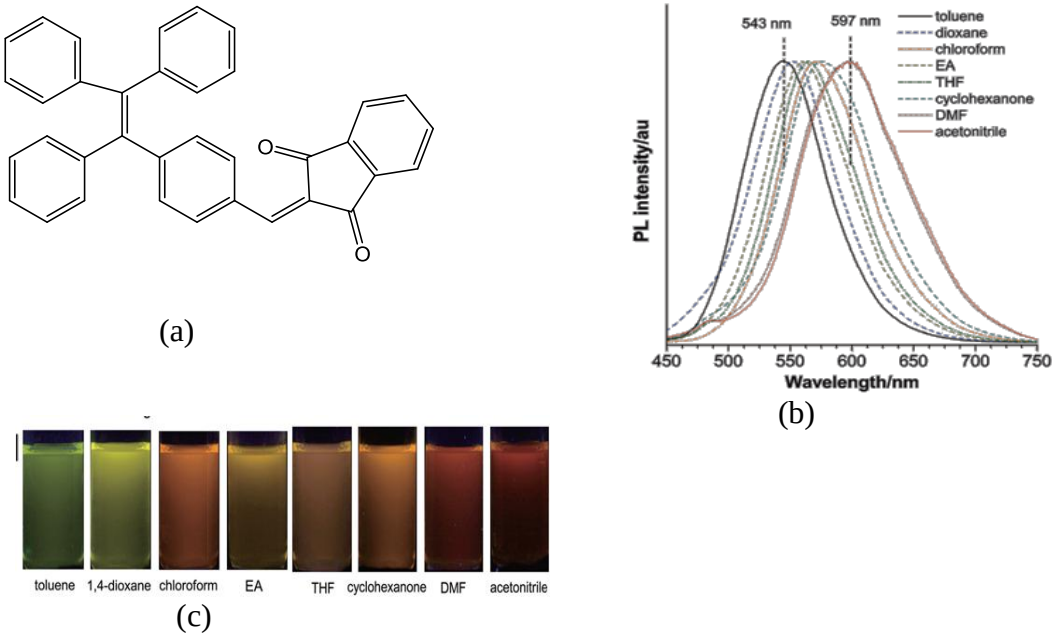

(a) (b) (c)

Figure 23 (a) Structure of 1,3 indandione modified –tetraphenylethylene (IND-TPE), (b) Fluorescence of IND-TPE in different solvents showing solvatochormic behaviour and (c) Images of IND-TPE solutions in different solvents under the UV lamp illumination at 365nm.[87]

The potential applications of AIE as vapochromic sensor was recently extended to polymeric systems.[107] The detection of VOCs using TPE/Polymer systems were investigated by Tang et al.[108] Polyacrylates were prepared through radical polymerization of the TPE containing di- and tetracrylates (Figure 33a). The TPE/Polymer system on exposure to dichloromethane showed excellent reversible vapochromic response (Figure 34b).

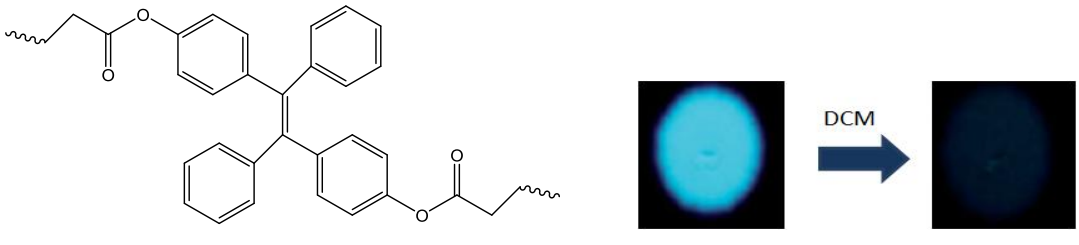

(a) (b)

Figure 24 (a)TPE-attached to polyacrylates and (b) Images of the spots of the polymer on thin layer chromatography (TLC) plates depicting vapochromism on exposure to dichloromethane.[108]

1.5. Solvatochromic probes as sensors for the detection of VOCs

The change in colour of a chromogenic material on changing the polarity of the solvent is described as solvatochromism. The phenomenon was first termed by Hantz schlater[109] however since then, the meaning of this term has broadened. Depending of the polarity index of the solvent, solvatochromism can be either positive or negative corresponding to bathochromic and hypsochromic shifts respectively.[110] Solvatochromism occurs due to differential salvation of the ground and first excited state of the chromophore resulting in the stabilization of either of the two states. Accordingly when excited state is more stabilized than the ground state in higher polar medium, bathochromic shift occurs and vice versa.[110]

Since the absorption process is very fast than the time required for the displacement of nuclei (Franck Condon principle) and results in redistribution of electrons and consequently changes in dipole moment. Like FMRs, solvatochromic molecules also contain both donor and acceptor moieties connected by conjugated part. However, their flexibility is restricted even in the free environment. The ICT chromophores, also known as push-pull chromophore, are simply represented by an electron donor (D) linked to an electron acceptor (A) through π-conjugated linker having dipole character.[111] This ensures that during photoexcitation, the charge is transferred from donor to acceptor forming a excited state with higher dipole moment (μ). Consequently, the excited state then relaxes through interaction with the solvent dipoles resulting in bathochromic shift in polar solvents as represented. Due to the ICT, the dipole moment increases in the excited state (μ_e) with respect to the dipole moment of the ground state (μ_g) on photoexcitation.[110,112–114] The polar solvent molecules are assumed to form a cage around the solavtochromic dye molecule which then undergoes relaxation to the minimize energy of the excited state of solute molecules (Figure 25). Since the lowering of the energy is much larger in higher polar solvents than the lower polar solvents, bathochromic shift results in polar medium. When the lifetime of the solvent reorganisation around the chromophore is shorter than excited state lifetime, fluorescence results from the molecules in equilibrium with salvation shell (F' in figure 25). In case of the higher polar solvents the bathochromic shift is accompanied by non radiative emission due to higher decrease in energy of the chromophore. Higher viscous solvent may hinder the solvent reorganization[112] thereby resulting in emission from Franck Condon state with a slightly

shifted emission spectra.

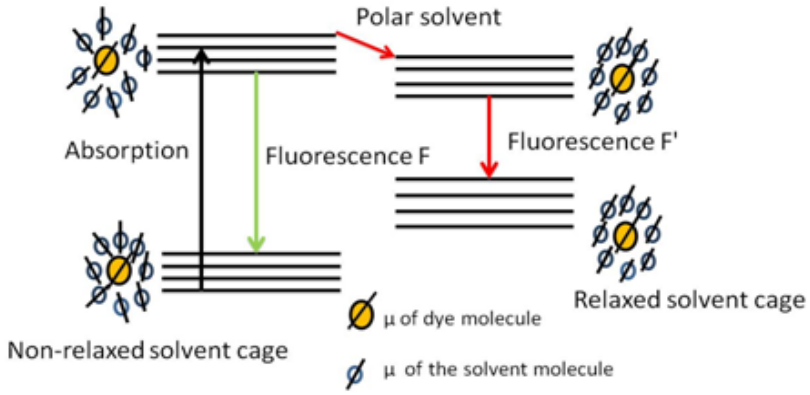

Figure 25 Representation of solvent cage around the salvatochromic dye with the orientation of the dipole moment in non-polar (left) and polar solvent (right).[51]

Solvatochromism depends on the chemical and physical properties of the chromophore as well as the solvent that together describe the strength of intermolecular solute-solvent interactions. The exact environmental effects of a solvatochromic probe are still under investigation.

The sensitivity of chromophores to the polarity of the medium is explored for the development of novel sensors for the detection of solvents based on their polarity. The solavtochromic probes have been also used to monitor biophysical properties of biomembranes including polarity which play important role in organization and function of these membranes.[115] Loew et al. use styryl-pyrinidium, charge transfer dyes, to detect transmembrane potential since they are vertically oriented in biomembranes.[116] Solvatochromic probe has also proved as powerful tool to detect bimolecular interactions with better response than fluorescence resonance energy transfer (FRET) and fluorescence anisotropy.[117]

The typical polar sensitivity of different solvatochromic probes has been explored for chemical sensing applications. For example Prodan, Nile red, Dapoxyl derivatives etc. (Figure 26) display typical solvatochromic behaviour and have demonstrated the chemical sensing ability. With the time, the solvatochromic features of the chromophores have been enhanced by certain modification methods. Recently, Kucherek et al. developed fluorene analogues of prodan (7-diethylamino-9,9-dimethyl-9H-fluorene p-2-carbaldehyde, (FR0)) by

substituting napthelene with fluorene, indicating significantly higher solvatochromic features than prodan.[118] (Figure 27)

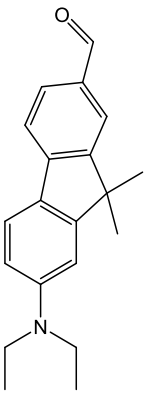

Prodan

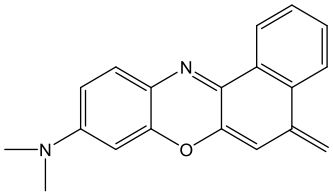

Nile Red

Figure 26 Molecular structures of well known solvatochromic dyes prodan and nile red.

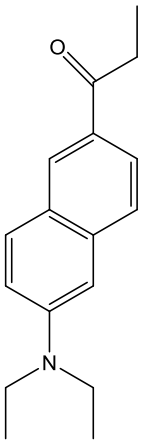

(a)

(b)

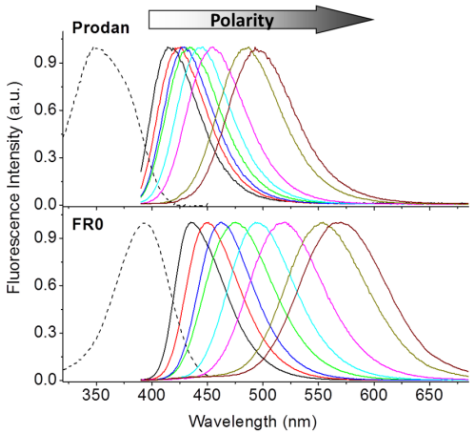

(c)

Figure 27 (a) Molecular structure, (b) fluorescence of FR0 in different solvents and (c) comparison of solvatochromic behaviour of prodan and FR0 in different solvents.[118]

Certain dyes display negative solvatochromic behaviour when exposed to high polar solvents. Reichardt's betaine (2,5- diphenyl-4-(2,4,6-triphenyl-1-pyridinio)-phenolate) (Figure 28a) features outstanding negative solvatochromic response on exposure to higher polar solvents.[110] Accordingly, hyposchromic shift of about 350 nm was reported on changing the solvent from tetrahydrofuran to methanol (Figure 28b).[119] Clearly this behaviour can be attributed to the better relaxation of highly dipolar zwitterionic ground state than the less dipolar first excited state. Such behaviour is favoured due to some typical properties of betaine molecule which involves large permanent dipole moment, lager polarizable π-

electronic system and the highly basic electron pair donor phenolate oxygen for the better interaction with H-bonding solvents.[120]

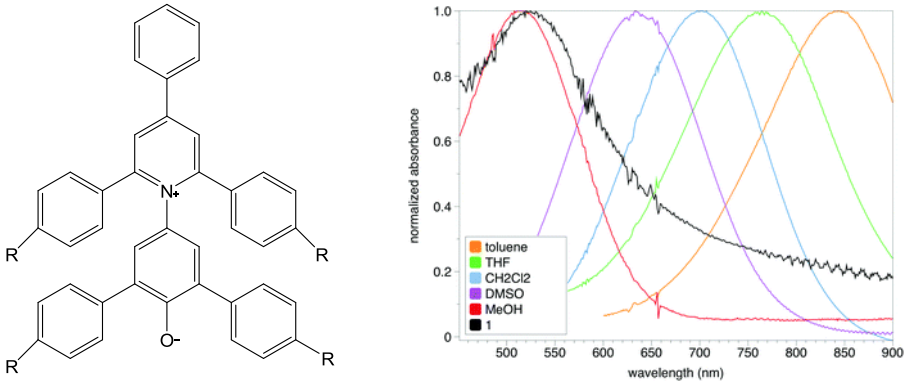

Figure 28 (a) Molecular structure of Reichardt's Betaine dye. (b) Normalized absorption of Reichardt's dye in different solvents indicating negative solvatochromism.[120]

Ryan et al. reported the application of solvatochromism in selective detection of hydrogen-bond-donating solvents.[121] Accordingly, the emission of the dye 6-(3-aminophenyl) -1,3,5-triazine-2,4-diamine (MADAT) (Figure 29a) remains unchanged in all aprotic solvents (polar or non-polar) while it is red shifted in all protic solvents (Figure 26b). It was found that strongly hydrogen bonding solvents resulted in complete quenching of MADATs emission. Interestingly, there seems to be no effect on solvent stabilization of the dye. The selective response of the MADAT towards protic solvents was assumed to be the due to hydrogen-bonding interactions from the nitrogen atoms in 1,3,5 triazine ring.

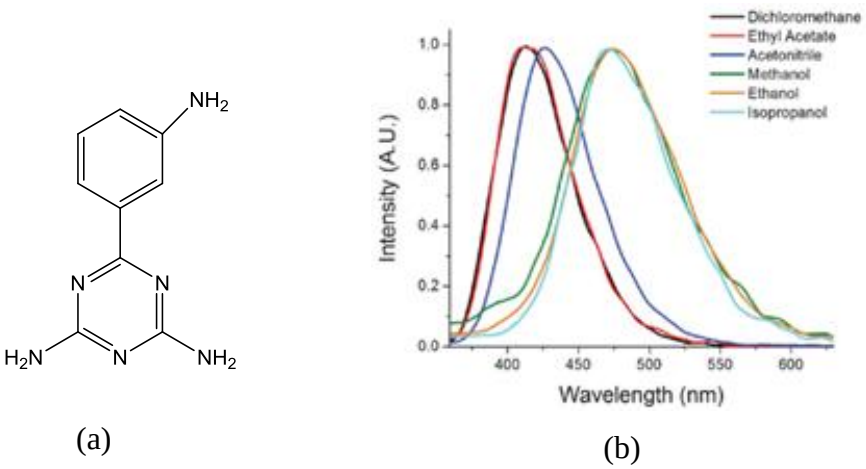

Figure 29 (a) Molecular structure of 6-(3-aminophenyl)-1,3,5-triazine-2,4-diamine (MADAT) (b) Emission spectra of MADAT in some protic and aprotic solvents.[121]

Consequently, this kind of solvatochromic dye has potential application in monitoring the protic solvents without the effect of their polarity.

Many workers have reported the development of colorimetric sensor array based on different chromogenic dyes for the detection of different organic solvents.[122,123] Recently Jacquelin et al. reported the colorometric sensor array composed of seven solvatochromic dyes (4 positive solvatochromic and 3 negative solvatochromic) in semi-liquid matrices to detect different organic solvents (Figure 30).[122] The dyes change colour on the basis of polarity and allow the measurement of physical changes in matrix on solvent adsorption. They were successfully able to distinguish the analytes with limited chemical reactivity. The colorometric sensor array was prepared by printing highly viscous dye/solvent liquid on porous polypropylene membranes. Interestingly, solvatochromic probes embedded in polymer films have also shown promising application in the detection of VOCs. Polymers play a vital role in enhancing the sensing ability of the probe. Polymers act as sorbent phase, interact and concentrate VOCs. Evaporation of solvent resulted in dyes in semi-fluid environment. The dyes were mixed in different matrices (polar, non-polar) to improve the chemical diversity of the sensor array.

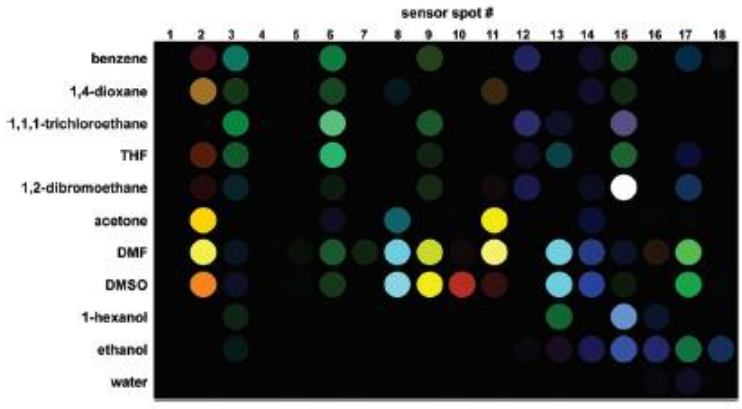

Figure 30 Colorometric sensor array detection of different organic solvents at 10% of their saturation vapour pressure after 5 min of exposure.[122]

The sensing features of solvatochromic polymer films for the detection of organic solvents were also demonstrated by Krech and co -workers on exposing the negative solvatochromic dye, Richardt's betaine (RDye), in different polymers including poly(isobutylene), poly(epichlorohydrin), polystyrene etc. to different VOCs.[124] The effect of polymer properties on solvatochromic response at the lower vapour concentration was reported.

Notably, RDye has higher dipolar zwitterionic ground state and less polar excited state facilitated by the ICT form the phenoxide group to pyridinium moiety on photoexcitation.[110] Eventually, this gives rise to blue shift in polar medium. They concluded that RDye in non polar polymer film exhibit better response to polar solvents and vice versa. Furthermore, due to the preferential solvation of RDye in polymer films by methanol, the detection of lower concentration of polar solvents in water was demonstrated.

Recently an interesting solvatochromic sensor array of conjugate polymer polydiacetylene (PDA) was reported.[125] The colour change of PDA from blue to red due to conformational changes in its backbone on exposure to VOCs was demonstrated (Figure 31). VOCs response was improved by incorporating PDA in different polymer matrices including polyvinylpyrrolidone (PVP), polyethylene glycol (PEG), polyacrylic acid (PAA) and poly (4-vinyl pyridine (P4VP)). Consequently, these polymers condense and concentrate vapours of VOCs differently, resulting in better and variable solvatochromic response of PDA on exposure to different solvents.

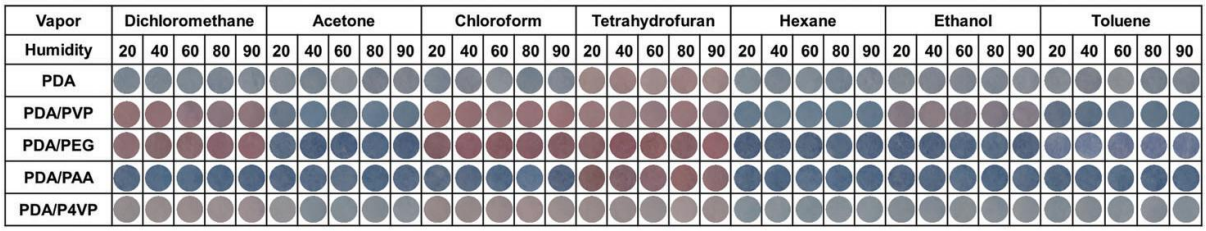

Figure 31 Solvatochromic sensor array of different PDA/ Polymer films on exposure to different vapours under relative humidity between 20% and 90% [126]

1.6. Polymers as supporting materials for fluorescent molecules

Polymers continue to remain the most preferred supporting material for the fluorescent dyes since they can be easily processed to thin films. Generally, a polymer can be thermoplastic, elastomeric or thermosetting depending on difference in the method of polymerization, effect of heating, softness or hardness of the material etc. Thermoplastic polymers are characterized by long flexible chains connected to back bone by covalent bonding. They can be easily hardened or softened by decreasing or increasing the temperature respectively. The electrons

are found in the low lying orbitals with a large energy gap resulting in absorption in near UV. Consequently they are transparent to wavelengths above 200nm and hence do not alter the efficiency of dyes.[127] Such excellent properties make them potentially suitable as supporting material for most of fluorescent dyes. Typically used thermoplastic materials for fluorescent dyes are Poly (methyl methacrylate) (PMMA), Polycarbonate (PC), etc. (Figure 32).

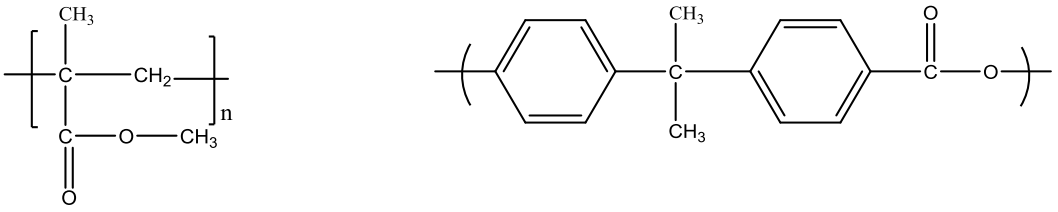

Poly(methyl methacrylate)

Polycarbonate

Figure 32 Structure of the monomeric units of PMMA and PC

Thermosetting polymers on the other hand are covalently crosslinked materials with three dimensional structures making them hard and rigid (e.g. epoxy resins). They have also been used as the supporting matrix for the aggrochromic dyes for the detection of different organic solvents.[128] The characteristics of elastomers range between thermoplastic and thermosetting polymers e.g. rubber.

1.6.1. Preparation of dye/Polymer films

Fluorescent dyes are either immobilized by simple mixing[129] or by covalent attachment.[130] Both methods have certain advantages or disadvantages associated, while physical entrapment method of dyes is a simple, cost effective and fast method for the preparation of the fluorescent polymer film, covalent attachment is considered to be more efficient but less favourable in terms of cost and time. In both cases, the control of the dispersion of dyes plays the main role in their final application.[131] Accordingly, aggregation of dyes could alter their optical properties which could make them less suitable for the practical applications.[132–135]

Dye dispersion in polymers by simple mixing can be realized either by solution casting or in the molten polymer matrix by mechanical process. The dyes having higher compatibility with the polymer matrix can be prepared easily without synthesizing new polymer. The final solution mixture is poured into the mould resulting into thin dry films after solvent

evaporation (Figure 33a). In case the two are incompatible, miscibility cannot occur by solution casting which otherwise can give rise to phase separation. The problem is overcome by applying mechanical treatment involving shearing forces that overcome the interfacial tension thereby resisting the deformation and break-up of dye agglomerates (Figure 33 b).[127] The dispersion is mainly controlled by the affinity of dye with polymer. The miscibility is allowed through non-covalent intermolecular interactions including hydrogen bonding, dipole-dipole and van der walls forces.[127] These specific interactions tune the photophysical properties of the system resulting in innovative characteristics and response to external changes. The thermoplastic polymers like PMMA, PC, PS etc. are supposed to be highly compatible with dyes due to the presence of functional repeating units and hence the fluorescent polymer films of such materials can be realised easily by solvent casting.[136]

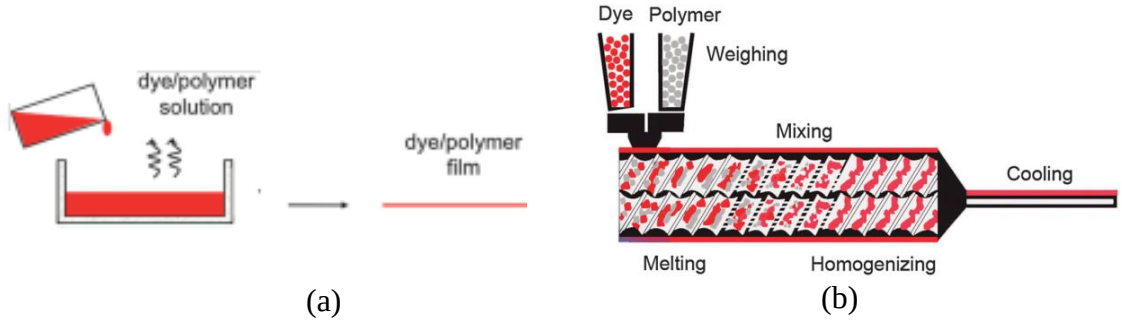

Figure 33 Preparation of dye-polymer film by (a) solution casting (b) melt-extrusion process.[127]

Covalent attachment of dyes with polymers can be realized by many synthetic routes (Figure 34). It either involves directly linking the fluorescent dye with the polymer (Figure 34a) or formation of a copolymer with a random or block distribution of coloured residues (Figure 34b).[127] Alternatively, the covalently linking of the dye with the polymer can also occur after polymerisation provided the polymer possess reactive functional groups, causing the limitation of this method (Figure 34c).[137,138] In such cases, the monomer is labelled with the fluorophore and then allowed to undergo polymerization to form linear polymers (Figure34d).

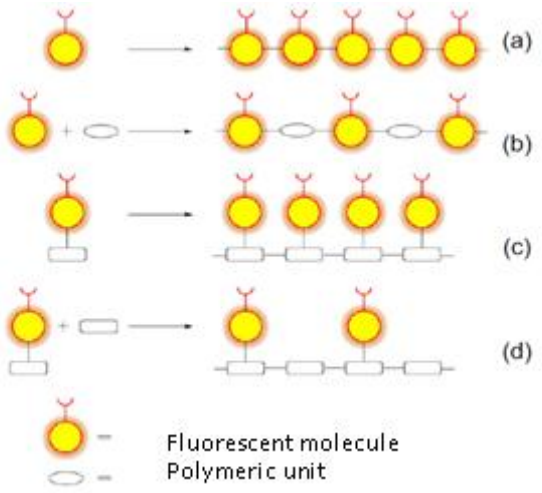

Figure 34 Synthetic routes for the preparation of covalently linked fluorescent dyes with polymers.[107]

1.7. Vapour permeation in polymers

To understand the vapochromic or salvatochromic nature of the fluorescent polymer films it is essential to know the phenomenon of solvent permeation processes through the polymers and the factors that control these processes. The polymers are permeable to different vapours/gases to different levels. Permeability of vapours in a polymer has been well explored for the fascinating applications in gas separation processes.[139] Consequently, many researchers are interested to understand the mechanism of the permeation and diffusion of solvent molecules through the polymeric materials. Notably, the permeability of solvent molecules in glassy polymers is lower than the rubbery polymers. Permeation of the gases/vapours through the polymer is the net result of the two different processes, thermodynamic dissolution of vapour in the polymer and the kinetic process of diffusion of gas through the polymer matrix.[140]

1.7.1. Effect of diffusion

The permeation occurs in sequence of steps: adsorption, diffusion and desorption. Molecular diffusion determines the rate of permeation as it is the limiting factor and occurs due to the concentration difference between the two interfaces of the polymer. Motion of both polymer chains and solvent occurs during diffusion.[141] Since the motion of polymer segments is slower than the solvent, the former is the limiting step in diffusion process. According to

Fick's law of mass diffusion, "rate of the transfer of the diffusing substances through the unit area of cross section is proportional to the concentration gradient normal to the section"[142] The permeation equation is obtained by combining Fick's law of diffusion with Henry's law of solubility and is given by:

$$J = \frac{D.S\ (P_2 - P_1)}{h} \qquad (5)$$

J is the rate of transfer per unit area of the section (permeation), D is the diffusion coefficient, S is solubility coefficient of the vapour, h is the film thickness (polymer film thickness here), P_1 and P_2 are the partial pressures on two different sides of the film.

Polymer selectivity of two gases A and B is expressed by ideal separation factor α*(A/B) defined by

$$\alpha^*(A/B) = \frac{P(A)}{P(B)} = \frac{D(A)}{D(B)} \times \frac{S(A)}{S(B)} \qquad (6)$$

where P(A) and P(B) are the permeability coefficients , D(A) and D(B) represents diffusion coefficient of each gas and S(A) and S(B) their solubility coefficients respectively.

1.7.2. Effect of pressure

Pressure dependence of permeability is different for rubbery and glassy polymers.[143] It is observed that the permeability of the gas in glassy polymer decreases with increase in pressure initially but increases after the plasticization of the polymer. In rubbery state polymers, the pressure dependence of gas solubility is also evident. For less soluble gases, permeability is independent on the pressure. In case of organic vapours, the permeability depends on the vapour pressure since they are much soluble in rubbery polymers. The permeability of gases in glassy polymers in relation to pressure is described satisfactorily by "dual-mode" sorption model considering the heterogeneity of the glassy polymers.[144–146] Dual mode sorption is the sum of the Henry's and Langmuir sorption[147,148] and is given by

$$C = C_D + C_H = K_D p + \frac{C'_H bp}{1} + bp \qquad (7)$$

Where C_D is the Henry's sorption, C_H is the Langmuir sorption, p is the applied pressure of the gas, K_D is the Henry's solubility coefficient, C'_H is the Langmuir saturation constant and b

represents the Langmuir affinity constant.

According to this model, the permeability and solubility coefficients decrease and diffusion coefficients increase with increase in pressure of gas at high pressure.[139] Furthermore, at low pressure, permeation, diffusion and solubility coefficients are independent of pressure. However, at higher concentration of the gases all three coefficients increase with increase in pressure in glassy polymers. Stern et al. reported the effect of pressure on the permeability by using free volume theory. According to their results, the increase in the pressure of the gas may result in two effects opposite to each other. Accordingly, on increasing the pressure, the concentration of the gas dissolved increases resulting in further increase in free volume. However, the hydrostatic pressure generated can work against the process and hence decrease the free volume. The overall change in the free volume determines the permeability coefficient.[149]

1.7.3. Effect of solubility parameter (δ) and Flory-Huggins interaction parameter (χ)

There are many polymer solution theories that explain the solvent –polymer interaction.[146,150] However these theories have some limitations of increased complexity of calculations or unavailability of the data required for the calculations. The most widely accepted theory is that of Flory-Huggins theory of polymer solutions, introduced independently by P.J.Flory [151] and M.L.Huggins.[152] According to this theory, free energy of mixing of polymer and solvent is given by

$$\Delta G_{mix} = RT(n_1\ In\ \phi_1\ + n_2\ ln\phi_2 + n_1\phi_2\ \chi_{12}) \qquad (8)$$

Where ΔG_{mix} is the free energy of mixing, R is the gas constant , T is the temperature, n_1 and n_2 are the number of the moles of the gas and polymer respectively, ϕ_1 and ϕ_2 corresponds to the volume fractions of solvent and polymer respectively and χ_{12} is the unit less quantity described as Flory –Huggins interaction parameter .

The smaller value of χ_{12} indicates better solvent-polymer interaction. Negative values of χ indicate the contribution of the polar interactions between solvent and polymer. The value of χ is slightly sensitive to the polymers with higher molecular weight.[143] χ is assumed to be independent of the relative concentration of polymer and the solvent.[153]

Another way of describing the solvent-polymer interaction is expressed by solubility

parameter (δ). The value of δ defines the compatibility of a solvent with the polymer. Notably, for better solvent-polymer compatibility, the solubility parameter of both solvent and polymer has to be similar or very close (a difference less than 0.5). Any deviation with such difference results in unfavourable interaction between the solvent and the polymer. This parameter was introduced by J.H. Hildebrand and is valid for a single component unlike Flory-Huggins which represents both solvent and polymer. The solubility parameter is given by square root of cohesive energy density.[150]

$$\delta = -\frac{U}{V} = \left(\frac{\Delta H - RT}{V}\right)^{\frac{1}{2}} \qquad (9)$$

Where U is the internal pressure of the solvent, V is the volume, ΔH change in enthalpy, R is the gas constant, T is the absolute temperature.

The cohesive energy is the increase in internal energy and cohesive energy density represents the energy required to break all intermolecular interactions. This parameter was previously used for non-polar solvents but has been extended for polar solvents also. The Hildebrand solubility parameter was further modified by Hensen and co-workers for large scale application of the polar and hydrogen bonding systems.[155]

$$\delta_t^2 = \delta_d^2 + \delta_p^2 + \delta_h^2 \qquad (10)$$

Where δ_t^2= Hansen's total solubility parameter, δ_d^2, δ_p^2, δ_h^2 are the contribution to solubility parameter due to dispersion, polarity and hydrogen bonding respectively.

1.7.4. Effect of polymer free volume

Free volume is the internal space in the polymer for the chains to move (Figure 35). Free volume is in the form of channels and holes of molecular size and are filled by solvent molecules during exposure to VOCs.[139] Higher the free volume inside a polymer, lower is the viscosity, thereby lower hindrance to the transport of the gaseous molecules. The free volume in glassy polymers is assumed to exist as isolated microvoids. The molecules in these voids may dissolve and diffuse through the dense polymer matrix. Consequently, an equilibrium is established between the sorption and dissolution.[141]

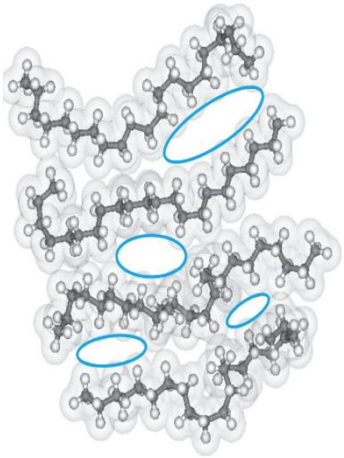

Figure 35 The representation of free volume in a polymer matrix.

Diffusion coefficient and free volume are related to each other by [149]

$$D = A\ exp\left(-\frac{\mathrm{B}}{\mathrm{f_v}}\right) \qquad (11)$$

Where D is the diffusion coefficient, f_v is the fractional free volume of the glassy polymer, A and B are the constant characteristics of a given solvent-polymer system.

Free volume can be subdivided into two types (a) interstitial free volume present among all the molecules and (b) hole free volume which is localized.[156] The energy of redistribution for interstitial volume is too large while redistribution of hole free volume requires no energy hence the latter is available for the molecular transport.[157]

1.7.5. Effect of molecular weight of polymers

The mechanical properties of a polymer highly depend on its molecular weight. Higher the molecular weight, higher the viscosity. Accordingly, the molecular weight must influence the transport of solvent within polymer. Consequently, the higher weight polymers reduce the transport process due to decrease in number of chain ends.[143] Notably the chain ends form sites for the molecules to be adsorbed into glassy polymer. Higher degree of cross linking reduces the free volume and hence decreases the transport process. Furthermore, large molecular weight polymer have higher disentanglement resulting in higher degree of swelling before dissolution.[139]

1.7.6. Effect of the solvent

Solvent properties including vapour pressure, polarity, shape, size etc also affects the solvent-polymer interaction and consequently their diffusion. Solvents with same interaction parameter but higher vapour pressure display better interaction with polymers than the lower vapour pressure solvents. Polarity of solvents can also influence the permittivity of solvents within the matrix. Accordingly, polar solvents interact differently with different polymers. The shape and size of the solvent molecules cannot be ignored when the interaction is not significant. Berens et al reported that the diffusion of n-alkanes and other elongated molecules are higher by a factor up to 10^3 than the diffusion of spherical molecules of similar molecular weight indicating the molecules having long alkyl chain move along their long dimension in glassy polymers.[147]

1.8. Relation of glass transition temperature (T_g) with the viscosity of the polymer

Glass transition temperature (T_g) of Polymer plays a crucial role in many polymer applications. The effect of T_g on the transport of vapours inside the matrix cannot be ignored. Glassy Polymers with higher T_g have reduced segmental mobility and thereby lower diffusivity contrary to the rubbery polymers.

The continuous progress in this research field led to the development of an interesting equation known as Williams-Landel-Ferry (WLS) equation. This equation relates the influence of temperature on the viscosity and the mobility of the polymer chains particularly at the glass transition temperature (T_g).

$$\log\left(\frac{\eta}{\eta_g}\right) = -17.44(T - T_g)/[51.60 + (T - T_g) \qquad (12)$$

Where η and η_g are the viscosities at temperature T and glass transition temperature T_g.

1.9. Structural and morphological changes in glassy polymer on exposure to VOCs

Glassy polymers are rigid than the rubbery polymers hence they are less favourable to the solvent permeation. However, there are some factors that allow the solvent molecules to interact with the polymer to some extent depending on the interaction parameter, solubility parameter, vapour pressure, polarity etc. The compatible solvents after interaction with the polymer diffuse into the matrix. Consequently, there is some plasticization of the matrix indicated by the swallowed gel-like morphology. At such point, large free volume is available due to freely chain mobility. After certain point of time the dissolution of the polymer starts. However sometimes the polymer cracks and no gel layer is formed. The cracking is caused by the increase in stress concentration at the interface between swallowed and solid part of the polymer.[158] It depends on how fast the osmotic pressure inside the polymer is relieved. The dissolution of polymer is related interaction parameter and temperature as

$$\chi = \frac{\Delta\omega}{KT} \qquad (13)$$

Where χ is the Flory-Huggins interaction parameter, $\Delta\omega$ is the difference in energy of the pure solvent and solution, K is the Boltzmann constant and T is the temperature.

Solvent exposure of polymer films can also induce crystallization termed as solvent-induced crystallization (SINC). Exposure of polymer to the well interacting solvents results in plasticization of the polymer, thereby reducing the T_g and the difference between T_g and melting point (T_m) is increased resulting in room temperature crystallization.[159] The relation between the depressions of melting point of polymer with the addition of solvent can be calculated using Flory's equation

$$\frac{1}{T_m} - \frac{1}{T_m^0} = \frac{R\,V_P}{\Delta H_m\,V_s}\,(\phi_s - \chi\phi_s^2) \qquad (14)$$

Where T_m and T^0_m is the melting point of solvent and pure polymer, ϕ_s is the solvent volume fraction, V_S and V_P are molar volumes of the solvent and the polymer and ΔH_m is the molar heat of fusion, R is the gas constant and χ is the interaction parameter

Solvent induced crystallization of bisphenol A polycarbonate (PC) has been effectively

investigated by many workers.[159–162] Solvent permeation is followed by easier movement of the polymer chains, hence there is less hindrance to the formation of thermodynamically favourable crystalline state. Titwow et al. reported the crystallization of bisphenol A polycarbonate (PC) by chlorinated hydrocarbons. The solvents used were 1,2-dichloroethane and chloroform, since they are considered to be good solvents for PC. Crystallization begins to occur when the partial pressure of the solvent is equal or higher than the solubility transition and is favoured by delayed desorption and whitening of the polymer.[163] Crystallization rates are maximum at the temperature when the thermodynamic driving force is balanced by the decrease in chain mobility with cooling.[164] Furthermore, the increase in molar mass increases the crystallization of polymers on exposure to solvent. Due to crystallization process, the mechanical properties of a polymer also changes as reported in case of PC. It was observed from the reflected light micrograms that the behaviour of PC changed from ductile to fragile after the solvent (acetone) exposure and the crystallization is induced. The crystalline phase structure morphology of the solvent exposed PC films is the spherulite form whose size depends on the polymer molar mass. This is attributed to the higher number of the repeating units in PC, which increases greater number of folding sites available.

The solvent induced crystallization of glassy syndiotactic polystyrene has been reported as well.[165] The polymer films were immersed in solvents of different solubility parameter including dichloromethane, chloroform and cyclohexane and the resulted crystallization process was ascribed to the sorption of these solvents. The molecular mechanism of the solvent-induced crystallization of the glassy syndiotactic polystyrene was fully investigated by Tashiro etal.[166] They showed that after the exposure of polymer to different organic solvents the formation of the regular helical conformation started to increase with time. Furthermore, it was noted that crystal lattices starts to form at the time when the long segments of helical form the aggregation structure. The rate of crystallization directly depends on the type of the solvent used.

Solvent mediated crystallization of 9,9-dialkyl-fluorene polymers has been also investigated. The influence of the side chain structure on the crystallization of the polymer was reported.[167]

Swelling of polymer occurs if the solvent and the polymers thermodynamically incompatible or have different solubility parameters. When the solubility parameter of the polymer and the solvent is similar, the polymer chains at the polymer-solvent interface will disentangle from

swallowed polymer. The degree of swelling is determined by the relative rate of transport of solvent and the disentanglement. Higher the transport rate, better the swelling of polymer and faster the disentanglement, lower the swelling.[168]

Chapter 2

2. Fluorescent molecular rotors as vapochromic sensors

2.1. Introduction

FMRs have become rather popular in the last 5–10 years thanks to their easy applicability as non-mechanical viscosity sensors, tools for protein characterization, and local microviscosity imaging.[68,78,93,106,169–178] Remarkably, their sensitivity towards viscosity changes has reached a precision comparable to that of commercial mechanical rheometers with shorter measurement time.[67]

The sensitivity of FMRs towards viscosity has already been explored for the development of vapochromic sensors.[85] Accordingly, these molecules display significant sensitivity to the viscosity changes when dispersed in polymer films. However, the investigation of the applications of FMRs for vapochromism is still in its initial stages and needs further research to understand the mechanism fully. In the previous study, the vapochromic behaviour FMRs sensitive to only viscosity has been investigated. However, in addition to viscosity, the local polarity can make significant changes on the photophysics of FMRs which are also sensitive to polarity. Most of the FMRs are slightly sensitive to polarity due to the complex dipolar properties of the accessible excited states.[68] This limitation restricts their application for determining the polarity sensitive changes in the environment. The introduction of intramolecular charge (ICT) character can induce the polar sensitivity in FMRs to a significant level. Consequently, sensitivity to both viscosity and polarity sensitivity might broaden their application for sensing purpose. However, the synthesis of such molecular design is a challenging task. It has been reported that FMRs based on triphenyl amine (TPA) display significant sensitivity to both viscosity and polarity.[179] To explore such fascinating properties of FMRs, different kinds of TPA based FMRs are under consideration.

Publications
1. P. Minei, M. Koenig, A. Battisti, M. Ahmad, V. Barone, T. Torres, D. M. Guldi, G. Brancato, G. Bottari and A. Pucci, *J. Mater. Chem. C*, 2014, **2**, 9224–9232.
2. P. Minei, M. Ahmad, V. Barone, G. Brancato, E. Passaglia, G. Bottari and A. Pucci, *Polym. Adv. Technol.*, 2016, **27**, 429–435.55

Recently, a prototype for a new class of FMRs, namely 4-(diphenylamino)phthalonitrile (**DPAP**) (Fig. 1a), was reported and its sensitivity towards solvent polarity and viscosity was probed using photophysical and computational methods.[179]

DPAP presents a contrasting deactivation pattern of the intramolecular charge transfer (ICT) state in low or high polar media. On one hand, in low and medium polar solvents **DPAP** shows a strong emission. On the other hand, in high polar and protic solvents the rotor's ICT state is stabilized and decays primarily non-radiatively. In addition to the aforementioned trends, an increase in **DPAP** emission was observed upon increasing the solvent viscosity as a result of a decrease of rotor flexibility, which in turn favours a radiative deactivation process. More recently, amorphous aggregation-induced emission (AIE) nanoparticles based on **DPAP** have been prepared and were transformed into highly emissive, rhomboidal nanocrystals using an ultrasound stimulus.[180]

Different polymers characteristics including interaction parameter, polarity etc. have already been shown as significant factors in defining the vapochromic response of the fluorophore inside the polymer matrix.[84–86,107,170,181–185] Differently, solvents with better polymer interaction influence the fluorescence behaviour of fluorophore to a significant level while as poorly interacting solvents hardly influence the fluorescence of films during exposure to VOCs.[83–86] There are still a number of physico-chemical properties and effects concerning these materials that have not been fully investigated. The influence of the polymer thickness on vapochromic behaviour of fluorescent polymer films is one such parameter that needs to be addressed. The fluorescence behaviour of the thin polymer films was investigated by shundo et al.[186] They studied the fluorescence behaviour of 6-(N-(7-nitrobenz-2-oxa-1,3-diazol-4-yl) hexanioc acid (NBD) in thin polymer films of different polarity. The fluorescence behaviour of polymer films depends on the dispersion of the dyes in the polymer. Accordingly, the unusual behaviour of fluorescence was reported in polymer films where the dye aggregates as film thickness decreases.[186] In case of better miscible dyes, surface and interfacial effects are assumed to play the considerable role.[186] Notably, the ratio of surface and interfacial areas to the total volume increases on decreasing the film thickness. Interestingly, the segmental mobility at surface is increased compared to mobility of chains in bulk.[186] Such changes in the polymer films must also influence the vapochromic behaviour of FMRs in polymer films with different thickness. Furthermore, it must be noted also that the permeation rate of solvent is also affected by the polymer film thickness and is inversely proportional to the thickness of the film. Considering this fact, the solvent is expected to

permeate easily in thinner films than the thicker polymer films. Consequently, such process must favour rapid and higher solvation the dye molecules inside the matrix resulting in fast vapochromic response than thicker films on exposure to VOCs.

Herein, we report on the emission properties of **DPAP** dispersed (0.05-0.1 wt. %) within transparent thermoplastic matrices such as poly(methyl methacrylate) (PMMA) and polycarbonate (PC) as a function of the exposure to different VOCs. The results are discussed in terms of sensitivity and reproducibility of the vapochromic response of the polymer systems.

Moreover, to validate the effect of thickness on the vapochromic response, we focused on the emission properties of a newly synthesized FMR, namely 4-(triphenylamino) phthalonitrile (**TPAP**, Figure 1b) in PC films of different thickness as a function of exposure time to different solvent vapours. **TPAP** is a highly-flexible FMR with strong polarity and viscosity sensitivity.[187] **TPAP** has an extended π-conjugated system that results in a significant distance between the electron-accepting cyano and the electron-donating amino groups, which, in turn, affects its electronic and spectroscopic features with respect to solvent polarity and viscosity. In particular, in the present study we have investigated, in some detail, the effect of the thickness on the vapochromic response of **TPAP**/PC films, in terms of both the spectral signal features and the kinetics of its response.

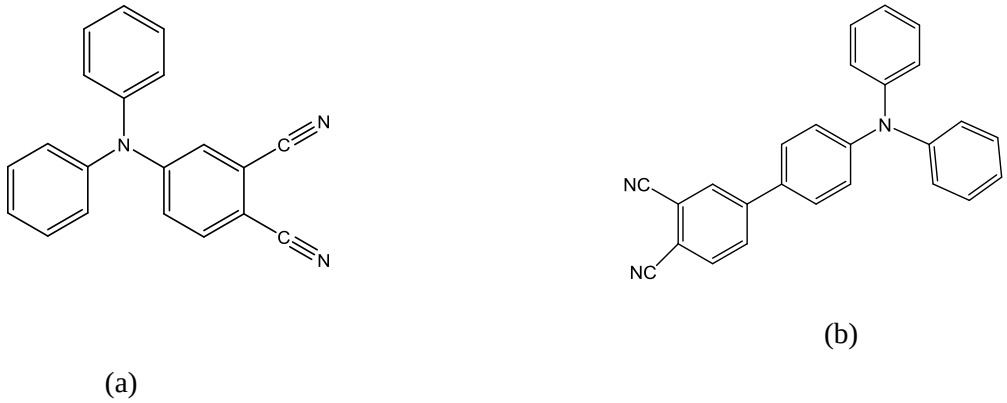

Figure 1 Molecular structure of (a) 4-(diphenylamino) phthalonitrile (**DPAP**) and (b) 4-(triphenylamino) phthalonitrile (**TPAP**).

2.2. Experiments

2.2.1. Materials and Methods

DPAP was prepared following the synthetic procedures reported in the literature.[179] **TPAP** was prepared following a standard, transition metal-catalysed cross-coupling reaction between 4-iodo-phthalonitrile and 4-boronic acid-triphenylamine.[188]

All the solvents (n-hexane, toluene, acetonitrile (CH_3CN), tetrahydrofuran (THF), chloroform ($CHCl_3$)) were purchased from Sigma-Aldrich and used as received. Poly (methyl methacrylate) (PMMA, Aldrich, Mw = 350,000 g/mol, acid number <1 mg KOH/g) and random copolymer polycarbonate-polysiloxane LEXAN® EXL 1414T (PC, SABIC, Mw = 220,000 g/mol with 1.5 wt. % Si) were used as received.

Table 1 Vapour pressure of different solvents at 20 °C,[189] polarity index,[190] PMMA-solvent Flory–Huggins interaction parameter χ,[143] and solubility parameter difference $\Delta\delta$ (for PC)[191] for utilized solvents.

solvent	vapour pressure (mm Hg)	polarity index	χ^a	$\Delta\delta$ $((cal/cm^3)^{1/2})^b$
***n*-hexane**	124	0.1	0.530 [49]	2.5
toluene	28.5	2.4	0.450	0.9
THF	142	4.0	0.494	0.7
$CHCl_3$	158.4	4.1	0.44	0.5
CH_3CN	88.8	5.1	0.500 [49]	-3

[a] for PMMA; [b] for PC;$\Delta\delta = \delta_{PC} - \delta_{solvent}$; $\delta_{PC} = 9.8\ (cal/cm^3)^{1/2}$

2.2.2. Preparation of polymer films

2.2.2.1. Preparation of DPAP Polymer films

500 mg of PMMA were dissolved in 15 mL of chloroform under stirring for 10 minutes. Then, **DPAP** (0.05 or 0.1 wt.%) was added and the resulting solution casted into clean Teflon® Petri-dishes. In this way, 90-120 μm thick films of **DPAP**/PMMA were realized after solvent evaporation. The same procedure was adopted for the preparation of **DPAP**/PC films, except that dichloromethane was used as solvent for PC and clean glass Petri-dishes for film formation.

2.2.2.2. Preparation of TPAP/PC films

500 mg of PC were dissolved in 5 mL of chloroform under stirring for 10 minutes. Then, **TPAP** (0.05 wt. %) was added and the resulting viscous solution poured into clean glass dishes. A ZUA 2000 Universal Applicator (Zehntner Testing Instruments) was used to distribute the mixture over the glass in order to obtain films of different thickness (Fig. 2a). 20-80 μm thick films were realized after complete solvent evaporation.

2.2.3. Apparatus and Methods

UV-Vis spectra of DPAP/polymer films were recorded on Perkin Elmer Lambda 650 at room temperature. Fluorescence spectra ($\lambda_{exc.}$=325 nm) of both **DPAP** and TPAP in polymer films were measured on a Horiba Jobin-Yvon Fluorolog®-3 spectrofluorometer at room temperature in the dark by using the F-3000 Fibre Optic Mount apparatus coupled with optical fibre bundles. Light generated from the excitation spectrometer is directly focused to the dye/polymer film using an optical fibre bundles. Emission from the sample is then directed back through the bundle into the collection port of the sample compartment.

The vapochromic response of the **DPAP**/polymer films was tested by exposing a 2×2 cm dye/polymer film attached to an aluminium foil covering a 50 mL closed container (Fig. 2b)[84] to 20 mL of five organic solvents of different polarity at ambient temperature (20 °C) and atmospheric pressure, namely *n*-hexane, toluene, THF, $CHCl_3$, and CH_3CN, with similar conditions for each experiment. The experiments were collected after solvent saturation was reached. The concentration of about 10^4 ppm for toluene and 10^5 ppm for the other solvents were estimated taking into consideration their vapour pressures listed in Table 1.

TPAP/polymer films were also exposed to organic solvents of different polarities, namely, *n*-hexane, THF, $CHCl_3$, and CH_3CN, under similar conditions.

Microscopy images and lifetime measurements were collected by using a Leica TCS SP5 SMD inverted confocal microscope (Leica Microsystems AG, Wetzlar, Germany) equipped with an external pulsed diode laser (PicoQuant GmbH, Berlin, Germany) for excitation at 405 nm. The laser repetition rate was set to be 40 MHz. Each of the image sizes were 512×512 pixels and acquired with a scan speed of 400 Hz (lines per second). The pinhole aperture was set at 1.00 Airy. **DPAP**/polymer films fixed on microscope glass slides were viewed with a

100 × 1.3 NA oil immersion objective (Leica Microsystems). The images were collected using low excitation power at the sample (10-20 µW). Emissions were monitored in the 430-490 nm range by acoustic-optical tuneable beam splitter (AOBS) based built in detectors. Acquisition lasted until about 100-200 photons per pixel were collected, at photon counting rates of 100-500 kHz. Emission lifetime images (FLIM) of the **DPAP**/polymer were elaborated using Picoquant Symphotime software for FLIM analysis.

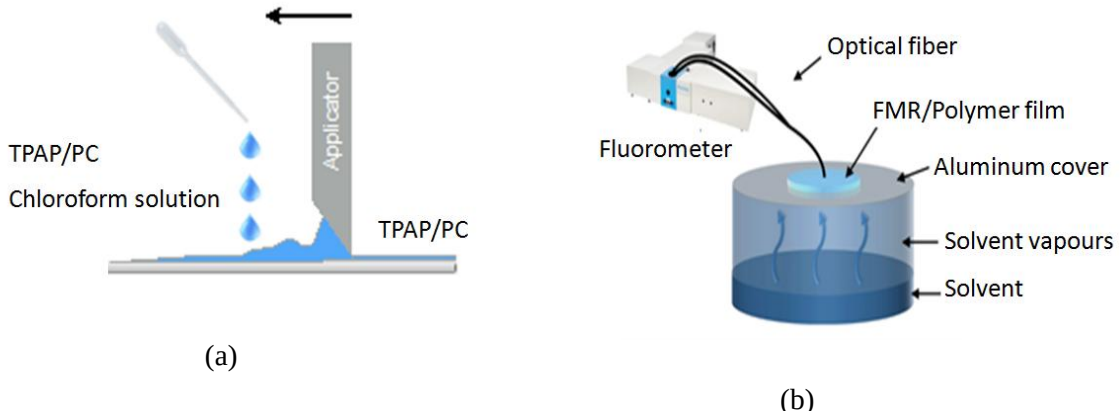

(a) (b)

Figure 2 (a) Schematic representation of **TPAP**/PC film preparation and (b) setup used to study the vapochromic behaviour of both **DPAP** and **TPAP** in polymer films.

Differential scanning calorimetry (DSC) was carried out under nitrogen atmosphere by using a Mettler DSC 30 instrument. Samples of 10–20 mg were heated from 40 to 300 °C at 10 °C/min. Melting enthalpies were evaluated from the integrated areas of melting peaks by using indium for calibration. PC crystalline content (f_c) was evaluated from the measured melting enthalpy (ΔH_m) taking into account the melting enthalpy of the perfect PC crystal ΔH^0_m =132 J/g[192] using the equation 1:

$$f_c = \frac{\Delta H_m}{\Delta H_m^0}.100 \qquad (1)$$

2.3. Results and Discussion

The solvatochromism of **DPAP** in various solvents has been fully described in previous study by some of us.[179] In the following the main results are summarized. **DPAP** shows a solvent-insensitive absorption with a broad band maximizing at around 325 nm.[179] On the other hand, **DPAP** emission is strongly solvatochromic, showing a red–shift of up to 120 nm when increasing the solvent polarity from cyclohexane ($\lambda_{em.}$ = 430 nm), to o-xylene ($\lambda_{em.}$ = 470 nm), to THF ($\lambda_{em.}$ = 505 nm), and to acetonitrile ($\lambda_{em.}$ = 550 nm). Beside such exceptional

sensitivity toward solvent polarity, **DPAP** displays a noteworthy response to viscosity.[179] In this respect, hampering **DPAP** intramolecular rotation upon increasing the viscosity of the medium prompts an increase of the rotor fluorescence intensity.

2.3.1. Spectroscopic characterization of DPAP/polymer films

DPAP was dispersed at different concentrations (0.05–0.1 wt. %) in poly(methyl methacrylate) (PMMA) and polycarbonate (PC) films by film casting. These concentrations were selected to realize polymer films with emission intensities that are not impacted by spurious effects stemming from high rotor concentration such as aggregation, self-quenching, self-absorption, etc. The **DPAP**/polymer films have a thickness of 90-120 μm, appear homogeneous, and have absorption features similar to those previously reported for **DPAP** in organic solvents (Figure 3)

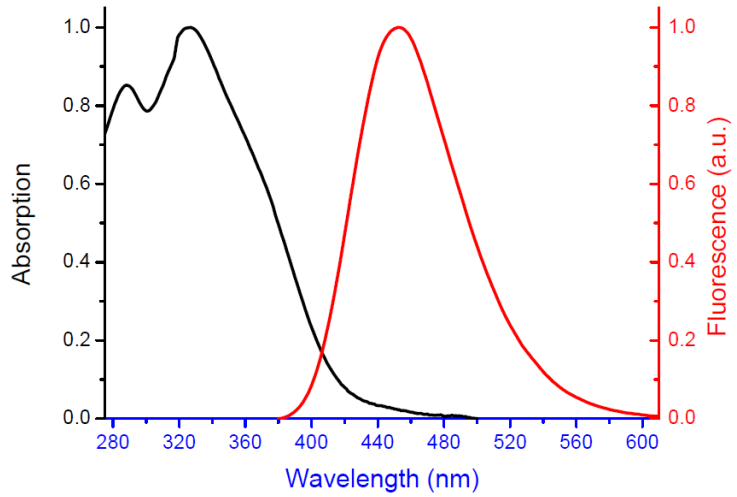

Figure 3 Absorption (black) and emission (red) spectra of 0.05 wt. % DPAP/PMMA ($\lambda_{exc.}$ = 325 nm).

PMMA and PC are amorphous polymers with glass transition temperatures of about 100–110 and 150 °C, respectively. Moreover, they only gave rise to residual emission upon 325 nm photoexcitation. DPAP was dispersed in PMMA and PC glassy matrices, in which the rotor intramolecular rotation is strongly hampered. Under such conditions, the radiative decay of DPAP is expected to dominate its photophysics. Recently, Iasilli *et al*. demonstrated that when tetraphenylethylene (TPE) is dispersed in a glassy polystyrene (PS) matrix, the reduced intramolecular rotation result in strong emission of the dye, whereas the emission is significantly weakened when viscous but not glassy polymer matrices are used.[170] In line with

these assumptions, both DPAP/polymer films gave rise to a similar bright blue-green emission characterized with maxima at about 450 nm (Fig. 4).

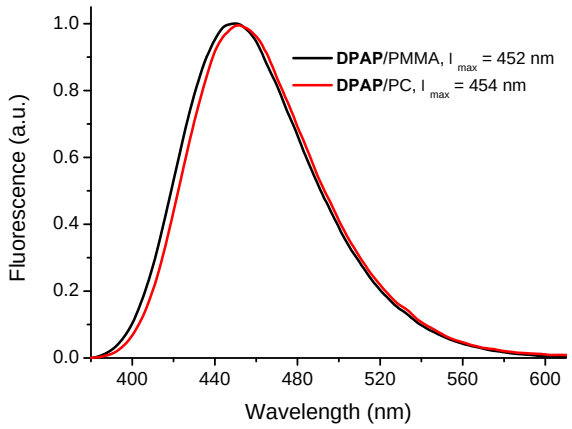

Figure 4 Fluorescence emission spectra of 0.05 wt. % DPAP/PMMA and DPAP/PC films ($\lambda_{exc.}$ = 325 nm).

Emission spectra of both films are almost identical with only a 2 nm difference in their maxima probably due to the similar dielectric constant of PMMA and PC (2.8 and 2.9, respectively). Likewise, the emission lifetimes of these DPAP/polymer films determined upon excitation at 297 or 403 nm were also similar, with values of 12.7 (PMMA) and 12.1 ns (PC) (Fig. 5) compare well with DPAP solutions in solvents such as CH_2Cl_2 or *o*-xylene.[179]

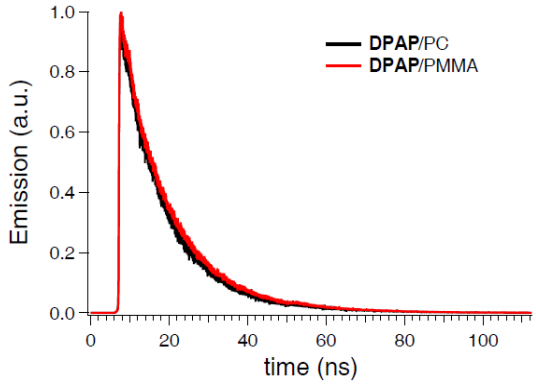

Figure 5 Fluorescence lifetime of **DPAP**/Polymer films ($\lambda_{exc.}$=403nm)

2.3.2. Effect of VOC exposure on the optical emission of DPAP/PMMA films

The DPAP/PMMA films were exposed to solvents with different vapour pressure, polarity index and Flory–Huggins interaction parameter (χ) (Table 1). It is worth noting that χ is small in the case of effective solvent/polymer interactions. Owing to the fact that the solvent uptake is likely to affect the polymer matrix viscosity and polarity, a vapochromic effect was expected to play an appreciable role.

The emission spectra of **DPAP**/PMMA films exposed to *n*-hexane, that is, the least polar and interacting solvent with PMMA, are reported in Fig. 6. In particular, no changes in the film emission – neither in intensity nor in position were noted even after 38 min. exposure to solvent vapours.

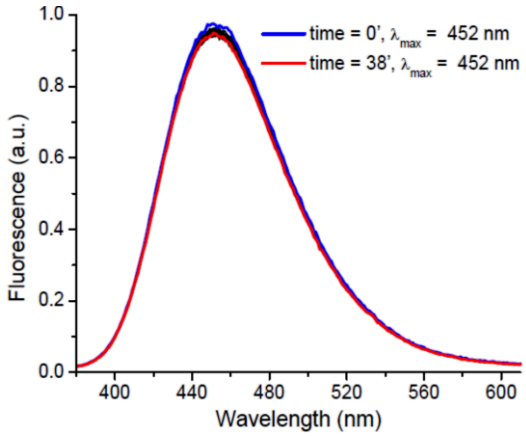

Figure 6 Emission spectra of 0.05 wt.% **DPAP**/PMMA film as a function of the exposure of *n*-hexane vapours ($\lambda_{exc.}$=325nm). The spectra were collected for 38 min with a time interval of 1min.

In stark contrast to the aforementioned case, the **DPAP**/PMMA emission was strongly impacted upon exposure to more polar and PMMA-interacting VOCs. The progressive change in the emission of **DPAP**/PMMA films exposed to toluene and THF vapours is shown in Fig. 7.

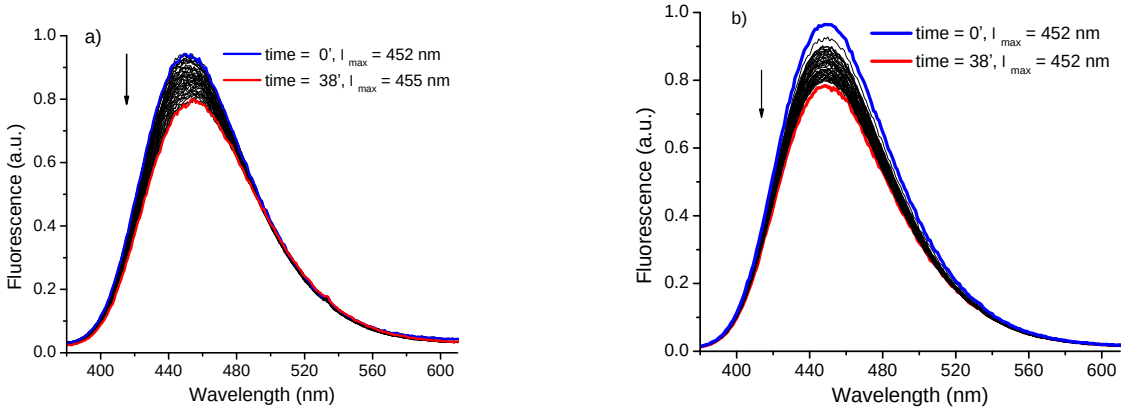

Figure 7 Progressive changes in the fluorescence emission of 0.05 wt.% DPAP/PMMA films as a function of exposure to (a) toluene and (b) THF vapours (λ_{exc} = 325 nm). The spectra were collected for 38 min. with a time interval of 1 min.

In both cases, the decrease in the **DPAP**/PMMA emission is mainly ascribed to the viscosity sensitivity of **DPAP** with increasing solvent uptake by the polymer matrix. Note that in the glassy state the PMMA matrix is characterized by a large fraction of free volume. The latter comes in the form of channels and cavities reaching molecular dimensions. Considering that solvent vapour fills these empty spaces, diffusion and swelling of the polymer starts from the outer surface layers inwards. In turn, an overall decrease of the local microviscosity evolves.[112] This phenomenon leads to a partial increase of **DPAP** mobility, which, in turn, favours its non-radiative deactivation.

A more evident change in the emission is observed for **DPAP**/PMMA films exposed to either CH_3CN or $CHCl_3$ vapours (Fig. 8), solvents which present a favourable combination of polarity index and χ parameter (Table 1). When vapours of CH_3CN and $CHCl_3$ penetrate into the polymer films, their emission intensity dropped reaching a minimum after 5 min. of vapour exposure. From there on, the emission remained unchanged. On the other hand, for CH_3CN and $CHCl_3$ a red–shifted emission is observed (28 and 49 nm, respectively). Interestingly, despite having the higher polarity index, CH_3CN displays a lower red-shift than $CHCl_3$. This finding can be rationalized considering that the magnitude of the red-shift in the DPAP-doped films emission upon solvent vapour exposure is the result of a subtle interplay between solvent polarity (*vide supra*)[179] and solvent/polymer interactions.

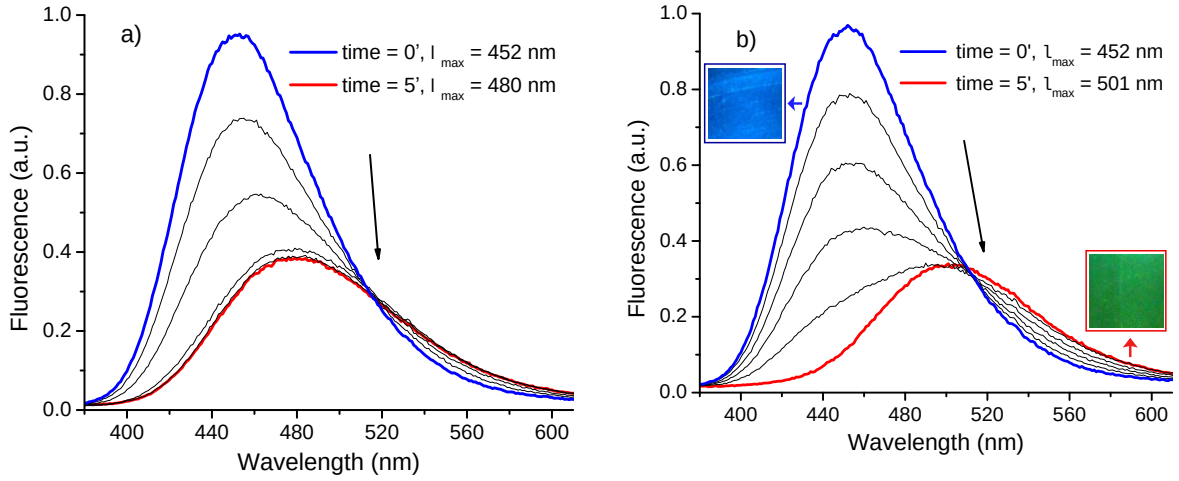

Figure 8 Progressive changes in the fluorescence emission of 0.05 wt.% **DPAP**/PMMA films as a function of exposure to (a) CH_3CN and (b) $CHCl_3$ (λ_{exc} = 325 nm) and (inset) pictures of the same film with the exposure time of $CHCl_3$ vapours taken under the illumination at 366 nm. The spectra were collected for 5 min. with a time interval of 1 min.

The solvent permeation into the film appears crucial for establishing the response time of the film. Similar findings have been recently reported for PMMA films doped with solvatochromic dyes. The vapochromic response resulted substantially delayed when methanol, the weakest interacting solvent with the matrix, or its mixture with dichloromethane, was utilised.[84] By contrast, vapour pressure appears unable to play an effective role in the phenomenon selectivity.

In Fig. 9, the relative emission variations of **DPAP**/PMMA films as a function of solvent vapours exposure time indicate that the largest and fastest vapochromic response occurs for films that are exposed to VOCs featuring high polarity and strong chemical interactions with the polymer matrix such as $CHCl_3$ and CH_3CN.

These results suggest that the selectivity of DPAP/PMMA films is determined by the chemical affinity of PMMA for the solvent vapours and by the solvent polarity. More specifically, solvents with χ values lower than 0.45 and polarity indices higher than 4 interact well with the PMMA matrix, thus providing the vapochromic behaviour.

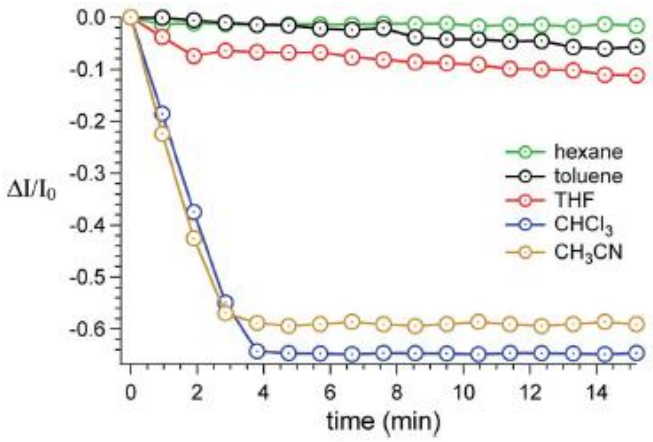

Figure 9 Relative fluorescence intensity variation of peak maximum ($\Delta I/I_0$) of 0.05 wt. % DPAP/PMMA films as a function of exposure time to different VOCs (λ_{exc} = 325 nm).

The kinetics of the vapochromic phenomenon was also affected by the DPAP concentration within the doped films. When 0.1 wt. % DPAP/PMMA films were exposed to $CHCl_3$, the minimum emission intensity was reached after a 16 min. exposure (Fig. 10a), as compared to 5 min. at lower rotor concentration. Fig. 10b documents that the vapochromism of DPAP/PMMA films is completely reversible. After desorption of $CHCl_3$ from the DPAP/PMMA films, the original emission is reinstalled and a second cycle of solvent exposure resulted in the same change in emission as observed during the first cycle. A similar reversible behaviour was observed for CH_3CN (data not shown).

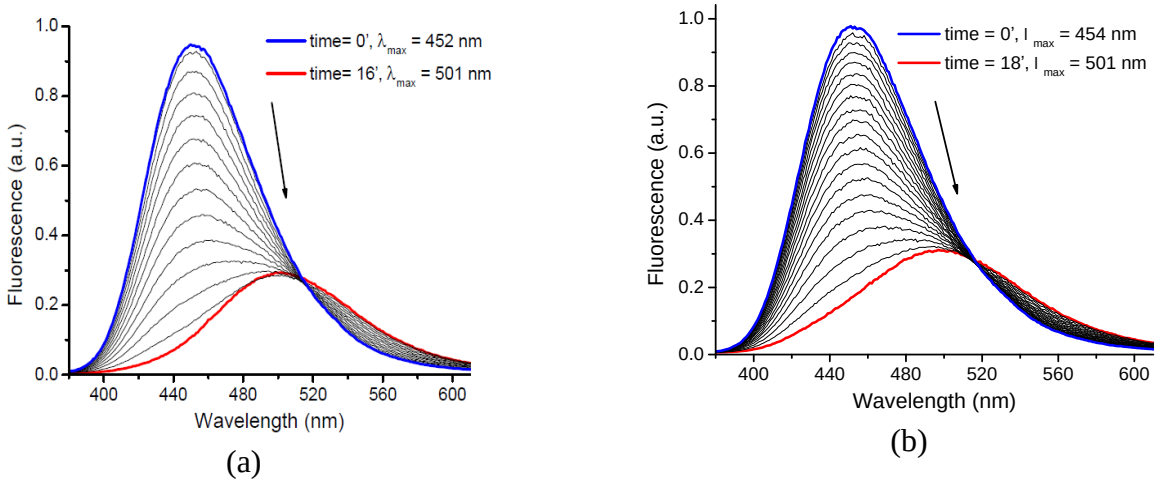

Figure 10 (a) Progressive changes in the fluorescence of 0.1wt.% **DPAP**/PMMA as a function of exposure to (a) $CHCl_3$ vapours and (b) second cycle of $CHCl_3$ vapours .($\lambda_{exc.}$=325nm). The spectra were collected for 16 and 18 min. respectively with a time interval of 1 min.

2.3.3. Effects of VOC exposure on the optical emission of DPAP/PC films

Considering that the Flory–Huggins interaction parameter, χ, is unavailable for some solvent/PC combinations, we used a semi-empirical relationship to predict solvent/PC interactions, which takes into account the solubility parameter difference Δδ, that is, the measure of the attractive strength between molecules of the material.[191] Notably, the Δδ (Δδ = δ_{PC} - $\delta_{solvent}$) is small for effective solvent/PC interactions (Table 1).

In Fig. 11 (a), the emission spectra of DPAP/PC films upon exposure to n-hexane as a function of time are presented. Similar to DPAP/PMMA, DPAP/PC films revealed no appreciable alterations in terms of their emission maximum and intensity even after 38 min. of solvent exposure.

When CH_3CN is used, the emission of the DPAP/PC films experiences a significant quenching and red-shift (25 nm), similar to the DPAP/PMMA (Fig. 11b).

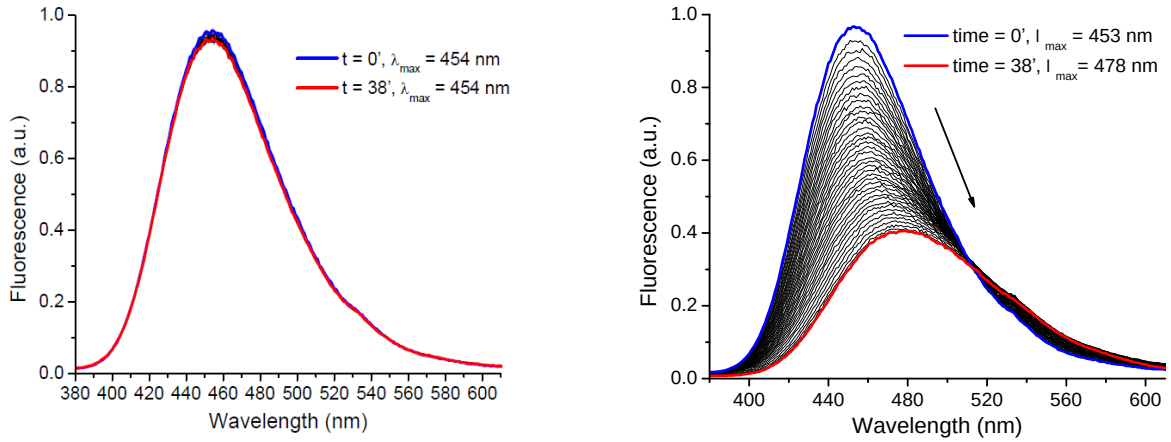

Figure 11 (a) Progressive changes in the emission of 0.05 wt. % DPAP/PC films as a function of exposure to (a) n-hexane vapours and (b) CH_3CN vapours ($\lambda_{exc.}$ = 325 nm). The spectra were collected for 38 min. with a time interval of 1 min.

An even more intriguing vapochromic response was noticed when highly PC–interacting solvents such as toluene, THF, and $CHCl_3$ were used (Fig. 12).

Toluene, THF, and $CHCl_3$ are an inception to rather unexpected emission behaviour. Following an initial drop in DPAP/PC emission intensity at short solvent vapours exposure times, a marked fluorescence enhancement combined with a red-shift was observed. To this

end, emission intensities recorded after 38 min. revealed an increase going from toluene to THF and $CHCl_3$. This trend is in accordance with the solubility parameter differences of these solvents.

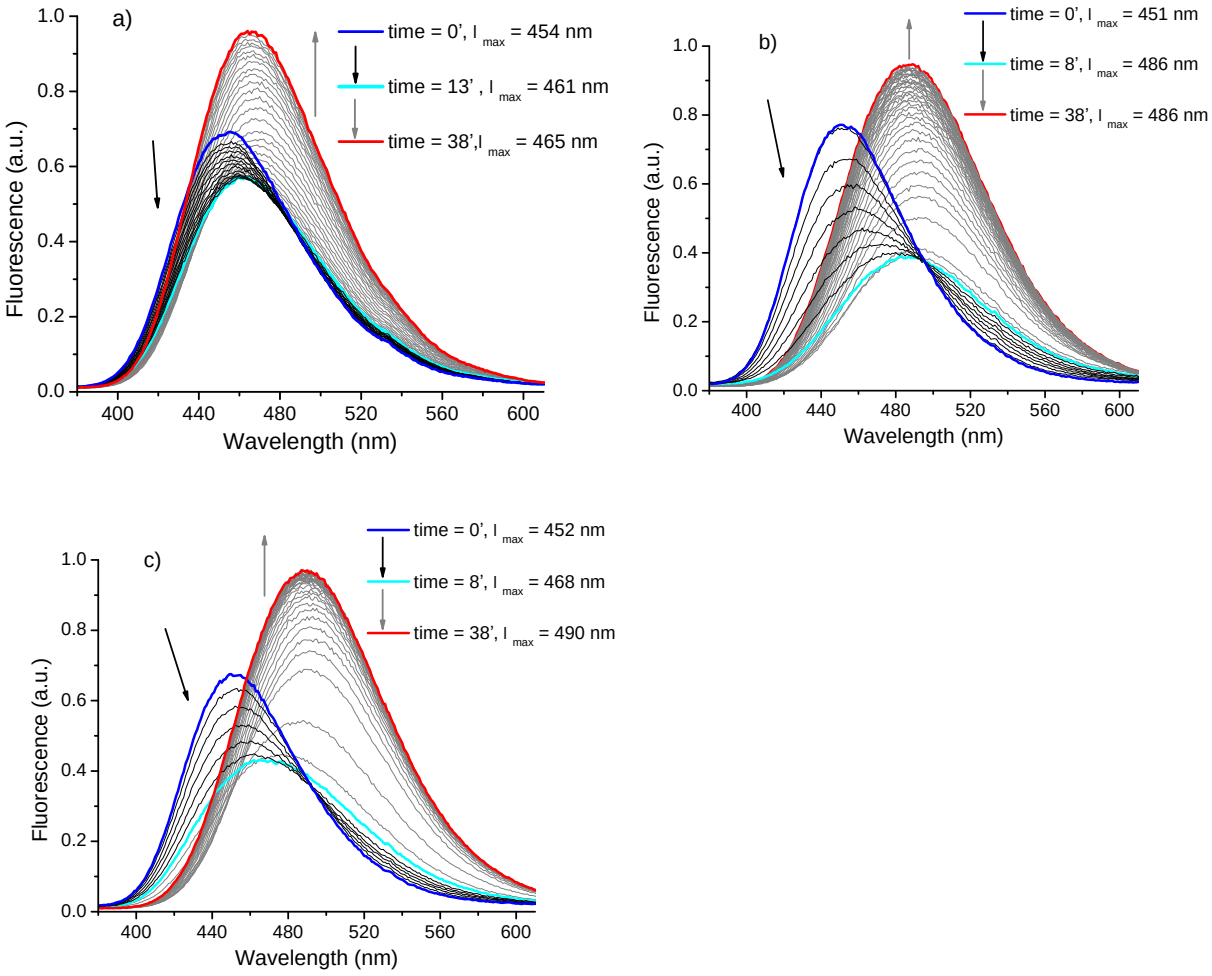

Figure 12 Progressive changes in the emission of 0.05 wt.% **DPAP**/PC films as a function of exposure to (a) toluene, (b) THF, and (c) $CHCl_3$ vapours (λ_{exc} = 325 nm).The spectra were collected for 38 min. with a time interval of 1 min.

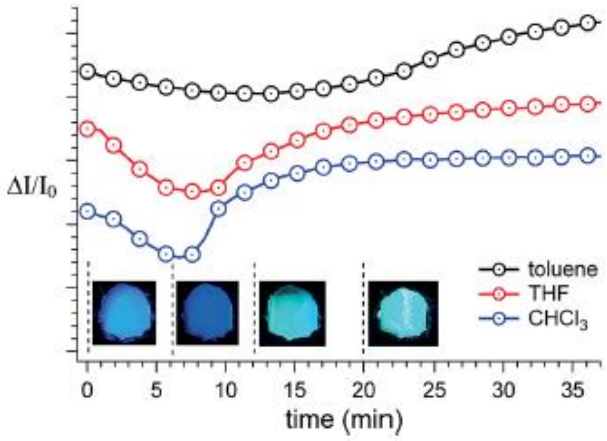

Figure 12 Relative fluorescence intensity variation of peak maximum ($\Delta I/I_0$) of the 0.05 wt.% **DPAP**/PC films as a function of the exposure time to toluene, THF and $CHCl_3$ vapors ($\lambda_{exc.}$ = 325 nm). Pictures of the same **DPAP**/PC film at 0, 6, 12 and 20 min. (from left to right) of exposure time to $CHCl_3$ vapors. The pictures were taken under the illumination at 366 nm.

Notably, the aforementioned emission enhancement occurred already after 7-8 min. of $CHCl_3$ exposure, whereas it appeared slower for THF (9-10 min.) and toluene (13-14 min.) (Fig.13)

Interestingly, the emission red-shift maximizes for **DPAP**/PC films exposed to $CHCl_3$ vapours (38 nm) which, compared to toluene and THF, is the solvent with the higher polarity index and lower PC-solubility parameter difference $\Delta\delta$. Such changes in the **DPAP**/PC film emission could be visualized by naked-eye (Fig. 13). On the other hand, the smaller emission red-shift (11 nm) was observed for films exposed to toluene, which has the lower polarity index and the higher $\Delta\delta$ value.

Inspection of the **DPAP**/PC films immediately after $CHCl_3$ exposure under visible light revealed an evident change of film morphology (Fig. 14a). In the area exposed to $CHCl_3$, the films gave rise to clear whitening combined with an evident embrittlement. These morphological changes are accompanied by a strong modification of the emitted light of the film from blue to intense green. Next, emission imaging studies were carried out investigating the morphology of **DPAP**/PC films before (Fig. 14b) and after (Fig. 14c) $CHCl_3$ exposure. In particular, the films were subjected to solvent vapours for 38 min. and analysed by means of confocal scanning laser fluorescence microscopy using a laser source at 405 nm and an emission in the 430–490 nm range.

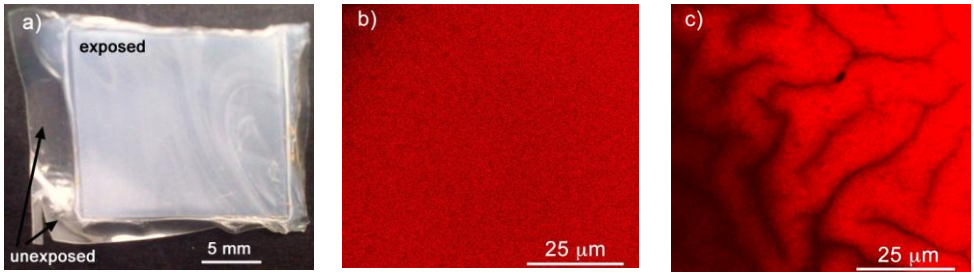

Figure 14 (a) Digital picture of 0.05 wt.% **DPAP**/PC film immediately after exposure to $CHCl_3$ vapours for 38 min. under visible light. Confocal microscope images of **DPAP**/PC films with emission collection in the 430–490 nm range (b) before and (c) after exposure to $CHCl_3$ vapours for 38 min. In this latter case, after the $CHCl_3$ vapour exposure, the **DPAP**/PC film was placed at room temperature and atmospheric pressure for 40 min. allowing the desorption of the trapped solvent molecules from the polymeric matrix. Note that the emission images are in pseudocolors.

Prior to solvent exposure, the film surface appears smooth and homogeneous. After solvent exposure, the area of the film placed in contact with $CHCl_3$ revealed a strong modification of its texture, the appearance of numerous surface cracks, and a significant increase in the emission.

The effect of the solvent desorption on the emission properties of the $CHCl_3$-exposed **DPAP**/PC films was also investigated. In this case, the original **DPAP**/PC emission maximum was almost completely recovered upon solvent desorption (458 nm (Fig. 15a, red spectrum) versus 452 nm (Fig. 15a, green spectrum) for $CHCl_3$–exposed and pristine **DPAP**/PC films, respectively). In other words, when $CHCl_3$ starts to desorb from the doped matrix, the film emission is accordingly shifted to lower wavelengths in line with the different effective polarity of PC and $CHCl_3$. However, to our surprise, after $CHCl_3$ desorption **DPAP**/PC films showed a fluorescence intensity that was much higher than that of the pristine film before solvent exposure (Fig. 15a, red spectrum).

The second cycle of $CHCl_3$ exposure showed a similar trend to the first cycle, that is, a film fluorescence emission drop flanked by a red-shift of the emission maximum, but without the marked fluorescence enhancement (Fig. 15b). Similar results were also registered when using toluene (data not shown) and THF (Fig. 16), highly interacting VOCs for PC.

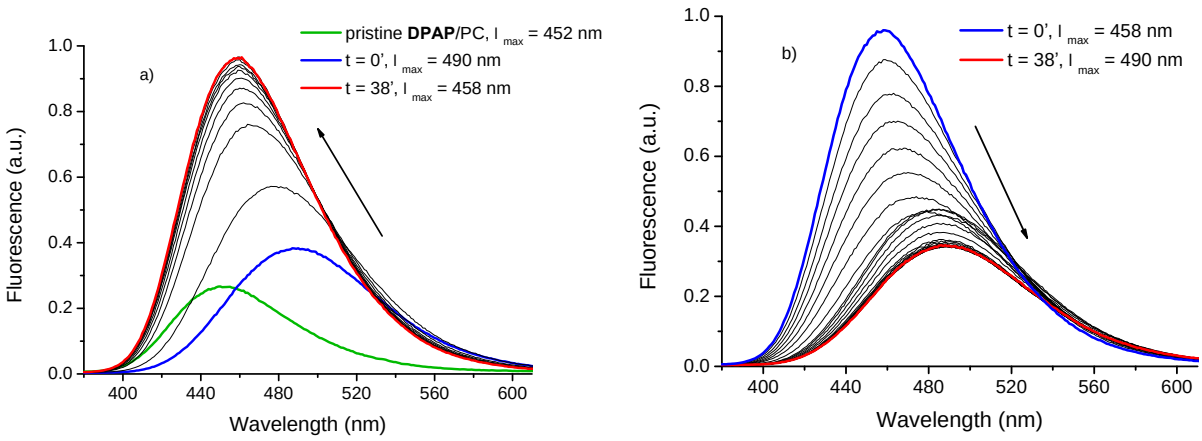

Figure 15 Progressive changes in the emission of $CHCl_3$−exposed 0.05 wt.% **DPAP**/PC films (after equilibration in the presence of the same solvent vapours) as a function of (a) $CHCl_3$ desorption of a $CHCl_3$−exposed **DPAP**/PC film after equilibration in the presence of the same solvent vapors. The emission spectrum of the pristine **DPAP**/PC film is shown in green. (b) Second cycle exposure to $CHCl_3$ vapors (λ_{exc} = 325 nm). In both experiments the spectra were collected for 38 min. with a time interval of 1 min.

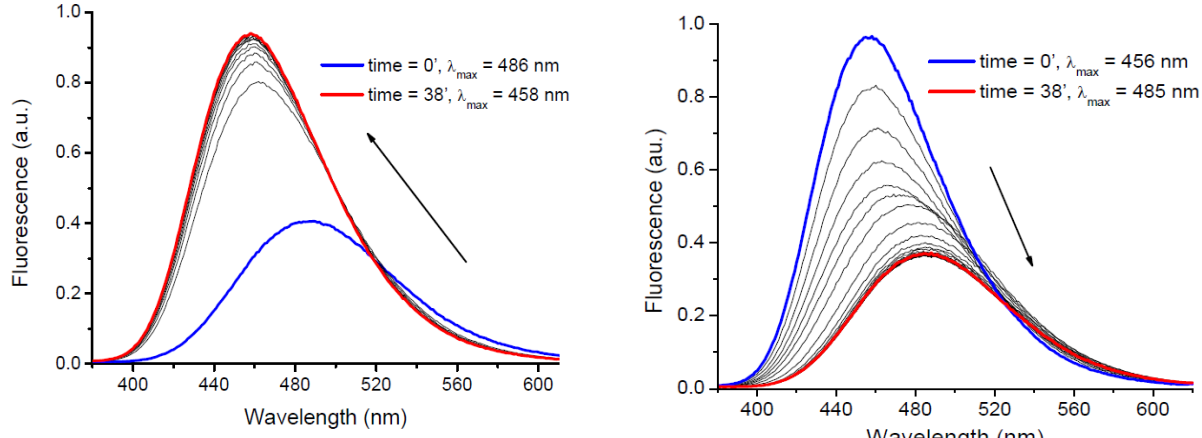

Figure 16 Progressive changes in the emission of THF−exposed 0.05 wt.% **DPAP**/PC films (after equilibration in the presence of the same solvent vapors) as a function of (a) THF desorption of a THF−exposed **DPAP**/PC film after equilibration in the presence of the same solvent vapors and (b) second cycle exposure to THF vapors (λ_{exc} = 325 nm).

We hypothesize that the phenomenon associated with the emission increase of the **DPAP**/PC films noted during the first $CHCl_3$ exposure cycle could be related to changes in the internal flexibility of **DPAP** triggered by some irreversible solvent-induced modification of the PC matrix at the molecular level. More specifically, an increase of the viscosity of the solvent-exposed PC matrix is expected to occur which could lead to an increase in the rotor fluorescence intensity. Changes with respect to the appearances of **DPAP**/PC films upon

solvent exposure, that is, from transparent to opaque, suggest crystallization of the polymeric matrix. Crystallization, in turn, is likely to hamper the internal motion of **DPAP** present in the PC phase.

To validate our hypothesis, we probed the thermal properties of **DPAP**/PC films before and after $CHCl_3$ exposure by comparing their first heating DSC scans (Fig. 17).

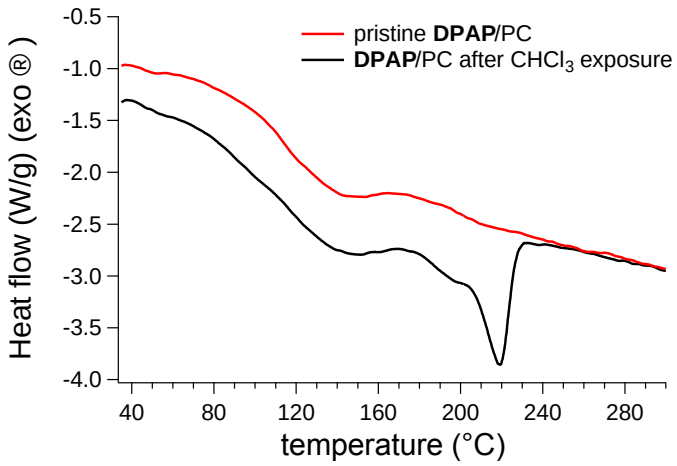

Figure 17 First heating DSC scans of pristine (red trace) and $CHCl_3$-treated (black trace) 0.05 wt. % **DPAP**/PC films. The $CHCl_3$-treated films were prepared exposing the **DPAP**/PC films to $CHCl_3$ vapours for 40 min. and the resulting films let to stand at room temperature and atmospheric pressure for 40 min. in order to eliminate solvent molecules trapped in the polymeric matrix.

During the first heating scan both pristine and $CHCl_3$-exposed films displayed a glass transition temperature (T_g) at around 150 °C. However, in contrast to the pristine **DPAP**/PC films which may be regarded essentially as amorphous materials, the solvent-exposed system showed a strong endothermic peak at around 220 °C which supports the existence of a crystalline phase.

The crystallization of PC is of considerable interest and has been investigated as found in the literature.[192] PC features poor crystallization because of its rigid macromolecular chains. Attempts have been made to induce crystallization of PC by exposure to organic solvents in the vapour or liquid state.[160,163,193] Under these conditions, the crystallization rate was strongly enhanced due to the role of the absorbed solvent as plasticizers. As such, their presence increases the mobility of polymer segments and, thus, enables crystallization to occur even at room temperature. The crystallinity (f_c) of PC, as a function of $CHCl_3$ or THF exposure was calculated using Eq. 1 (see experimental part) and is reported in Table 2.

Table 2 0.05 wt. % DPAP/PC crystallinity (f_c) as a function of CH_3CN, $CHCl_3$ and THF vapour exposure time.

Sample	solvent	time (min)	f_c (%)
DPAP/PC	-	-	0
DPAP/PC	CH_3CN	30	~0
DPAP/PC	THF	30	7.15
DPAP/PC	$CHCl_3$	10	2.00
DPAP/PC	$CHCl_3$	30	9.38

After 10 min. of exposure to $CHCl_3$, **DPAP**/PC films exhibited only 2% of crystallinity, which increased and plateaued at 9% with increasing the vapour exposure time up to 30 min. This suggests that small changes in the PC crystallinity do not affect significantly the viscosity of the doped PC matrix as documented by the decrease in the rotor emission intensity in the film, which is mainly related to the polarity of the environment. On the other hand, at longer vapour exposure a higher degree of crystallinity is reached, which in turn induces an increased viscosity in the matrix and an enhancement in **DPAP** emission intensity. Additionally, the impact of THF on both the emission and crystallinity of the rotor-doped films was smaller than with $CHCl_3$, which is in agreement with its higher solubility parameter difference $\Delta\delta$ (Table 1). Prolonged exposure to VOCs for longer than 38 min. did not cause detectable variations of both the emission response and phase behaviour of the PC matrix.

Compared to PMMA, the selectivity of **DPAP**/PC films is more determined by the chemical affinity of PC for the solvent vapours since acetonitrile, the most polar solvent, is not able to induce polymer crystallization.

Interestingly, **DPAP** emission studies in mixtures of *o*-xylene and silicone oil 500, whose polarity is comparable with that of PC, corroborate the findings made with **DPAP**/PC films. With increasing solvent viscosity, that is, increasing the content of silicone oil in the mixtures, a similar emission enhancement evolved (Fig. 18a). Changing the viscosity resulted, however, in no appreciable changes of the 12.5 ns emission lifetimes (Fig. 18b). Both trends are in good agreement with the results gathered for the **DPAP**/PC films. Note that **DPAP**/PC films before and after THF exposure reveal the same lifetimes of around 12.1 ns (Fig. 18c). This substantiates the hypothesis of a hindered mobility of **DPAP** when going from amorphous to crystalline PC.

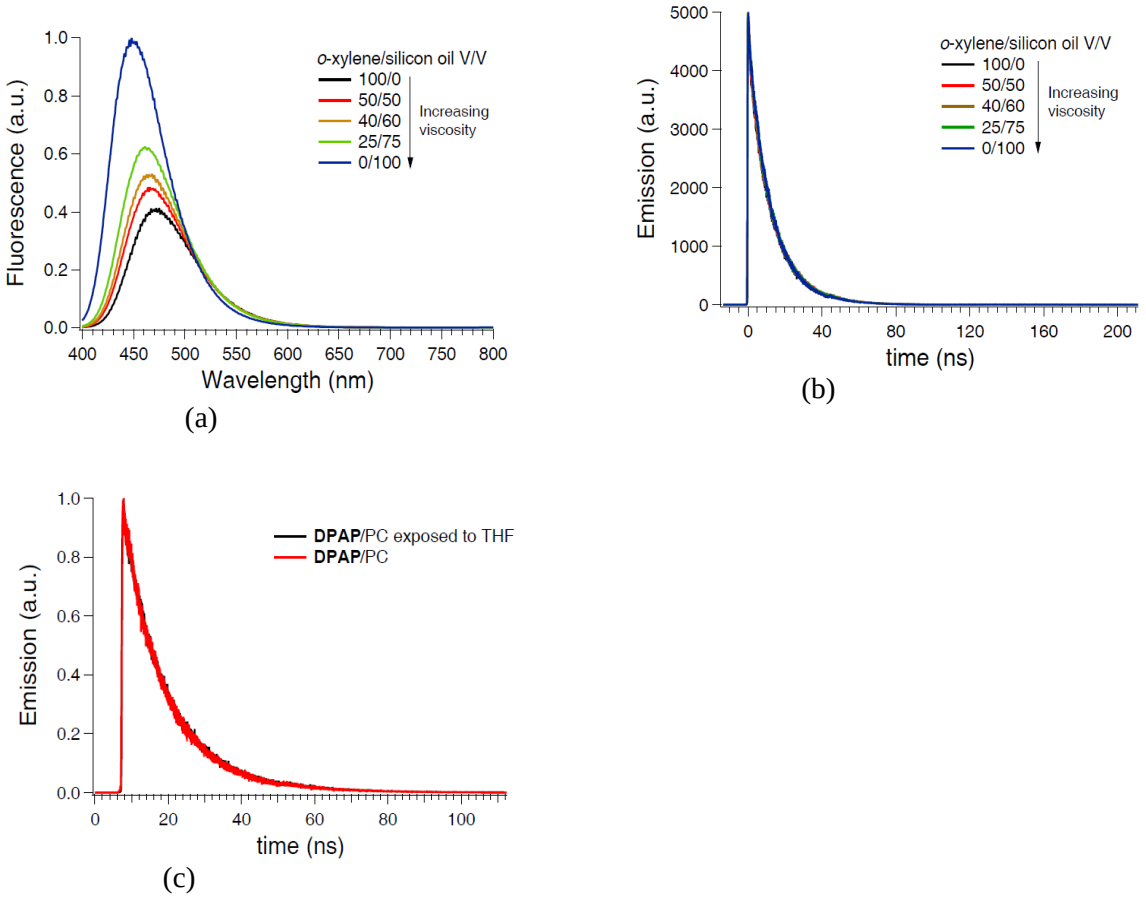

Figure 18 (a) Fluorescence of DPAP in mixtures of *o*-xylene/silicon oil of different fractions ($\lambda_{exc.}$=328nm). Fluorescence lifetime profile of (b) DPAP mixtures of *o*-xylene/silicon oil and (c) DPAP/PC films before and after exposure to THF ($\lambda_{exc.}$=403nm). The solvent was allowed to desorb from the film under room temperature and pressure.

2.4. Effect of polymer thickness on the vapochromic behaviour of TPAP/PC films

TPAP is a FMR showing a solvent-insensitive absorption and a noteworthy fluorescence sensitivity to viscosity.[187] The intramolecular charge transfer (ICT) character in TPAP is favoured by the amino electron donor and electron accepting nitrile moieties.[180] From the quantum mechanical (QM) calculations, it was shown that nitrogen atom is coplanar in the optimized structure of TPAP. The phenyl groups assume propeller shaped configuration due to the steric hindrance.[180] Contrary, the rotation of 1,2-dicyanobenzene unit is allowed

by the small energetic barrier as calculated from QM calculations. Furthermore, it was also shown that **TPAP** is able to form stable fluorescent nanoparticles with enhanced aggregation induced emission properties.[180] The spectral properties of TPAP display two absorption bands in each solvent at 390 and 285nm. The emission spectra in different polar solvents clearly supported the solvatochromic nature of molecular rotor with a Stokes shift of about 200nm in strongly polar solvents.[180]

As a result, by hampering the **TPAP** intramolecular rotations through a highly viscous medium, enhanced fluorescence intensity is generally obtained. As reported, in the film preparation, **TPAP** was dispersed in PC films at a concentration of 0.05 wt. %.
Highly homogeneous **TPAP**/PC films with controlled thickness of 80 μm were prepared. Note that PC is an amorphous polymer, characterized by a glass transition temperature (Tg) of about 150 °C, in which the **TPAP** intramolecular rotations are strongly hampered. Under such conditions, the radiative decay of **TPAP** is expected to dominate its photophysics. In line with these assumptions, **TPAP**/PC films gave rise to a bright blue emission characterized by a single unstructured broad band peaked at about 450 nm (Figure 20) with an emission lifetime of 4.2 ns (Figure 19).

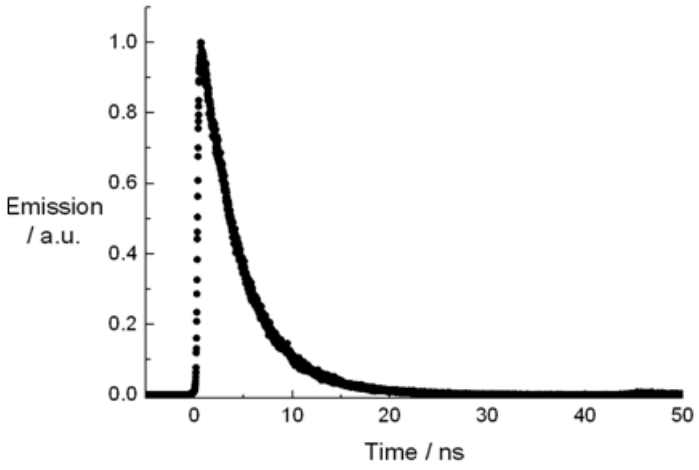

Figure 19 Fluorescence lifetime profiles of 60 μm thick 0.05 wt. % **TPAP**/PC films (λ_{exc} = 403 nm).

The **TPAP**/PC films were exposed to solvents with different vapour pressure and polarity index. We used a semi-empirical relationship to predict solvent/PC interactions, which takes into account the solubility parameter difference Δδ, that is, the measure of the attractive strength between molecules of the material.[191] Notably, the Δδ ($\Delta\delta = \delta_{PC} - \delta_{solvent}$) is small for effective solvent/PC interactions (Table 1).

2.4.1. Effects of VOC exposure on the optical emission of TPAP/PC films

In Figure 20a, the emission spectra of **TPAP**/PC films upon exposure to *n*-hexane vapours as a function of time are presented. No appreciable alterations in terms of their emission maximum and intensity even after 25 min. of solvent exposure are observed, being *n*-hexane the least polar and interacting solvent with PC.

A more evident change in the emission is observed for TPAP/PC films exposed to CH_3CN (Figure 20b), a solvent with the highest polarity index (Table 1). The emission of the TPAP/PC film experiences a significant quenching and red-shift (34 nm). Note that in the glassy state the PC matrix is characterized by a large fraction of free volume, generally in the form of channels and cavities reaching molecular dimensions. Considering that solvent vapours may fill up such empty spaces, diffusion and swelling of the polymer starts from the outer surface layers inwards. As a consequence, an overall decrease of the local microviscosity evolves.[112] This phenomenon leads to an increase of TPAP mobility, which, in turn, favours its non-radiative deactivation from the non-emissive TICT state. Moreover, a red–shifted emission of more than 30 nm is observed due the polar nature of CH_3CN.[194]

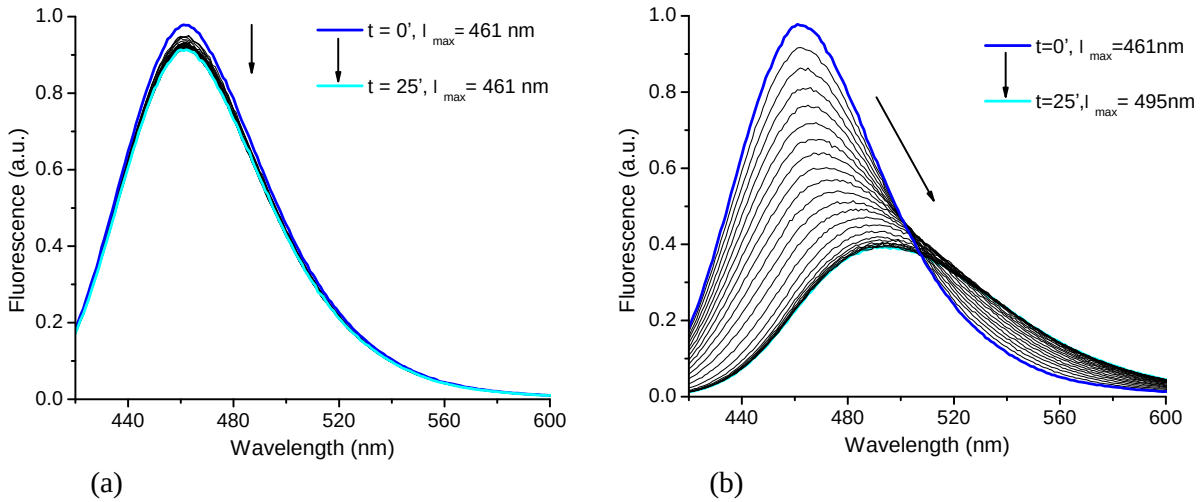

Figure 20 Progressive changes in the emission of 0.05 wt. % **TPAP**/PC films as a function of exposure to (a) *n*-hexane vapours and (b) CH_3CN ($\lambda_{exc.}$ = 325 nm). The spectra were collected for 25 min with a time interval of 1 min.

A striking vapochromic response was recorded when THF and $CHCl_3$ were used as solvents (Fig. 21), i.e. solvents which present a favourable combination of polarity index and $\Delta\delta$

parameter (Table 2). During the first 10 min, the decrease in the **TPAP**/PC emission is mainly ascribed to the viscosity sensitivity of **TPAP** with increasing solvent uptake by the PC matrix. After the initial drop in **TPAP**/PC emission intensity, a marked fluorescence enhancement was observed in both cases (Figure 21). Both fluorescence intensity variations and wavelength shifts appear slightly more pronounced when the **TPAP**/PC film is exposed to THF vapours, notwithstanding the similar polarity index and $\Delta\delta$ parameter of THF and $CHCl_3$.

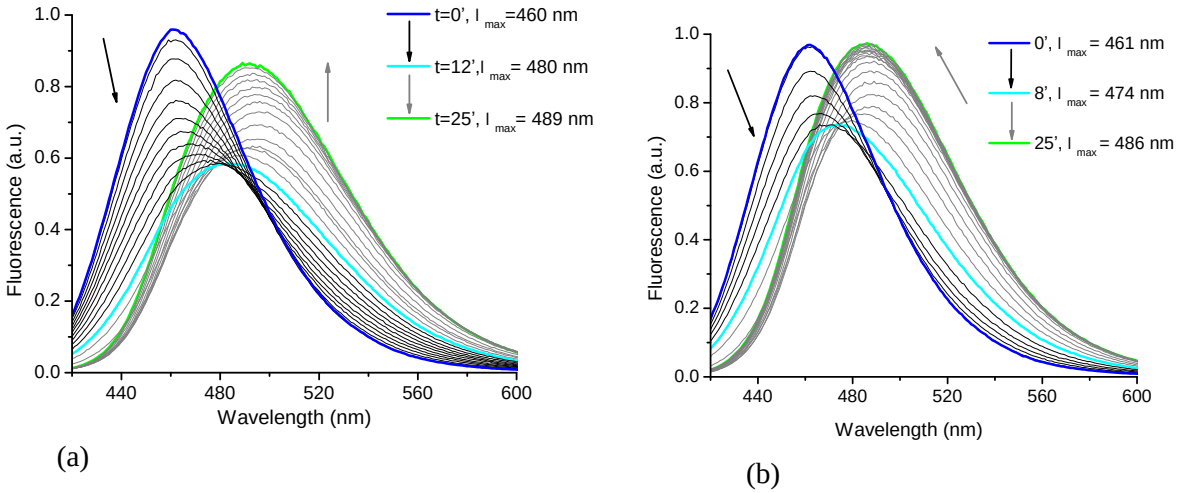

Figure 21 Progressive changes in the emission of 0.05 wt. % **TPAP**/PC films as a function of exposure to (a) THF and (b) $CHCl_3$ vapours ($\lambda_{exc.}$ = 325 nm). The spectra were collected for 25 min with a time interval of 1 min.

It was reported that the exposure of PC to strongly interacting organic solvents ($\Delta\delta$ = 0.7 for THF and 0.5 for $CHCl_3$) in the vapour or liquid state effectively enhances the polymer crystallization rate due to the role of the absorbed solvents as plasticizers.[160,163,193] As a result of the solvent uptake, the mobility of the polymeric segments increases, triggering the crystallization of the polymer that can occur at room temperature under such conditions. This crystallization process due to THF and $CHCl_3$ exposures reduces the flexibility of the polymer-embedded **TPAP**, hampering its internal motions and, in turn, enhancing its radiative decay process.

Emission imaging studies were carried out investigating the morphology of **TPAP**/PC films before (Figure 22a) and after (Figure 22b) $CHCl_3$ exposure. In particular, the films were subjected to $CHCl_3$ vapours for 25 min and analysed by means of confocal scanning laser fluorescence microscopy using a laser source at 405 nm and an emission in the 430–490 nm range. Before $CHCl_3$ exposure, the film surface appeared smooth and homogeneous (Figure

22a). Conversely, after solvent exposure, the area of the film placed in contact with $CHCl_3$ vapours revealed a strong modification of its texture with the formation of micro-sized granules, in agreement with the polymer crystallization process in the plastic film (Figure 22b).[162]

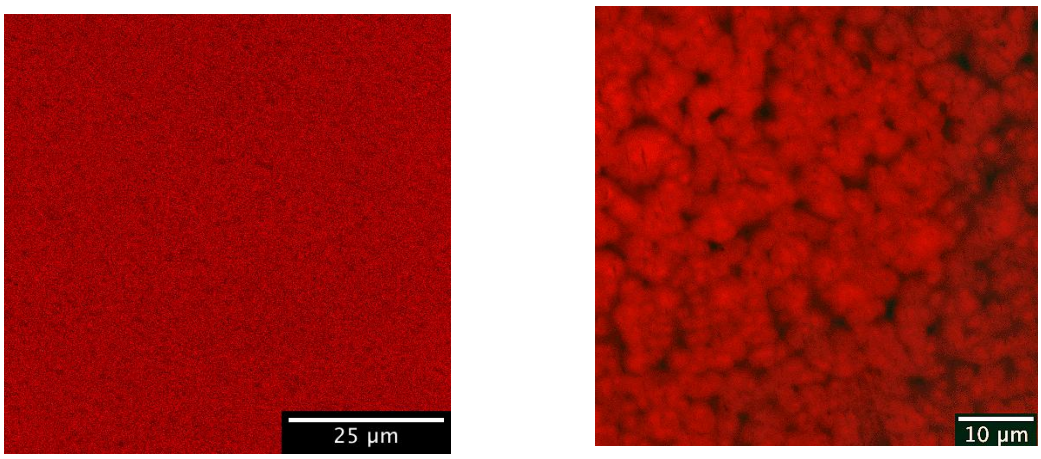

(a) (b)

Figure 22 Confocal microscope images of 60 µm thick TPAP/PC films with emission collection in the 430–490 nm range (a) before and (b) after exposure to $CHCl_3$ vapours for 25 min. In this latter case, after the $CHCl_3$ vapour exposure, the TPAP/PC film was placed at room temperature and atmospheric pressure for 40 min. allowing the desorption of the trapped solvent molecules from the polymeric matrix. Note that the emission images are in pseudocolors.

Upon solvent desorption of the **TPAP**/PC films, a second and a third cycle of THF and $CHCl_3$ exposure were also carried out. Fluorescence studies on these films showed a similar trend in the fluorescence variation to the one observed for the first cycle, that is, a film fluorescence emission drop flanked by a red-shift of the emission maximum. However, in this case, and differently from the first cycle, no fluorescence enhancement was observed increasing the exposure to the solvent vapours (Figure 23). From these results we can conclude that the expected kinetically-irreversible crystallization process occurring in the **TPAP**/PC films can be considered mostly completed after the first 25 min of $CHCl_3$ exposure.[17]

In order to give an insight into the nature of the investigated phenomenon, the effect of film thickness on the vapochromic behaviour of **TPAP**/PC films was investigated. Following the procedure described in the preceding section, highly homogeneous **TPAP**/PC films with different and controlled thickness in the range between 20 and 60 µm were prepared. $CHCl_3$

was selected as the solvent due to the most favourable Δδ parameter. The emission spectra of **TPAP**/PC films exposed to $CHCl_3$ vapours are reported in Figure 24 as a function of exposure time. Four different film thicknesses were considered, namely 20 µm, 25 µm, 40 µm and 60 µm.

In all cases, the **TPAP**/PC fluorescence was observed to change upon solvent exposure. During the first 5 min, the decrease in the **TPAP**/PC emission is mainly ascribed to the viscosity sensitivity of **TPAP** with increasing $CHCl_3$ uptake by the polymer matrix. It is worth noticing that the increase in film thickness strongly affects the extent of emission variation within the first 5 min of $CHCl_3$ exposure. More specifically, **TPAP**/PC films with lower thickness give rise to higher fluorescence variation within the same time interval, as a result of a more complete sorption process with respect to thicker films.

Interestingly, the extent of fluorescence recovery of **TPAP**/PC films, i.e. the difference between the emission intensity at t = 25 min and that at t = 5 min, appeared influenced by film thickness. More specifically, thinner films presented smaller fluorescence variations with respect to thicker films, possibly due to differences in the solvent-induced crystallization process.

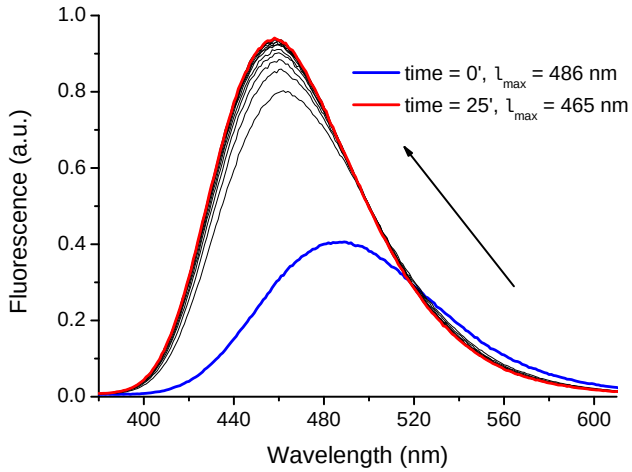

Figure 23 Progressive changes in the emission of a $CHCl_3$–exposed 0.05 wt.% TPAP/PC film (after its equilibration in the presence of $CHCl_3$ vapors) as a function of $CHCl_3$ desorption (λ_{exc} = 325 nm). TPAP/PC film thickness = 80 µm. The spectra were collected for 25 min with a time interval of 1 min and normalized at the emission maximum after 25 min of exposure.

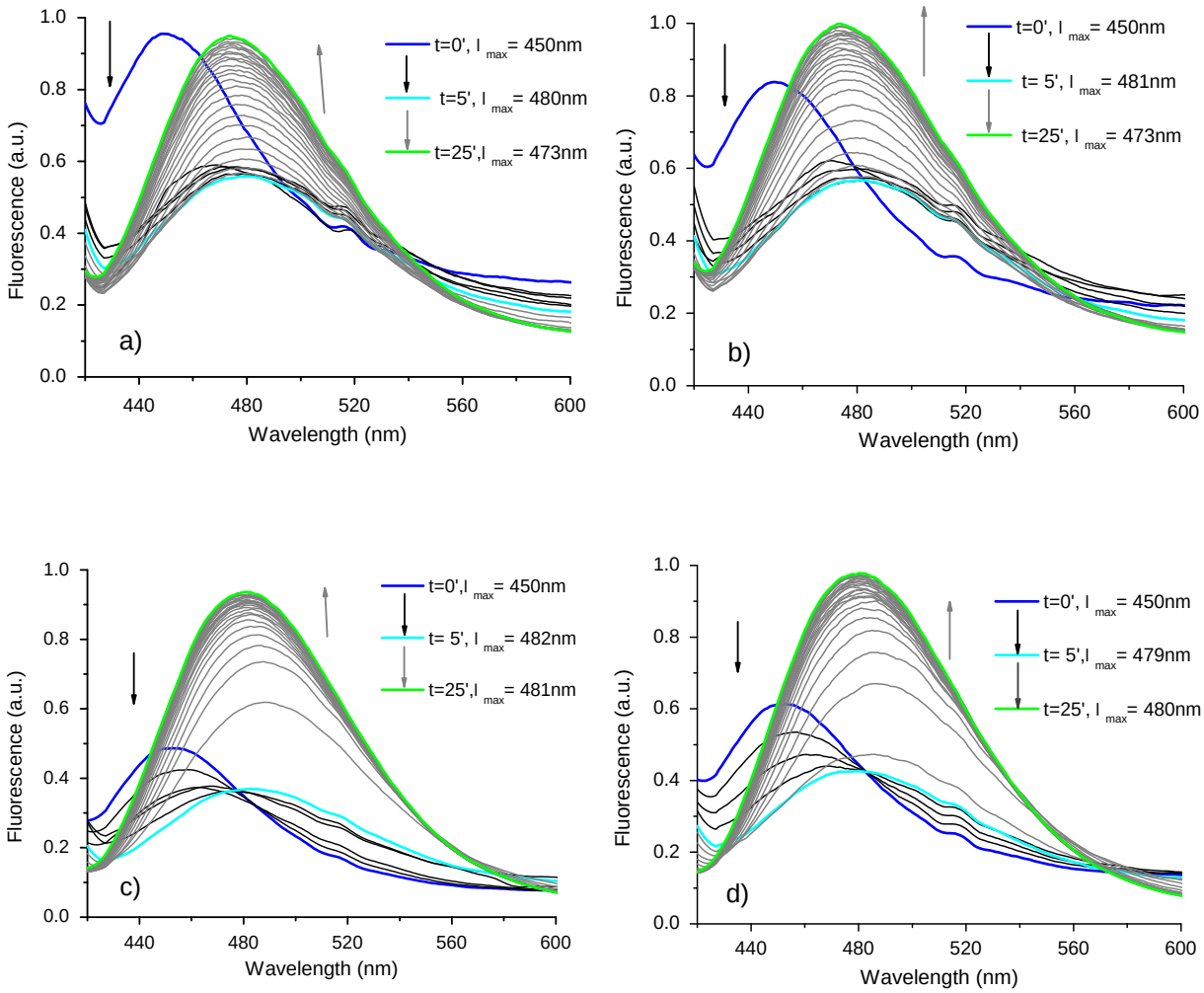

Figure 24 Emission of 0.05 wt. % TPAP/PC films as a function of exposure time to $CHCl_3$ vapours (λ_{exc} = 325 nm). PC film thickness: a) 20 µm; b) 25 µm; c) 40 µm; d) 60 µm. The spectra were collected during 25 min with a time interval of 1 min and normalized at the emission maximum after 25 min of exposure. All the spectra were normalized to the emission maxima.

Notably, **TPAP**/PC films with 20-25 µm thickness showed at the end of the vapour exposure (t = 25 min) an emission wavelength about 7-8 nm blue-shifted with respect to their thicker counterparts. This phenomenon could be also explained in terms of the faster $CHCl_3$ desorption occurring in thin films, leading to an overall lower polarity of the material.

Optical inspection of the **TPAP**/PC films immediately after $CHCl_3$ exposure under near-UV light (366 nm) revealed a clear change of the fluorescence from blue to green (Figure 8), thus allowing the detection of the vapochromic response with a naked eye. Notably, the **TPAP**/PC film with higher thickness (60 µm, figure 25b, against 20 µm, figure 25a) possibly revealed a more evident vapochromic response with the emission variation from blue to green.

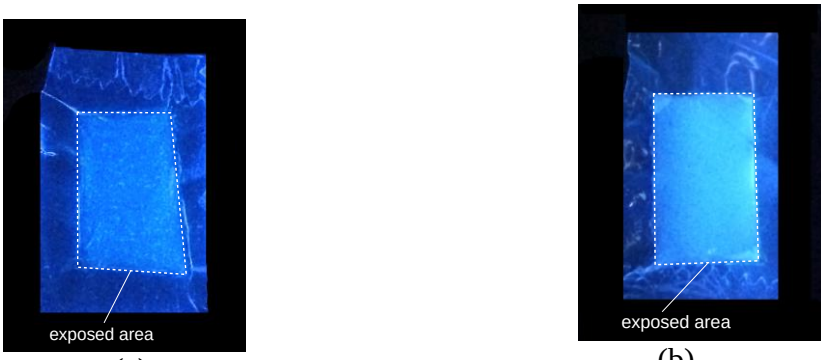

(a) (b)

Figure 25 (a) Picture of **TPAP**/PC films (about 1 x 2 cm) with a thickness of (a) 20 µm and (b) 60 µm after 25 min of exposure to $CHCl_3$ vapours. The picture was taken under the illumination at 366 nm. Films areas exposed and unexposed to the $CHCl_3$ vapours are clearly distinguishable.

These findings can be related to the differences in emission intensity and frequency, as observed by spectroscopic investigations, comparing the spectra of **TPAP**/PC films with thickness of 20 µm and 60 µm (Figures 23a and 23d, respectively).

2.4.2. Differential Scanning Calorimetry (DSC) of TPAP/PC films

To further validate our findings, we eventually probed the thermal properties of **TPAP**/PC films at variable thickness, before and after $CHCl_3$ exposure, by comparing their first heating DSC scans (Figure 26). During the first heating scan, both pristine and $CHCl_3$-exposed films displayed a T_g at around 150 °C. However, in contrast to the pristine **TPAP**/PC films which may be regarded essentially as amorphous materials, the solvent-exposed system displayed the progressive formation of endothermic peaks from 140 up to 240 °C with two main signals at around 185 °C and 220 °C which support the co-existence of a crystalline phase, as similarly observed after acetone exposure of PC-based samples.[160] After cooling, during the second heating scan, all the samples appeared as completely amorphous showing only the T_g at around 150 °C (Figure 26).

It is worth noticing that upon $CHCl_3$ exposure, the crystallinity of TPAP/PC films progressively increases upon increasing the film thickness (Figure 27 and Table 3). This result can be related to the fact that in thinner TPAP/PC films the diffusion of $CHCl_3$ into the amorphous polymer is nearly complete before the crystallization process is completed. Furthermore, as crystallization proceeds, solvent is rejected from the crystalline regions of the

polymer, thus limiting the crystallization process.[159]

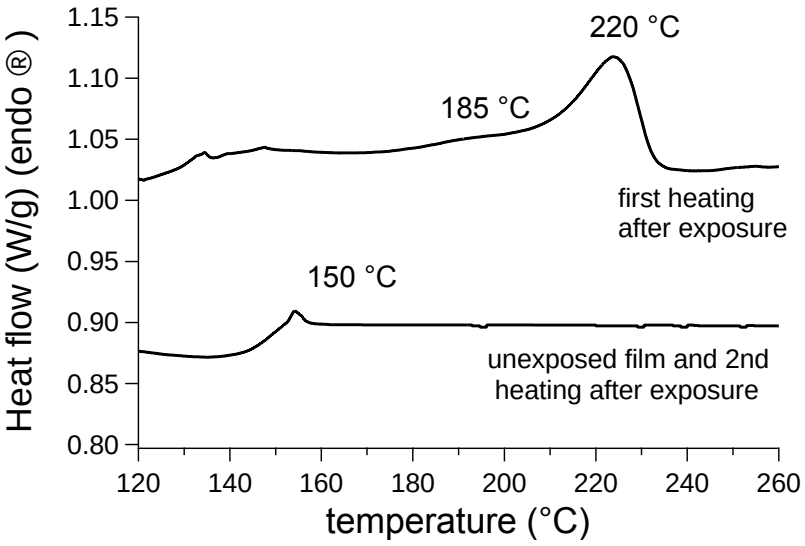

Figure 26 DSC scans of pristine and $CHCl_3$-treated 60 µm thick (both first and second heating) 0.05 wt. % **TPAP**/PC films.

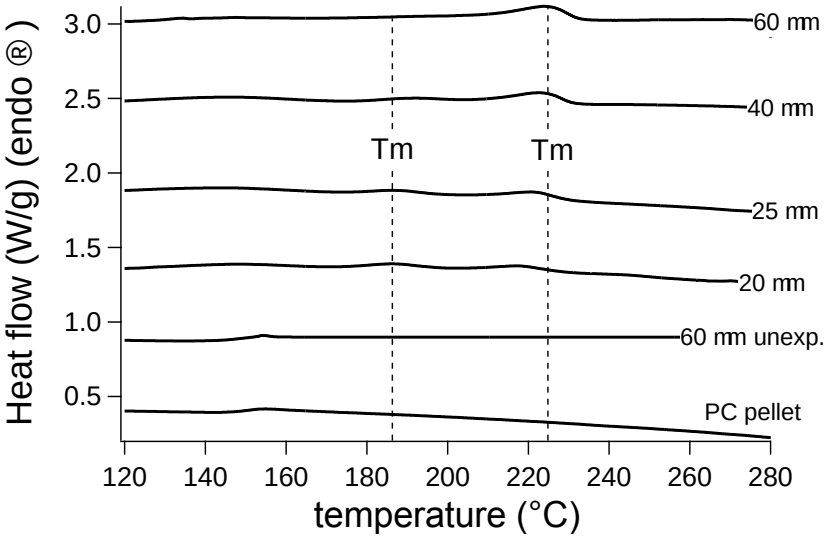

Figure 27.First heating DSC scans of pristine PC pellet and 0.05 wt. % **TPAP**/PC films with different thickness. The $CHCl_3$-treated films were prepared exposing the **TPAP**/PC films to $CHCl_3$ vapours for 25 min and the resulting films let to stand at room temperature and atmospheric pressure for 1 hour in order to eliminate solvent molecules trapped in the polymeric matrix.

Table 3 Crystallinity (f_c) calculated for PC pellet and **TPAP**/PC films with different thickness unexposed or exposed for 25 min to $CHCl_3$ vapours

Sample	f_c (%)
PC pellet[a]	0
60 μm TPAP/PC film[a]	0
20 μm TPAP/PC film[b]	5.70
25 μm TPAP/PC film[b]	6.30
40 μm TPAP/PC film[b]	7.40
60 μm TPAP/PC film[b]	8.80

[a] unexposed, [b] exposed to $CHCl_3$ vapours

In Figure 28, the crystallinity content in PC films with different thickness is compared with the fluorescence intensity variation $(I-I_0)/I_0$, where I and I_0 are the fluorescence intensities after 25 min. and 5 min. of $CHCl_3$ exposure, respectively. As expected, the fluorescence increase does agree quite well with the PC film crystalline content, suggesting that the vapochromic response is governed by morphology variations in the PC film bulk.

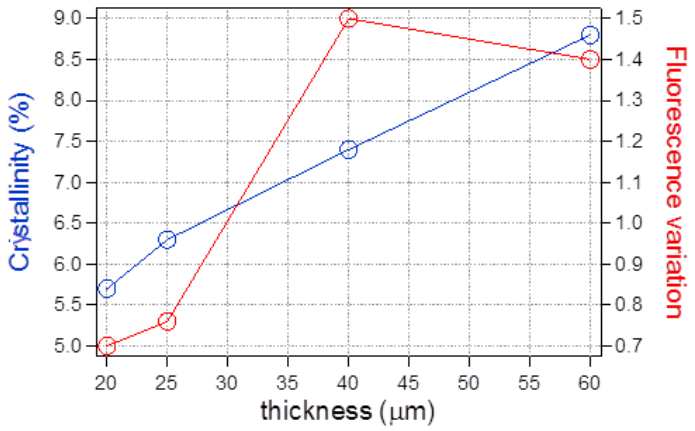

Figure 28 Crystallinity (blue circles) and fluorescence intensity variation (red circles) of $CHCl_3$-exposed **TPAP**/PC films with different thickness.

Conversely, the apparent slight decrease in the fluorescence of the thickest PC film (60 μm) is likely due to the micro-phase separation of **TPAP** molecules which occurs in the PC bulk during the crystallization process. Indeed, such a phenomenon can adversely affect the homogeneous fluorescence response of the macroscopic film.

2.5. Conclusions

We have demonstrated that a FMR, namely **DPAP**, characterized by high sensitivity toward solvent polarity and viscosity, once embedded into plastic materials, confers new vapochromic characteristics to the resulting films.

DPAP exhibits viscosity- and polarity-dependent emission properties when dispersed at low loadings (<0.1 wt. %) in PMMA plastic films and exposed to saturated atmospheres of polar and well-interacting VOCs. These films showed a significant decrease and red-shift of their emission due to solvent-induced changes in the local polarity and viscosity of the medium. On the contrary, the film emission remained unaffected when low polar and barely interacting VOCs were tested. The overall vapochromic response of these **DPAP**/polymer films was even more marked when PC was used. In this case, an initial solvent-induced red-shift and decrease in emission, as observed for the PMMA-based systems, was accompanied by a further red-shift and increase in the film fluorescence intensity at longer solvent-exposure time. This effect is attributed to a polymer crystallization process in the plastic films upon solvent uptake, which provokes a general increase in the viscosity of the matrix. This process reduces the flexibility of the embedded **DPAP**, hampering its internal motions and, in turn, enhancing its radiative decay process.

In light of this peculiar response, **DPAP**-enriched plastic films respond to vapours of different organic solvents, providing a reproducible emission signal even after several successive cycles of vapour exposure. Solvent permeation into the film is crucial in establishing the response time of the film.

We have also demonstrated that a recently synthesised FMR, namely **TPAP**, characterized by a high sensitivity toward solvent polarity and viscosity, once embedded into PC films of different thickness, confers interesting vapochromic features to the resulting films. In particular, **TPAP** exhibits viscosity- and polarity-dependent emission properties when dispersed at low loadings (0.05 wt.%) in PC plastic films and exposed to a saturated atmosphere of VOCs, such as CH_3CN, THF and $CHCl_3$, which present a favourable combination of polarity index and solubility parameter difference $\Delta\delta$. The obtained dye-enriched films showed a decrease and red-shift of emission due to solvent-induced changes in the local polarity and viscosity of the polymeric matrix. Moreover, for THF and $CHCl_3$ as solvents, the optical response was accompanied by an increase in the film fluorescence intensity at longer solvent-exposure time. This effect is attributed to a PC crystallization

process in the plastic films upon solvent uptake, which causes a significant increase in the matrix viscosity. This process reduces the flexibility of the embedded **TPAP**, specifically hampering the intramolecular rotational motions and, in turn, enhancing the radiative decay pathway. Notably, the vapochromic behaviour of such films was strongly influenced by the film thickness. More specifically, the increase in film thickness strongly affects the extent of emission variation within the first 5 min of $CHCl_3$ exposure. **TPAP**/PC films with smaller thickness resulted in higher fluorescence variation within the same time interval, possibly due to a more complete sorption process with respect to thicker films. On the other hand, thicker films determined the largest fluorescence intensity variation during the second stage of solvent exposure, allowing more defined vapochromic behaviour with colour emission changes from blue to green. This effect is attributed to a more complete crystallization process occurring in thicker films.

The results of this work were published in (a) Journal of Material Chemistry C, **2014**, 2, 9224-9232 and (b) Polymer Advanced Technologies, **2016**, 27, 429-435

Chapter 3

3. Solvatochromic Probe for the Selective Detection of Volatile Organic Solvents (VOCs)

3.1. Introduction

Nowadays, chromogenic fluorescent (fluorogenic) materials are highly desirable since their optical properties in emission are well sensitive to different external stimuli such as viscosity and polarity of the environment.[115,137,195] This feature has been explored for many classes of fluorogenic polymers triggered by potential applications in the field of chemical optical indicators and polymer sensors.[87,95,127,196,197] The fluorogenic polymer films can easily detect the presence of well-interacting volatile organic compounds (VOCs) such as chloroform and toluene. Nevertheless, even if the explored vapochromism resulted very promising for applications in thin film as accessible optical indicators, the concomitant responses towards viscosity and polarity variations like those reported in Chapter 1 should be averted in certain applications since they might compromise device sensitivity and selectivity. Selectivity is indeed one of the major issues that optical indicators and colorimetric sensors to VOCs are facing today.[198] Notably, the selective identification of aromatic or chlorinated VOCs is extremely important since they have adverse effects on human health.[4] Inspired by previous results on vapochromism, in the present study we focus attention on the solvatochromic features of the 3-[2-(4-nitrophenyl) ethenyl]-1-(2-ethylhexyl)-2-methylindole (NPEMI-E) (Fig. 1). NPEMI-E has been already studied by our group[199,200] for the preparation of stable indole-derived glass blends having very high photorefractive gain. Notably, the presence of asymmetric 2-ethylhexyl group on the nitrogen atom of indole ring hinders the crystallization and aggregation of the molecule, while the electron-withdrawing nitro group in conjugation with the indole ring serves to promote the intramolecular charge transfer (ICT) behaviour upon excitation.

Publication
M. Ahmad, I. Platonova, A. Battisti, P. Minei, G. Brancato and A. Pucci, Journal of Polymer Science Part B: Polymer Physics, **2017** in press: DOI: 10.1002/polb.24367

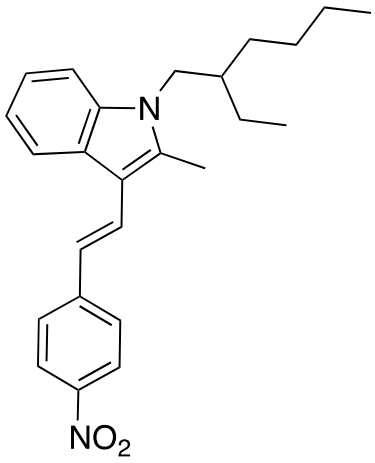

Figure 1 Molecular structure of 3-[2-(4-nitrophenyl) ethenyl]-1-(2-ethylhexyl)-2-methylindole (NPEMI-E).

Herein, we reported the excellent solubility of NPEMI-E in many classes of solvents flanked by a pronounced change in colour depending on solvent polarity. Conversely, no variation of the emission features was detected by changing the solution viscosity. The photophysical properties of the dye, such as the ICT character of its excited state and the observed bathochromic shift in emission, were investigated by means of quantum mechanical calculations. The derived solvatochromic features suggested the incorporation of NPEMI-E in a transparent and amorphous polycarbonate (PC) matrix to investigate their potential vapochromism towards the exposure to volatile organic compounds with different polarities. PC was chosen because of its excellent transmittance of light, high impact strength and thermal stability. Furthermore, PC has a polarity index of 2.9, which can be useful for the selective detection of VOCs with high polarity such as chloroform. This work also proposed a new sensitive and cost-effective image processing tool, which can be effectively applied to all the optical sensors already reported in literature.[107]

3.2. Experimental

3.2.1. Materials and Methods

All solvents used (Table 1) were purchased from Sigma-Aldrich.

Table 1 Vapour pressure, polarity[190], solubility parameter difference Δδ (PC)[191] and refractive index[190] of the utilized solvents.

Solvent	Vapour pressure (mmHg)	Polarity index	Δδ $(cal\ cm^{-3})^{1/2}$	Refractive index
***n*-hexane**	12.4	0.1	2.5	1.38
Et_2O	440	2.8	2.18	1.35
$CHCl_3$	158.4	4.1	0.5	1.44
Methanol	97.6	5.1	-5	1.32
THF	142	4.0	0.7	1.40
Toluene	28.5	2.4	0.9	1.49

Polycarbonate (PC), (SABIC, LEXAN® Mw 220000 g $mole^{-1}$ with 1.5 wt% Si) was used as polymer matrix. 3-[2-(4-nitrophenyl)ethenyl]-1-(2-ethylhexyl)-2-methylindole (NPEMI-E) was available in the research group since it had already been synthesized for the optoelectronic applications.[201] ^{1}H NMR confirmed its chemical structure and purity.

^{1}H-NMR (δ, $CDCl_3$, 400 MHz) 0.87 – 0.99 (m, 6H), 1.24 – 1.49 (m, 8H), 1.83 – 2.07(m, 1H), 2.60 (s, 3H, CH_3 indol.), 4.03 (d, 2H, J = 7.69 Hz), 7.17 (d, 1H, J_{trans} = 16.12 Hz), 7.23 – 7.32 (m, 2H, indol.), 7.32 – 7.39 (m, 1H, indol.), 7.56 (d, 1H, J_{trans} = 16.11 Hz), 7.64 (d, 2H, benz., J = 8.79 Hz), 7.99 – 8.06 (m, 1H, indol.), 8.25 (d, 2H, benz., J = 8.79 Hz).

3.2.1.1. Preparation of dye doped polymer films

500 mg of PC was dissolved in 20 mL of $CHCl_3$ followed by the addition of aliquots (0.1 wt. %) of 10^{-3} M NPEMI-E stock $CHCl_3$ solution. The resulting clear mixture was then casted into clean Teflon petri-dishes and then left for slow solvent evaporation. Dry 70-80 micron thick films were finally obtained.

3.3. Apparatus and Methods

NMR spectra were recorded with a Bruker Advance DRX 400 at room temperature at 400 MHz (^{1}H) and were referred to the residual protons of deuterated solvents.

UV-Vis spectra of both NPEMI-E solutions and films were recorded with a Perkin Elmer Lambda 650 at room temperature.

Emission spectra were measured at room temperature by using a Horiba Jobin–Yvon Fluorolog®-3 spectrofluorometer equipped with a 450 W xenon arc lamp, double-grating excitation and single-grating emission monochromators.

The fluorescence quantum yield (ϕ_F) of NPEMI-E in different solvents was calculated with the comparative method of Williams by using quinine sulfate (ϕ_F = 0.54 in 0.1 M H_2SO_4) and fluorescein (ϕ_F = 0.79 in 0.1 M NaOH) standards.[202,203] Accordingly, 3 solutions of increasing concentration for each standard and dye were prepared followed by recording the absorption and emission spectra at the excitation wavelength ($\lambda_{exc.}$) of dye. For both compounds, the value of integrated fluorescence intensity (area relative to the fluorescence band) is plotted as a function of the absorbance at λ_{exc}. The ϕ_F was calculated using the following equation:

$$\phi_X = \phi_{ST}\left(\frac{Grad_X}{Grad_{ST}}\right)\left(\frac{n^2X}{n^2_{ST}}\right)$$

Where the subscripts ST and X are the standard and the chromophore respectively, Grad is the gradient from the integrated fluorescence intensity *vs* absorbance and *n* is the refractive index of the solvent (Table 1).

For NPEMI-E/PC films, measurements were performed in dark using F-3000 optic fibre mount apparatus coupled with optic fibre bundles. Light generated from the excitation spectrometer is directly focused on the sample using the optical fibre bundle. Emission from the sample is then directed back through the bundle into the collection port of the sample compartment.[84,194,204] The emission response of the films was tested by exposing the sample held by a steel tripod in a 50 mL beaker closed by a pierced aluminium foil lid (Fig. 2), to 20 mL of various organic solvents of different vapour pressure and PC solubility parameter $\Delta\delta$ (Table 1), at 25 °C and atmospheric pressure.

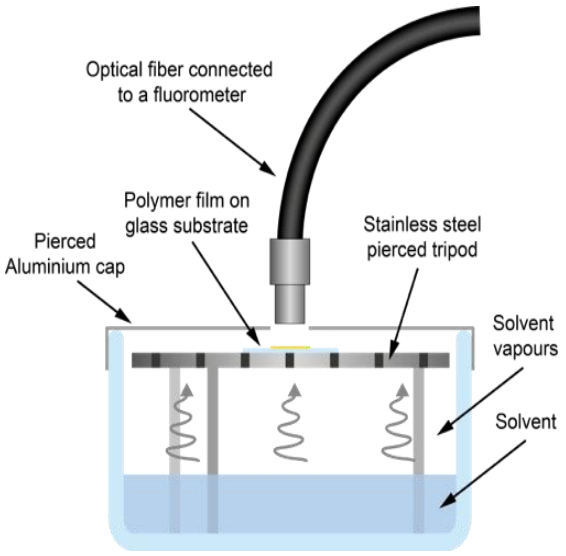

Figure 2 Setup used to study the solvatochromism of NPEMI-E/PC films.[86]

3.4. Hue-based quantification of vapochromism

The fluorescence colour changes of NPEMI-E/PC films upon exposure to $CHCl_3$ were investigated by means of the hue method described[205] and recently proposed[206,207] as a cost-effective tool to monitor variations in the absorption or emission wavelengths of colorimetric sensors. The hue method consists in converting RGB pictures of the fluorescent samples taken under UV irradiation (using a cheap conventional camera of any kind) to HSV stacks. HSV (Hue, Saturation and Value) is a colour format where the colour of each pixel is identified by the coordinates of its position in a cylindrical space.[208] The three different coordinates H, S and V can be determined as follows: H is the colour tone expressed as an angular value from 0° to 360°, that corresponds to the wavelength where the emitted light shows its maximum; S locates the point along the cylinder radius, accounting for colour purity; V is given by the maximum intensity of the signal produced by the pixel, locating the pixel itself along the cylinder axis. RGB images collected with any digital device can be easily converted in the relevant HSV stack by simple mathematical calculation; images can then be compared in terms of colour hue H without artefacts due to different illumination conditions, which would affect only the V and S parameters.[205] Notably, the H, S and V parameters are intrinsically connected with the properties of the emitted light. Considering the light spectrum, H reflects the emission wavelength, S the bandwidth of the peak and V its

height. Accordingly, hue values can be used to follow changes in the emission wavelength of a sample, without the need for optical discriminators such as filters or monochromators.

According to this technique, samples of NPEMI-E/PC films exposed to $CHCl_3$ vapours for different time spans were imaged using a Windows Nokia Lumia 625 Smartphone (main camera pixel resolution: 5.0 MP, f-number/aperture: f/2.4, camera focal length: 28 mm). Pictures were imported in open access software ImageJ (National Institute of Health, Bethesda, MD, USA; available for download at https://imagej.nih.gov/ij/), whose built-in plugin was used to transpose them to the HSV colour space, thus obtaining a stack of three images (H, S and V) for each picture. Average H values were obtained from selected areas of the H image and rescaled to span the 0-360° range. The S and V layers were used to evaluate the homogeneity of the pictures and to select the region of interest.

3.5. Quantum mechanical calculations

Quantum mechanical (QM) calculations of optical absorptions and emission transitions were performed using hybrid DFT functionals (here, B3LYP) and their long-range corrected extensions (here, CAM-B3LYP), which are generally considered suitable for describing molecular systems displaying extended electronic delocalization and their corresponding electronic excitations.[209–212] Solvent effects have been included implicitly by the polarisable continuum model (PCM).[213,214] All QM calculations were performed using the Gaussian09 software package.[215]

3.6. Results and Discussion

3.6.1. Spectroscopic characterization of NPEMI-E in solution

NPEMI-E is well soluble in all solvents characterized by both polar (protic or aprotic) and non-polar nature. The effect of polarity on optical absorption was confirmed by change in colour of dilute solutions (10^{-5} M) from pale yellow to intense orange under visible light (Fig. 3a), thus indicating a striking solvatochromism of the dye. Accordingly, under UV lamp ($\lambda_{exc.}$=366 nm), fluorescence changed from blue (*n*-heptane) to red ($CHCl_3$) (Fig. 3b), and it quenched in highly polar solvents including methanol.

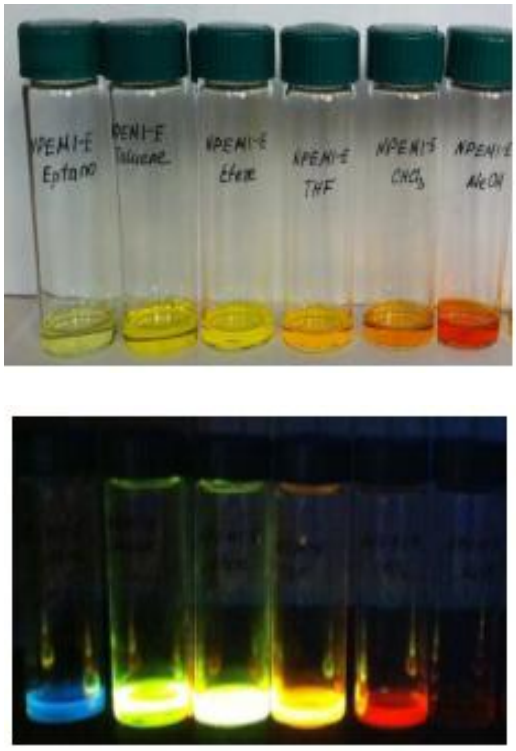

(a)

(b)

Figure 3 From left to right: NPEMI-E solution in *n*-heptane, toluene, diethylether, tetrahydrofuran, chloroform, methanol, (a) under visible light and (b) under the UV lamp illumination at 366 nm.

Absorption and emission spectra of NPEMI-E in different solvents at 10^{-5} M concentration were recorded. The absorption spectra in solution display three bands (Fig. 4a); while the first two bands were observed at about 230 nm and 280 nm corresponding to n-σ* and n-π* transitions respectively, the third band, issuing from the π-π* transition, splits into three different peaks at 400 nm, 415 nm and 435 nm only in the case of *n*-heptane as solvent. A possible explanation of such behaviour could be addressed to the interaction extent between dye and solvent that highlights the vibronic nature of the electronic transitions.[112]

A bathochromic shift is noted in absorption spectra as polarity increases from n-hexane (0.1) to DMSO (7.2), which depends on π-π* transition as n-σ* transition bands are not affected by the polarity. On the other hand, a slight hypsochromic shift in methanol is related to specific interactions between the dye and the solvent owing to the hydrogen bonding capability of the latter. Accordingly, upon π-π* excitation, the electron density on heteroatom (i.e., N) decreases as the hydrogen bonding increases resulting in a hypsochromic shift: stronger the hydrogen bonding, more pronounced the shift.[112] The emission spectra in different solvents (Fig. 4b) also highlighted the solvatochromic nature of NPEMI-E with a bathochromic shift of 7008 cm^{-1} in $CHCl_3$ and only 3562 cm^{-1} in *n*-heptane (Table 2). Notably, solvents with the

highest polarity index (MeOH and DMSO) completely quenched the emission of NPEMI-E in solution.

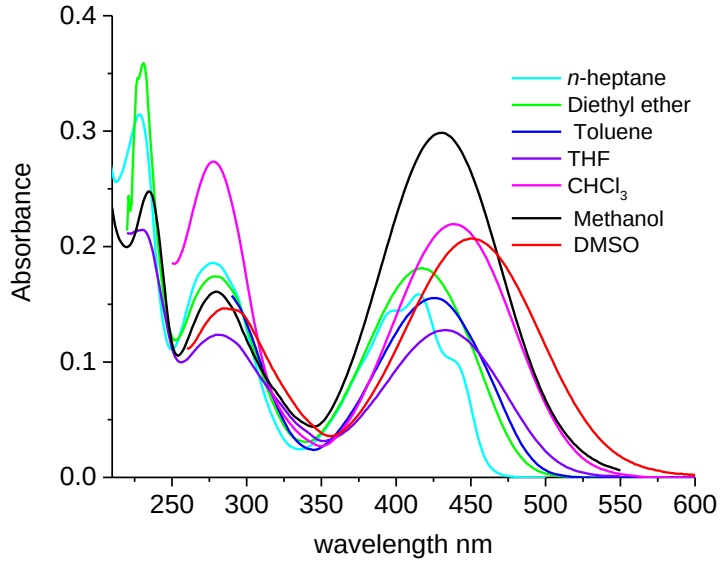

(a)

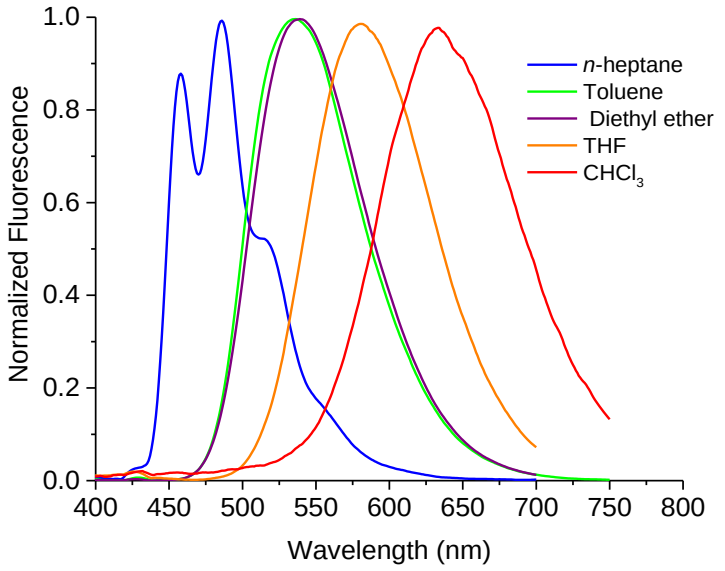

(b)

Figure 4 (a) Absorbance spectra (b) and normalized emission spectra ($\lambda_{exc.}$=380nm) of 10^{-5} M NPEMI-E solutions in different solvents.

The Stokes shifts (in wave number) are plotted against solvent orientation polarizability (Δf), i.e. a parameter described in the Lippert–Mataga equation $\Delta f = (J-1)/(2J+1)-(n^2-1)/(2n^2+1)$, where J is the dielectric constant and n is the refractive index of the solvent.[216–218] A variation in Stokes shift as a function of orientation polarizability (Δf) further confirmed the solvatochromic behaviour of NPEMI-E in different solvents (Fig. 5). The deviations from

linearity in some solvents is ascribed to contributions from specific interactions including intermolecular hydrogen bonding, acid-base interactions, and charge-transfer interactions which are ignored by Lippert-Mataga equation.[219–221]

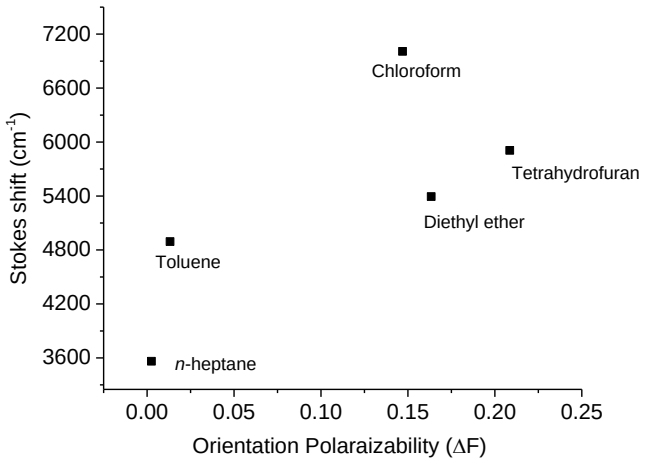

Figure 5 Stokes shift of NPEMI-E versus orientation polarizability (Δf) in different solvents. MeOH and DMSO contributions were omitted due to the negligible emission of the respective NPEMI-E solutions.

Table 2 Optical characterization of NPEMI-E in solvents of different polarity

Solvent	**Δf**	**Absorption λ_{max} (nm)**	**Emission λ_{max} (nm)**	**Stokes Shift (cm^{-1})**	**ϕ_F**
***n*-heptane**	0.0025	415	487	3562	0.03(a)
Toluene	0.0132	424(385[c])	535(480[c])	4893	0.18 (a)
Et_2O	0.1634	417	538	5393	0.23 (a)
THF	0.2086	432	580	5907	0.14 (b)
$CHCl_3$	0.1469	438(403[c])	632(523[c])	7008	0.02 (b)

(a) Quinine Sulphate (Excitation Wavelength = 380 nm)[202,203]
(b) Fluorescein (Excitation wavelength = 490 nm)[202,203]
(C) Results from QM calculations

ϕ_F for NPEMI-E in different solvents was calculated with the comparative method of Williams by using quinine sulphate and fluorescein standards. Notably, ϕ_F decreases in more polar solvents (Table 2). Such a photophysical effect is related to the fact that ICT states are mostly relaxed by non-radiative process resulting in lower fluorescence in polar solvents.[222]

3.6.2. Intramolecular charge transfer (ICT) mechanism

The photophysical nature of NPEMI-E was also effectively investigated by means of QM calculations. Notably, the potential energy surfaces (PESs) of NPEMI-E as a function of the dihedral angle around its double bond (θ), as issuing from both ground and first excited state, were evaluated in $CHCl_3$ (Fig. 6). PESs showed very similar parabola-like profiles centred in correspondence to the planar geometry. These results supported the view of a rather rigid character of the NPEMI-E structure, thus also suggesting the negligible effect of solvent viscosity on the optical features.

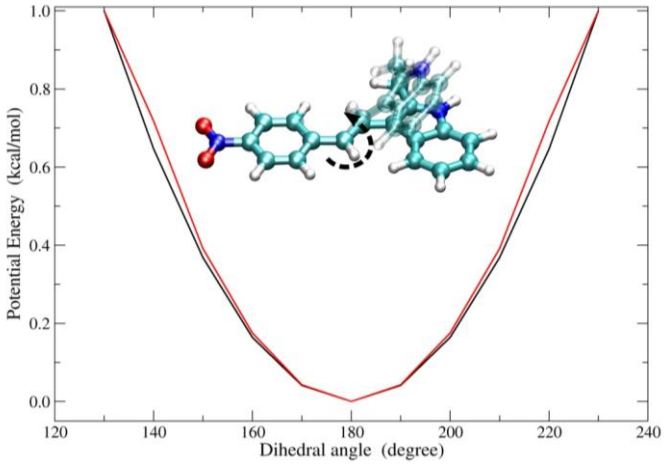

Figure 6 Potential energy surfaces of ground (black) and first excited-state (red) of NPEMI-E as a function of dihedral angle (θ) in $CHCl_3$. Also shown is NPEMI-E with dihedral angle (θ).

In contrast, NPEMI-E undergoes a significant change in dipole moment (μ) going from the ground state to the first excited state, in accordance to an intramolecular charge transfer (ICT). QM calculations of the dipole moment of NPEMI-E in $CHCl_3$, as computed at ground and excited state equilibrium geometries, provided a value of μ_g = 11.2 Debye and μ_e = 25.6 Debye, respectively. In toluene, μ_e (22.8 Debye) was also higher than μ_g (10.5 Debye), though the dipole moment change was somewhat smaller. Such a strong electronic rearrangement was also supported by the molecular orbitals involved in the first optical transition (Fig. 7), which suggested a partial shift of the electronic density from the indole moiety versus the nitro-phenyl group upon excitation. Note that, despite the appearance of a node in the lowest unoccupied molecular orbital (LUMO) in correspondence of the dye's double bond, the latter did not acquire a pure single-bond character in the excited state, as

previously proved by its PES. In turn, this also suggested a relevant role played by the ICT mechanism in NPEMI-E photophysics, in contrast with typical FMRs which undergo significant geometrical rearrangement, is accompanied by ICT. The increase in dipole moment change in $CHCl_3$ with respect to toluene strongly supported the observed bathochromic shift of NPEMI-E emission with solvent polarity, as a result of dipolar solvent relaxation.[112] In a nutshell, solvent reorganization around the chromophore stabilizes more its excited state than the ground state, thus leading to smaller optical transition energies upon emission and, as a consequence, red-shifted fluorescence spectra when going towards more polar solvents QM calculations of both excitation and emission transition energies of NPEMI-E showed a notable red-shift while going from toluene to $CHCl_3$ (Table 2), in qualitative agreement with experiments. Besides, the computed Stokes' shift consistently increased with solvent polarity, thus further supporting the primary role of the ICT mechanism. Note that deviations between theory and experiments are likely due to intrinsic approximations of the QM model and to the neglected vibronic effects, though the agreement is overall satisfactory and similar to previous computational studies on other molecular probes.[179]

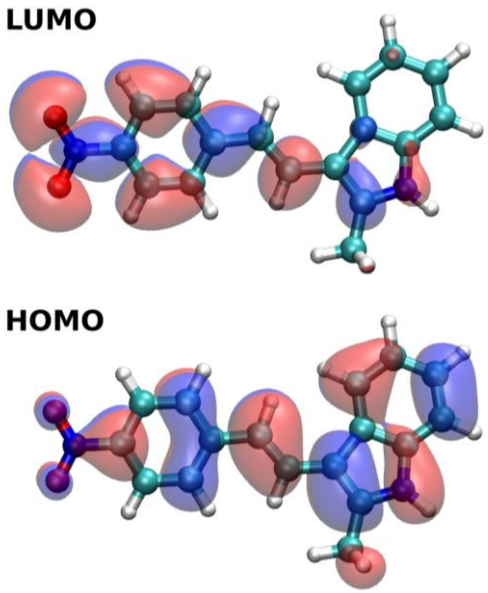

Figure 7 Structure of NPEMI-E showing molecular orbitals of LUMO and HOMO.

3.6.3. Spectroscopic characterization of NPEMI-E/polymer films

In order to explore the optical properties of NPEMI-E for VOCs sensing, a very small concentration (0.1 wt. %) of fluorophore was mixed in PC and films were obtained by solvent casting. Low concentrations of dye were preferred to avoid the effects of aggregation, self-quenching, and self-absorption of chromophore. All PC/NPEMI-E films appeared highly homogeneous and with a thickness of 70-80 μm.

The optical features of NPEMI-E/PC films revealed a Stokes shift of 120 nm (4870 cm^{-1}) (Fig. 8) and a greenish yellow upon excitation at 366 nm (Fig. 8, inset), thus reflecting the behaviour of toluene solution (Table 2) being polarity indices comparable (i.e., 2.4 for toluene and 2.9 for PC). This behaviour is in accordance with the effect of the polymer matrix on the optical properties of the fluorescent dyes, and suggests a possible and significant influence of vapours of volatile compounds with different polarity.[223,224]

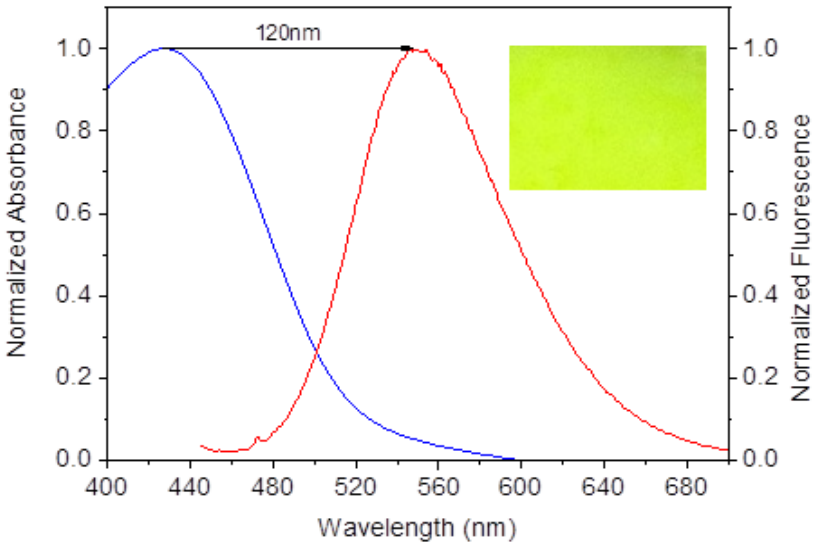

Figure 8 Normalized absorption (blue curve) and emission ($\lambda_{exc.}$=430nm, red curve) spectra of 70–80 μm NPEMI-E/PC film with 0.1 wt% of NPEMI-E. Inset: the same film under UV lamp excitation at 366 nm.

3.6.4. Effect of VOC exposure on the emission spectra of NPEMI-E/Polymer films

Aimed at investigating the vapochromism of NPEMI-E in a much broader way, six solvents of different polarity and with different solvent-polymer interaction were used including *n*-hexane, toluene, diethyl ether, THF, chloroform and methanol. The interaction of different VOCs with PC can be explained on the basis of solubility parameter difference (δ) between PC and solvent ($\Delta\delta = \delta_{PC}-\delta_{solvent}$), since, the Flory-Huggins interaction parameter of some solvents for PC is not available (Table 1). For a better polymer-solvent interaction, the value of δ for both polymer and solvent has to be similar. Fluorescence spectra of NPEMI-E/PC film on exposure to the *n*-hexane are reported in Fig. 9a. Notably, no change in the emission features occurred even after exposing the film up to 35 minutes. A graph of the variation of emission wavelength as a function of the exposure time was also reported and resulted in a constant straight line (Fig. 9a, inset). This result was addressed to the Δδ value of 2.5 (cal $cm^{-3})^{1/2}$ (Table 1), which evidences a feeble interaction between the polymer matrix and the solvent. This result was also confirmed by using a VOC with higher polarity index but similar solubility parameter difference such as diethyl ether (polarity index = 2.8; Δδ = 2.18 (cal $cm^{-3})^{1/2}$) Accordingly, on exposure to diethyl ether vapours, the emission spectra did not experience any variation in wavelength (Fig. 9b) being negligible the interaction with the PC matrix.

We further investigated the effect of toluene vapours on the vapochromic response of NPEMI-E/PC films. Notably, toluene is characterized by a similar polarity index (2.4) but a more favourable Δδ with respect to diethyl ether (0.9 cal $cm^{-3})^{1/2}$). Notwithstanding the appropriate Δδ, the emission resulted unaffected by solvent exposure, even after 35 min (Fig 9c). This was explained considering the similar polarity between the solvent and the PC matrix. As soon as the solvent molecules get (easily) in contact with the dispersed NPEMI-E, the fluorophore environment does not change in polarity, thus letting the fluorophore maintain the optical features unaltered.

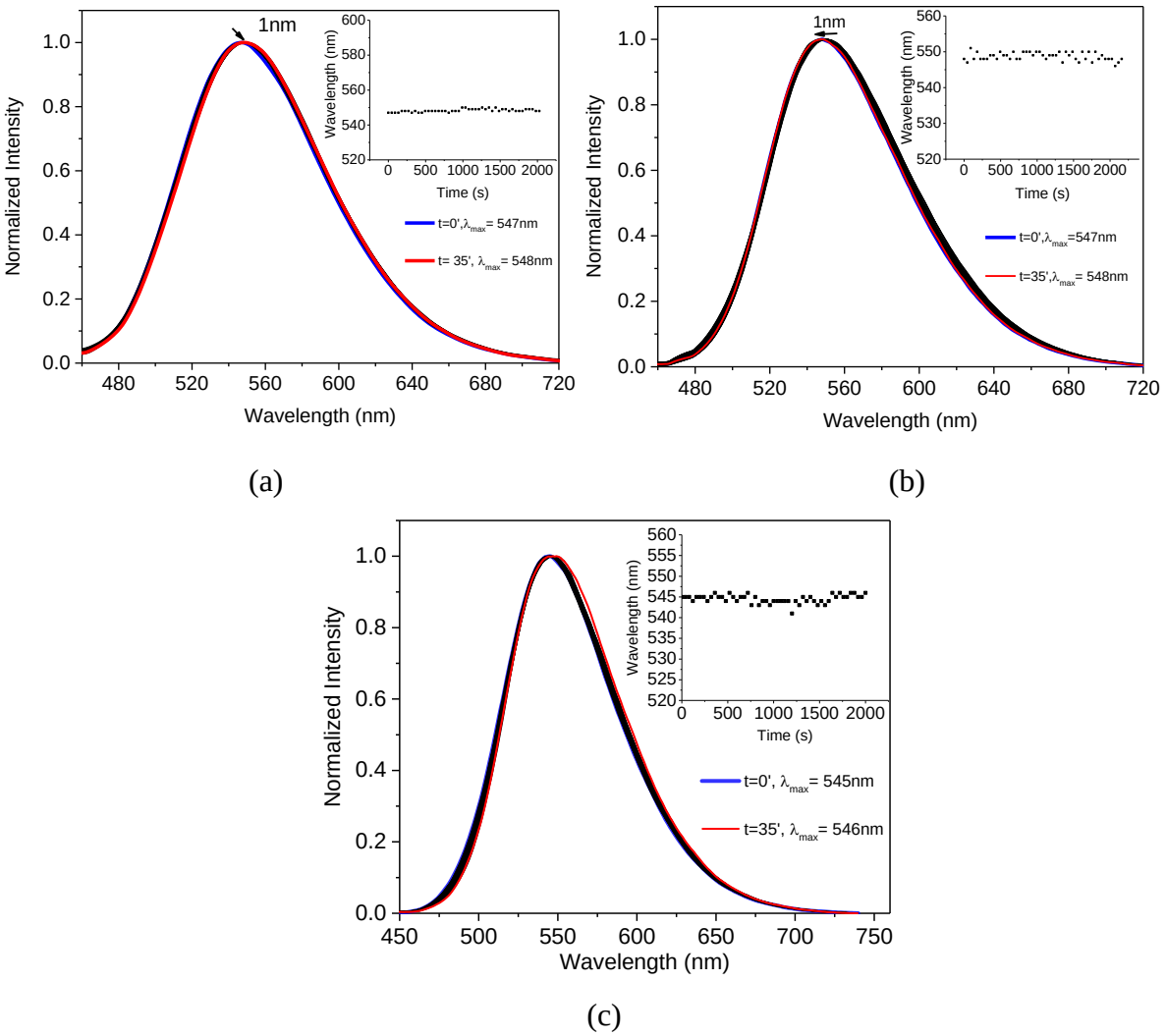

Figure 9 Normalized fluorescence intensity of NPEMI-E/PC exposed to the vapours of (a) *n*-hexane (b) Diethyl ether and (c) Toluene vapours for a time interval of 35 min (λ_{exc}.=430nm). Variation of maximum emission of PC/NPEMI-E as a function of exposure time to the vapours of n-hexane (inset a), diethyl ether (inset b), and toluene (inset c).

By contrast, a clear vapochromism was observed by exposing NPEMI-E/PC film to THF vapours (Fig. 10), i.e. a solvent that shows a good combination of low $\Delta\delta$ (i.e., 0.7 cal cm^{-3})$^{1/2}$) and polarity index (4.0). The THF molecules were able to diffuse into the PC matrix and to completely solvate the NPEMI-E molecules, thus promoting a shift in wavelength of 27 nm (from 543 to 570 nm) within 800 seconds (less than 13-14 min, with a time constant of 10^{-3} s^{-1}) of exposure. After that time, the emission wavelength remained mostly unchanged and a plateau was reached (Fig. 10, inset).

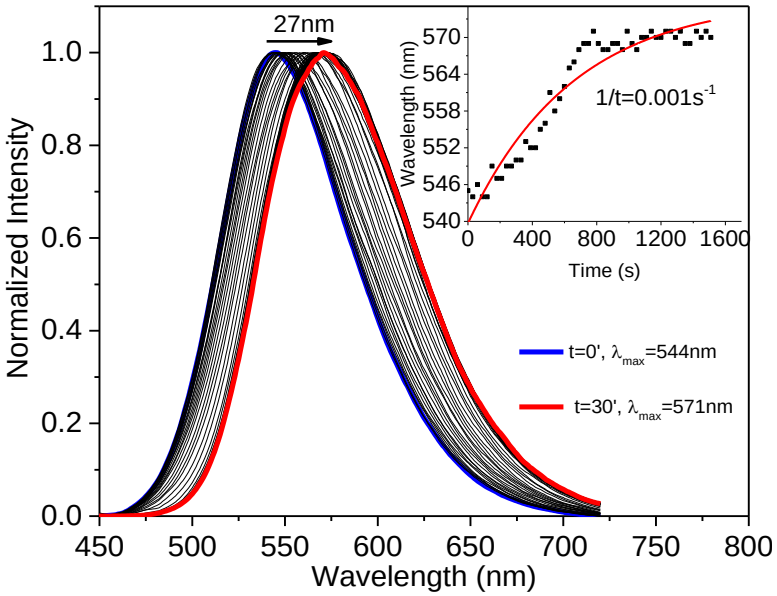

Figure 10 Fluorescence of NPEMI-E/PC exposed to THF for a time interval of 35 min ($\lambda_{exc.}$=430nm). Variation of the maximum emission of NPEMI-E/PC film as a function of exposure time to THF (▪). The wavelength shift with time exposure was fitted with mono-exponential ($y = y_{0+}A \cdot e^{(-x/t)}$) function with 1/t as time constant (solid line, inset).

It is worth noting that the use of $CHCl_3$ as VOC produced an even more pronounced vapochromic response. $CHCl_3$ is characterized by a higher polarity index and a more favourable $\Delta\delta$ (i.e., 4.1 and 0.5 cal $cm^{-3})^{1/2}$, respectively than THF. Notably, the strong solvent-polymer interaction fostered NPEMI-E solvation by the absorbed $CHCl_3$ vapours, which in turn caused a pronounced red-shift of the PC film emission wavelength of about 60 nm after a time interval of about 10 min only (Fig. 11). Moreover, the emission wavelength variation of the maximum as a function of $CHCl_3$ vapours exposure time further supports the evident solvatochromism (Fig. 11 inset). Data were fitted with good correlation using the mono-exponential growth function. Since the fitting procedure was not completely accurate in the initial part of the experiment we omitted to convert it into linear relationship. The time constant was about 4 times higher than that calculated for THF as VOC (i.e., $4 \cdot 10^{-3}$ s^{-1} against 10^{-3} s^{-1}), also promoted by the greater vapour pressure of $CHCl_3$ with respect that of the latter (i.e., 158.4 mm Hg against 142 mm Hg).

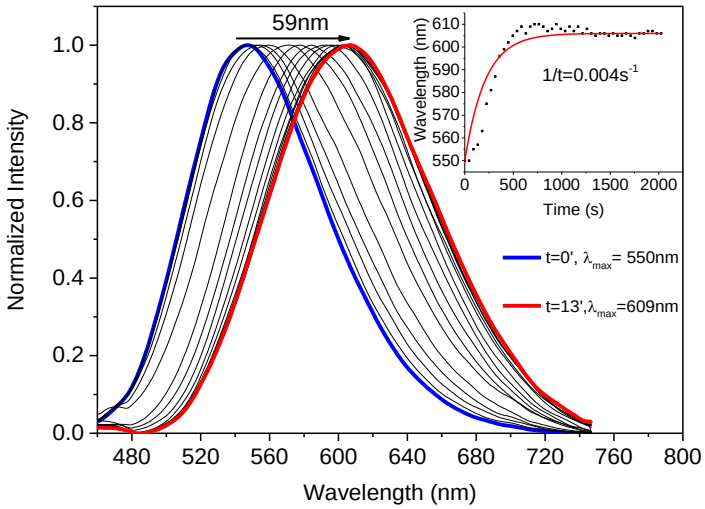

Figure 11 Normalized emission of NPEMI-E/PC exposed to $CHCl_3$ for a time interval of 13 min ($\lambda_{exc.}$=430nm). Variation of maximum emission of PC/NPEMI-E film as a function of exposure time to chloroform (▪).The wavelength shift with time exposure was fitted with mono-exponential ($y = y_{0+}A \cdot e^{(-x/t)}$) function with 1/t as time constant (solid line, inset).

The pronounced wavelength shift of about 60 nm produced a clear variation of the emission colour of the films from green to yellow and eventually to a dark yellow after a long time of exposure (about 30 min), which can be easily detected by the naked eye even during the first min of the experiments.

We finally tested the influence of MeOH vapours on the vapochromic behaviour of NPEMI-E/PC films. MeOH is a very polar solvent with the highest polarity index of 5.1 but with an adverse $\Delta\delta$ of -5 $(\text{cal cm}^{-3})^{1/2}$. Nevertheless, notwithstanding the highest $\Delta\delta$ for methanol and the lower vapour pressure compared to diethyl ether for example, NPEMI-E/PC films experienced a 10 nm shift in their emission wavelength (Fig. 12).

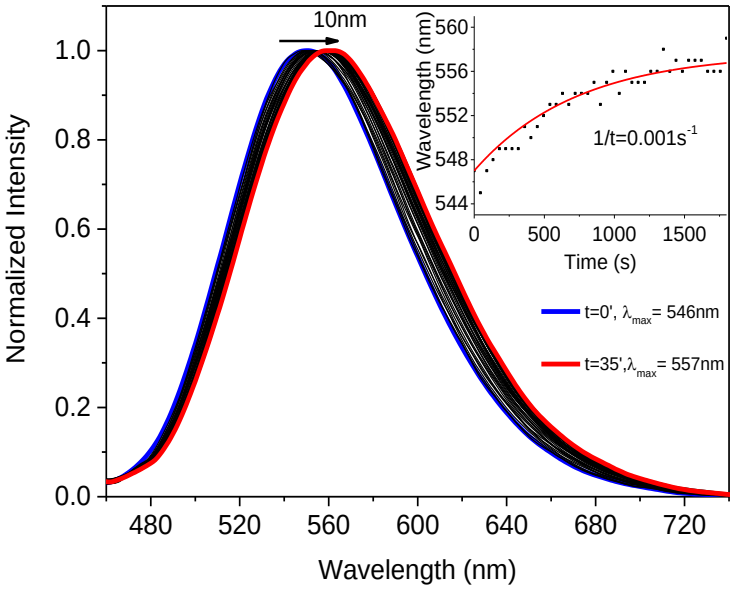

Figure 12 Fluorescence of NPEMI-E/PC film exposed to MeOH for a time interval of 35 min ($\lambda_{exc.}$=430nm). Variation of the maximum emission of NPEMI-E/PC film as a function of exposure time to methanol (▪).The wavelength shift with time exposure was fitted with mono-exponential ($y = y_0+A\cdot e(-x/t)$) function with 1/t as time constant (solid line, inset).

This phenomenon could be possibly addressed to the vapour molecules that get in contact with the PC surface where some NPEMI-E molecules could be distributed during the solvent evaporation.[225,226] Differently from dye molecules molecularly dissolved within the PC bulk, those at the surface can be promptly solvated by the incoming solvent, thus providing the shift in wavelength. Even if the high polarity index of MeOH should suggest a more pronounced wavelength shift, the solvatochromic effect is only partial since only fluorophore molecules at the film surfaces were affected by VOC solvation.

The remaining NPEMI-E molecules were not involved in the phenomenon being dispersed in the unaffected PC bulk. Overall, on the account of the reported experiments, NPEMI-E/PC films revealed the strongest vapochromic feature towards $CHCl_3$ vapours.

3.6.5. Reproducibility and reversibility of the behaviour of NPEMI-E/PC films

In order to explore the reproducibility and reversibility of the vapochromic response, the NPEMI-E/PC films exposed to $CHCl_3$ vapours were dried at 50 °C for 5 min in a ventilated stove to remove residual solvent from the film. This procedure was repeated after every exposure. The reproducibility depends on the NPEMI-E emission response while the reversibility feature is associated to the PC matrix, including the changes in polymer structure due to solvent interaction. Fig. 13 shows that NPEMI-E/PC films exhibited excellent reversibility and good reproducibility to successive cycles of $CHCl_3$ vapours exposure.

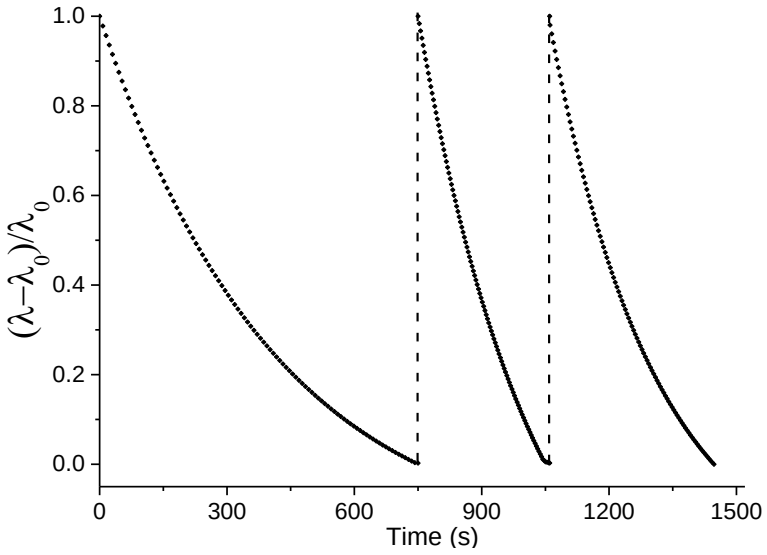

Figure 13 Variation of the wavelength at emission maximum of NPEMI-E/PC film on exposure to vapours of $CHCl_3$ for 3 successive cycles. The vertical dashed lines indicate storage time of 5 min at 50°C (λ_0 is the wavelength at emission maximum of the film before vapour exposure).

We speculated that the faster wavelength variation for the successive exposure cycles could be possibly addressed to a partial segregation of fluorophore at the surface induced during film dryness. The solvated NPEMI-E molecules were therefore forced to move closer to the film surface, thus rendering the successive vapochromism more prompt to occur.

3.6.6. HUE-based quantification of $CHCl_3$ exposure

NPEMI-E/PC samples exposed to $CHCl_3$ for different spans of time were imaged and the RGB pictures were converted to the HSV (Hue, Saturation and Value) colour space. Average H values were obtained from selected areas of the H image and rescaled to span the 0-360°

range. The S and V layers were used to evaluate the homogeneity of the pictures and to select the region of interest. Average H values showed a decrease with exposure time, reaching a plateau after about 10 min of exposure to solvent (Fig. 14a).

It is worth noting that this behaviour is in good agreement with the spectroscopic data shown in Fig. 10 and also accounts for the fluorescence colour variation that can be observed in Fig. 14b. The hue parameter allowed therefore for the effective extraction of spectral information from digital colour images of NPEMI-E/PC samples. This very simple and inexpensive method permitted to follow changes in the sample emission upon exposure to $CHCl_3$ without the need for wavelength discriminators.

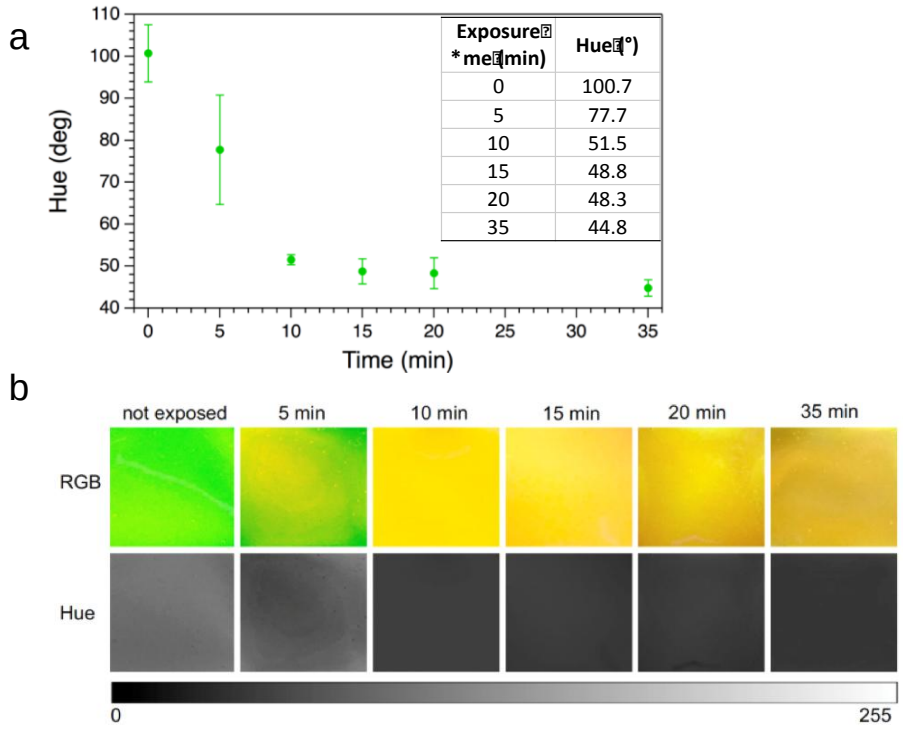

Figure 14 (a) Hue values vs $CHCl_3$ exposure time for NPEMI-E/PC films. (b) Images of NPEMI-E/PC samples after different exposure times to $CHCl_3$. Top: original RGB images. Bottom: hue layer after the conversion to HSV. Gray scale bar on the right refers to images in the bottom row only.

3.7. Conclusions

We have demonstrated that a solvatochromic fluorophore, namely NPEMI-E, when dispersed in films of PC experiences a selective and pronounced response towards polar and PC interacting VOCs such as chloroform. NPEMI-E showed excellent solubility in many classes of solvents with a change in colour, depending on solvent polarity. The experimental and computed Stokes' shift that consistently increased with solvent polarity supported the primary role of the ICT mechanism in the photophysics of the dye. When embedded in PC films at very low content (0.1 wt. %), NPEMI-E exhibited strong fluorescence variations visible to the naked eye upon exposure to saturated atmospheres of polar and well-interacting VOCs only. VOCs with an unfavourable solubility parameter difference ($\Delta\delta$) or polarity index (n-hexane, toluene and MeOH), were not active in promoting an effective vapochromic response. By contrast, a remarkable, fast and reversible vapochromic response was registered for chloroform vapours, and the phenomenon was effectively quantified by hue determination as well.

The results of this work were recently published in Journal of polymer science, part B: polymer physics **2017,** DOI: 10.1002/polb.24367

Chapter 4

4. Effect of Glass Transition Temperature (T_g) on the Vapochromism of FMR in Polymer.

4.1. Introduction

Many polymer properties can alter the sensitivity of the fluorescent molecules embedded within the matrix. In particular, for the application of vapochromism, solvent-polymer interaction or solubility parameter have been often reported to directly affect the response of the fluorescent dyes mixed with the polymer.[84,85,107,185] Consequently, better solvent-polymer interaction results in the significant vapochromic response of the fluorescent dye molecules. Apart from it, solvent properties including polarity and vapour pressure also influence the optical properties of the dye within the polymer matrix.

The optical properties of the fluorescent polymers are controlled by the specific interactions between the VOCs and the dye/polymer system.[84,85,107,194,204] Fluorophores can be either covalently attached with polymer or simply dispersed within the polymer matrix. Both methods have some advantages and disadvantages associated with them. Notably, the affinity of dye with the polymer prepared by simple dispersion is controlled by the non-covalent interactions including hydrogen bonding, dipole-dipole interaction and van der Waals forces.

A very typical property of the polymers that effectively impact their ultimate application is the glass transition temperature (T_g). Polymer engineering is highly interested in manipulating the polymer T_g for novel application of polymers. Polymer T_g is often used to explore the molecular mobility and other structural information, however, the nature of glass transition is still under debate.[227] T_g of a polymer determines the rigidity and flexibility of a polymer which define the reduced chain mobility and rapid molecular motion respectively. Consequently, the polymer films with different T_g are likely to show different motion of the macromolecular chains. Interestingly, the exposure of the polymer films with variable T_g to VOCs is supposed to influence the chain mobility, thereby altering the optical properties of fluorophore embedded inside the matrix. Accordingly, at lower T_g, higher chain mobility will favour the free rotation of FMR inside the film which can be reflected by non-emissive

deactivation. Contrary, the blends with higher T_g are supposed to restrict the rotation of FMR molecules inside the matrix and favour the strong fluorescence on photoexcitation.

To the best of our knowledge, the effect of T_g on vapochromic behaviour of dyes in polymers has not been investigated yet. Crenshaw et al. have reported the affect of polymer T_g on the chromogenic behaviour of blends for threshold temperature sensors.[228] Accordingly, it was found that by adjusting the T_g of the PMMA/PBMA blend on varying the composition of the individual polymers, the threshold of the temperature sensors can be modulated.

Herein, we report the affect of polymer T_g on vapochromic behaviour of a newly synthesized Fluorescent Molecular Rotor (FMR), **2-(methylbutyl)-2-cyano-3-Julolidine acrylate (MBCJA).** Accordingly, the photophysics of MBCJA depends on the viscosity of the medium. Higher viscous medium hinders the free rotation resulting in deactivation from locally excited (LE) state.[67,68] Differently, lower viscosity favours the formation of twisted intramolecular charge transfer (TICT) allowing the free rotation defined by the non-radiative decay.[59,68,69,229] A very small concentration (0.1wt. %) of MBCJA was mixed with two miscible polymers having totally different T_g, poly(methyl methacrylate) (PMMA) and poly(butyl methacrylate) (PBMA) with T_g of 105 and 20 °C (as measured from DSC) respectively. Mixing these two polymers in different compositions with desired amount of MBCJA resulted in new compatible polymer blends with different T_g. The compatibility of the blend is also supported by nearly similar solubility parameters of PMMA (δ= 9.76 cal $(cm^{-3})^{1/2}$ and PBMA (δ= 9.51 cal $(cm^{-3})^{1/2}$, a difference less than 0.5.[230]

4.2. Experimental

4.2.1. Materials and methods

Julolidine, N,N-dicyclohexylcarbodiimide (DCC), 9-(2,2-dicyanovinyl)julolidine, 9-(2-Carboxy-2-cyanovinyl)julolidine were purchased from Aldrich and used as recieved. Cyanoacetic acid was recrystallized form a mixture of toluene/acetone 2:3 v/v. 1,3 dicyclohexyl carbodiimide (DCC) was purified by dissolving in ethyl acetate followed by addition of powdered anhydrous sodium sulphate. The mixture was filtered and the filtrate was evaporated and dried. Dichloromethane was refluxed over CaH_2 for 2h and distilled under nitrogen. Tetrahydrofuran (THF) was refluxed over Na/K alloy for 3h and distilled under nitrogen. Finally, Triethylamine was refluxed over KOH for 3h and distilled under nitrogen.

4.2.2. Synthesis of 2-(methylbutyl)2-cyanoacetate (MBCA)

The reaction pathway for the synthesis of MBCA is shown in scheme 1.

To a solution of cyanoactic acid 0.86 g (10 mmol) and 2-methyl butanol (10 mmol) in anhydrous dichloromethane (20 mL), solution of 2.06g (10 mmol) of DCC in 10 mL anhydrous dichlomethane was added dropwise. The mixture was stirred for 10h at 50 °C and then stored to allow the formation of precipitate dicyclohexylurea (DCU), formed during the reaction. The DCU was filtered off and the filtrate was dried under vacuum and the residue was purified by column chromatography on silica gel (230-400 mesh) using dichloromethane as eluent (53% yield).

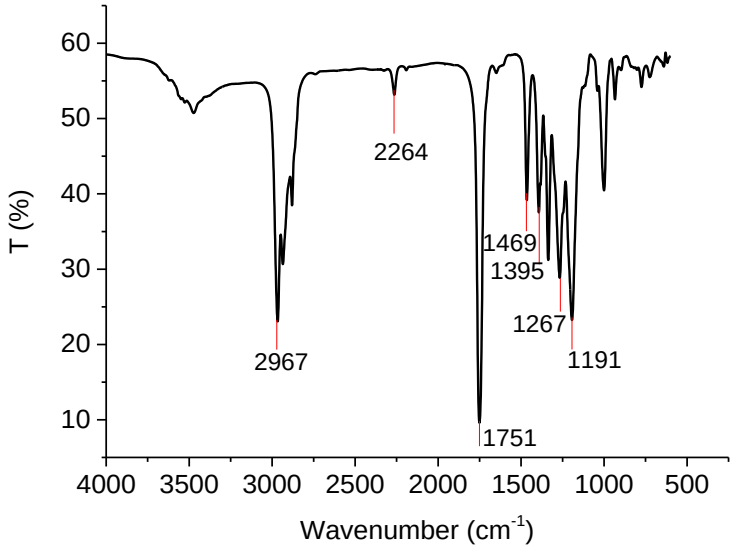

Figure 1 FT-IR characterization of MBCA

FT-IR (KBr cm^{-1}): 2967, 2264, 1751, 1469, 1395, 1267, 1191.

ν (cm^{-1})

- 2967 methyl C-H stretching
- 2264 C≡N stretching
- 1751 C=O stretching
- 1469 C–H bending
- 1395 C–H bending
- 1267 Ester asymmetric stretching
- 1191 C–O stretching

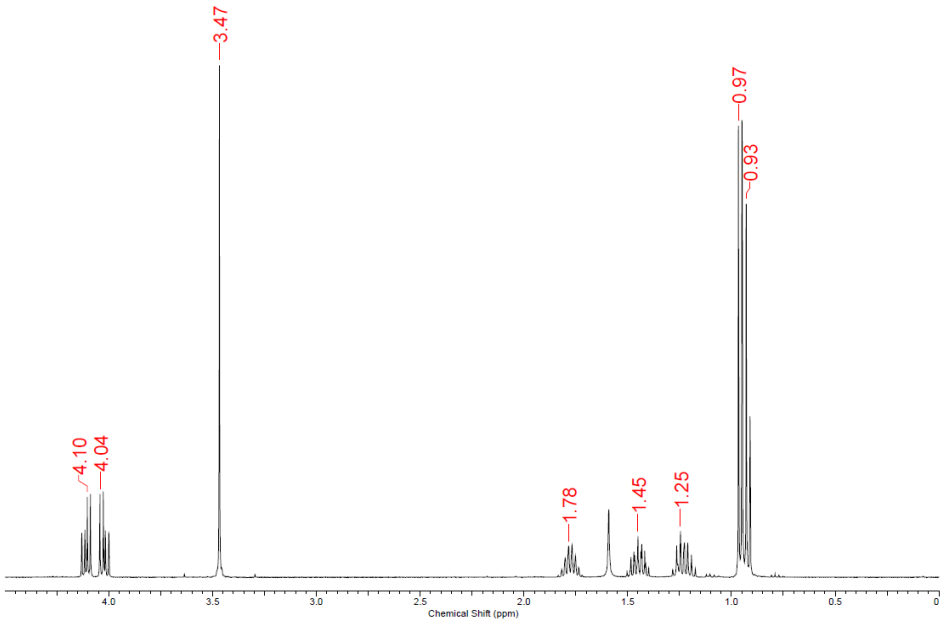

Figure 2 ^{1}H-NMR characterization of MBCA

^{1}H-NMR ($CDCl_3$): δ (ppm)= 4.10 (m, 2H, (COOC<u>H</u>2): 3.47 (s, 2H, $CNCH_2$), 1.78(m, 1H,-CH_2-C<u>H</u>), 1.45 (m, 2H, -CHC<u>H</u>$_2$$CH_3$):, 0.97 (t, 3H, -$CH_2$-C<u>H</u>$_3$): 0.93 (d, 3H, CHC<u>H</u>$_3$).

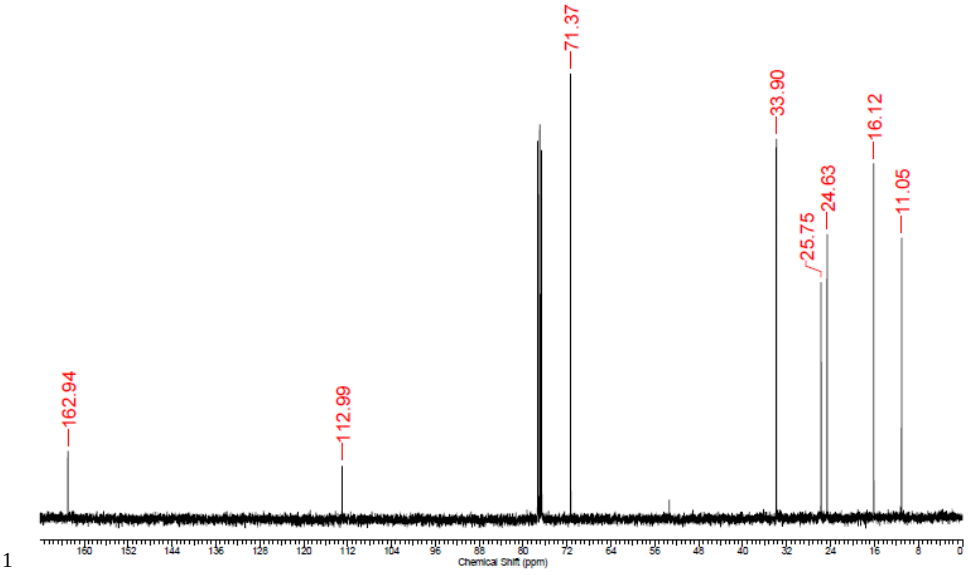

Figure 3 ^{13}C-NMR characterization of MBCA

^{13}C-NMR ($CDCl_3$): δ (ppm): 162.24 (COO), 112.99 (CN), 71.73 (O<u>C</u>CH), 33.90 (CH_2<u>C</u>H), 25.75 (CH<u>C</u>$H_2$$CH_3$), 24.63 (C<u>C</u>$H_2$COO), 16.12 (<u>C</u>$CH_3$), 11.05 ($CH_2$<u>C</u>$H_3$).

4.2.3. Synthesis of 9-formyljulolidine (FJUL)

FJUL was already synthesized in our group by the formylation of julolidine using Vilsmeier-Haak reaction.[85] To a solution of julolidine (0.5 mg, 2.88 mmol) and N,N-dimethylformamide (0.27 mL, 3.45 mmol) in anhydrous dichloromethane (5 mL), Phosphororus oxyxhloride (0.29 mL, 3.17 mmol) was added dropwise and stirred for 10 h at room temperature. The mixture was added with the aqueos sodium acetate solution (2 M) and stirred for 4 h at 0 °C. Extraction of organic layer was done with diethyl ether followed by drying under reduced pressure. The final crude product was purified under column chromatography on silica gel (230-400 mesh) using diethyl ether/n-hexane as eluent (60% yield) .

FT-IR (KBr, cm^{-1}): 2938, 2208, 1702, 1558, 1520, 1442, 1314, 1228, 1164,110.
^{1}H NMR ($CDCl_3$) (ppm): 7.93 (s, 1H, CHO), 7.51 (s, 2H, aromatic), 4.12 (t, 4H NCH_2), 2.7 (t, 4H $NCH_2CH_2C\underline{H}_2$), 1.9 (m, 4H $NCH_2C\underline{H}_2$).
^{13}C-NMR ($CDCl_3$) δ (ppm): 191.3 (CHO), 149.1 (=C-N aromatic) 128.5 to 122.0 (aromatic), 49.3(NCH_2), 28.1 to 20.4 ($NCH_2\underline{C}H_2\underline{C}H_2$).

4.2.4. Synthesis of 2-(methylbutyl)-2-cyano-3-julolidine acrylate (MBCJA)

Triethylamine (0.3 mL) (2.14 mmol) was added to a solution of MBCA (0.83g) (1.56 mmol) and (0.21 g) (1.06 mmol) of formyl julolidine (FJUL) in 20 mL of THF.
In order to enhance the yield of the reaction, 0.1mL of CH_3COOH and 10μL of pyperidine was added and reaction was stirrred for 48h at 70 °C. The reaction was completely monitored by TLC using CH_2Cl_2: n-hexane (4/6 v/v) as eluent. Sodium sulphate was then added and the solution was left for about 4 hrs and filtered off. The filtrate was then evaporated and the purified with column chromatography on silica gel (230-400 mesh) using $CHCl_3$ as eluent (61% yield).

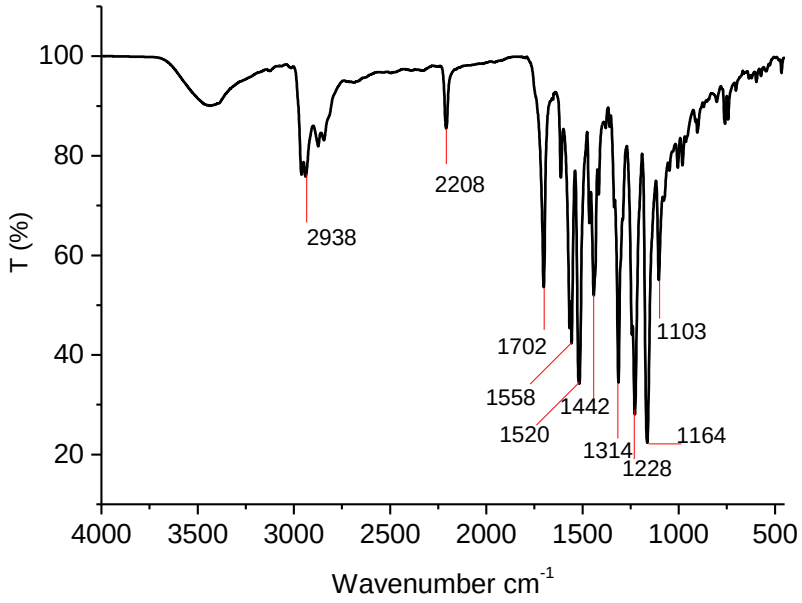

Figure 4 FT-IR characterization of MBCJA

FT-IR (KBr cm^{-1}): 2938, 2208, 1702, 1558, 1520, 1442, 1314, 1228, 1164, 1103

ν (cm^{-1})

- 2938 methyl C–H stretching
- 2208 C≡N stretching
- 1702 C=O stretching
- 1558 ring C–C stretching
- 1520 ring C–C stretching
- 1442 methyl bending
- 1314 CH_2 bending
- 1228 ester stretching
- 1164 ester stretching
- 1103 C-O stretching

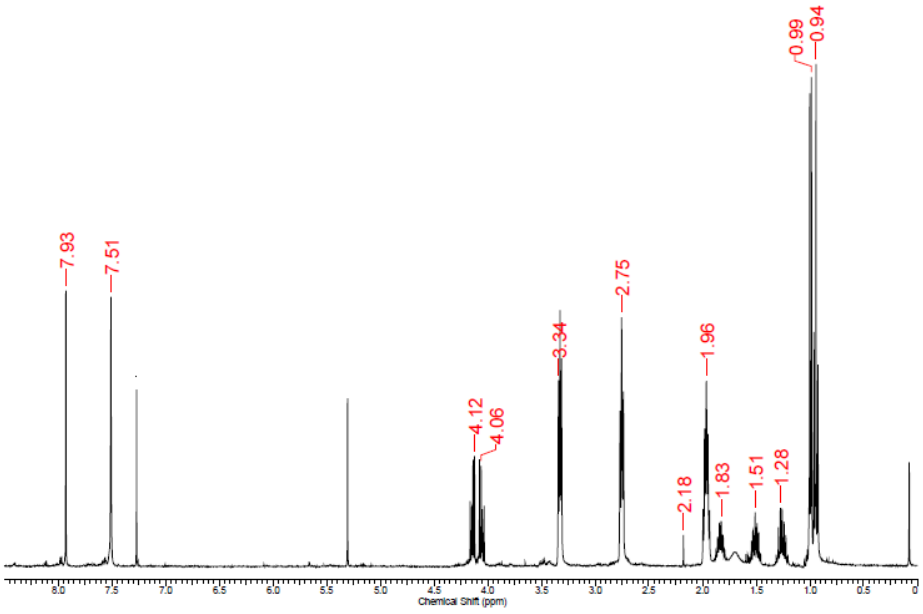

Figure 5 ^{1}H-NMR characterization of MBCJA

^{1}H-NMR ($CDCl_3$) δ (ppm): 7.93 (s, 1H, CNCCH) 7.51 (s, 2H, aromatic) 4.12 (t, 2H, $COOCH_2$) 3.34 (t, NCH_2), 2.75 (t, 4H, $NCH_2CH_2C\underline{H}_2$), 2.18 (m, $COOCH_2C\underline{H}$) 1.96 (m, 4H, $NCH_2C\underline{H}_2$) 1.51 (m, $CHC\underline{H}_2CH_3$) 1.28 (t, $CH_2C\underline{H}_3$) 0.99 (d, $CHC\underline{H}_3$)

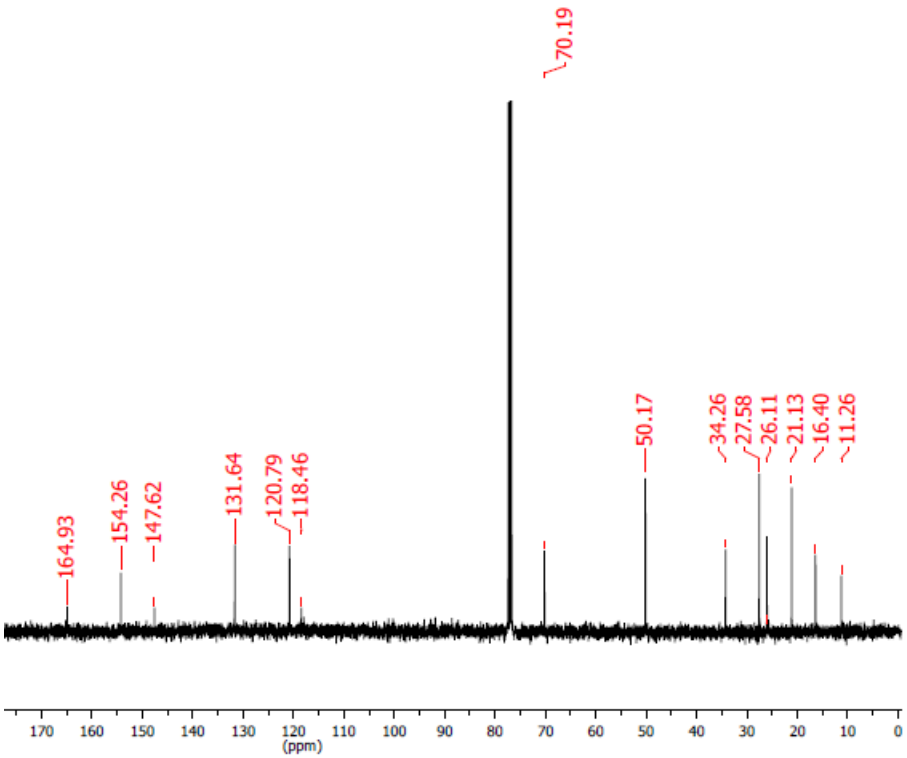

Figure 6 ^{13}C-NMR spectrum of MBCJA

^{13}C-NMR ($CDCl_3$) δ (ppm): 164.93(COO), 154.26 (Ph<u>C</u>H=CH), 147.62 (=C-N aromatic), 131.64 (aromatic C), 120.79 (CH_2 aromatic) 118.46 (CN), 70.19 (COO<u>C</u>H_2), 50.17 (NCH_2), 34.26 (CH_2<u>C</u>H), 27.58 (CH<u>C</u>H_2), 21.13 (NCH_2<u>C</u>H_2), 16.40 (CH<u>C</u>H_3) 11.26 (CH_2<u>C</u>H_3)

4.2.5. Preparation of PMMA/PBMA blend with MBCJA films

Molecular rotor containing blends of different compositions of PMMA/PBMA in the weight fraction of 0.8 : 0.2, 0.6 : 0.4, and 0.2 : 0.8 with pure PMMA and PBMA films were prepared. The desired amount of both PMMA and PBMA were disssolved seperately in $CHCl_3$ and then mixed together with 0.1wt.% of MBCJA solution. Pure PMMA and PBMA films with 0.1 wt.% of dye were also prepared accordingly. The air bubbles from the solution were completely removed under vaccum. Finally, the viscous solutions was casted into teflon dishes and left for drying and the resulting films were dried in vaccum againto ensure complete removal of solvent.

4.2.6. Characterization

FT-IR spectra were recorded with Perkin Elmer spectrum GXFT-IR at room temperature on KBr pellets. NMR spectra were recorded with Bruker Advance DRX 400 at room temperature at 400 MHz (^{1}H) and 100 MHz (^{13}C) in $CDCl_3$ solution.

Absorption spectra were measured with Perkin-Elmer Lambda 650 spectrometer at room temperature. Fluorescence spectra were recorded on a Horiba Jobin-Yvon Fluorolog®-3 spectrofluorometer at room temperature equipped with 450W xenon arc lamp double-grating excitation and single-grating emission monochromoters.

Fluorescence spectra of MBCJA/polymer films were measured on a Horiba Jobin-Yvon Fluorolog®-3 spectrofluorometer at room temperature in the dark by using the F-3000 Fibre Optic Mount apparatus coupled with optical fibre bundles. Light generated from the excitation spectrometer is directly focused to the MBCJA/polymer film using an optical fibre bundles. Emission from the sample is then directed back through the bundle into the collection port of the sample compartment. The emission response of the MBCJA/polymer films was tested by exposing a 2×2 cm portion of the film, attached to an aluminium foil covering a 50 mL closed container (Figure 1b), to 20 mL of different organic solvents.

DSC measurements for the MBCJA/Polymer films were done by using Mettler Toledo Stare system DSC 822e equipped with a cooling system under nitrogen atmosphere. The system was calibrated with two standards, indium with a fusion temperature 156.6 °C, and zinc with a fusion temperature of 419.5 °C. The samples were heated from -10 to 150 °C at a rate of 10 °C min^{-1} and cooled at the same rate.

4.3. Results and discussions

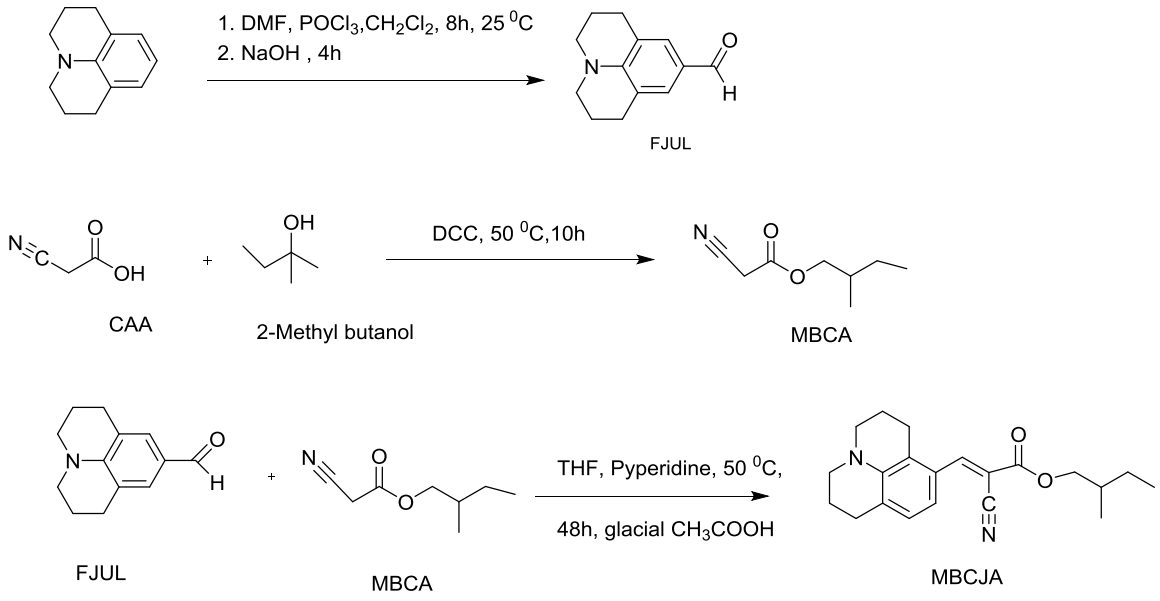

Scheme 1. Reaction pathway for the synthesis of MBCJA

The alkyl cyanoacetic ester (MBCA) was synthesized by dicyclohexyl carbodiimide esterfication of cyano acetic acid with 2-methyl butanol (Scheme 1). 9-formyl Julolidine was previously prepared with formylation of commercially available Julolidine with phosphorous oxychloride and dimethylformamide. Knovenegeal condensation of MBCA with 9-formyl Julolidine in presence of pyperidine, THF and triethyl amine resulted into the desired MBCJA (Scheme 1). To shift the equillibrium to the right side, glacial acetic acid was added also and the MBCJA was obtained with good yield (61%) after chromatographic purification.The fluorophore-polymer blend films were prepared by mixing 0.1wt.% of FMR with desired amount of of PMMA and PBMA in different compositions.

4.3.1. Optical properties of MBCJA in solution

To investigate the optical properties of MBCJA, both absorption and emission spectra of MBCJA in MeOH/glycerol mixtures was performed. MBCJA is a FMR and its optical properties are highly viscosity dependent, so the two solvents were chosen to prepare mixtures of variable viscosities. Absorption maxium was recorded at 449 nm when 99% MeOH was used but it shifted to 464 nm when 99% of glycerol was present in the solution (Figure 7). The emission spectra of MBCJA solutions ($\lambda_{exc.}$= 450 nm) in MeOH and glycerol was noted at around 491 nm and 503 nm respectively (Figure 8). The shift in both absorption and emission spectra clearly demonstrates that MBCJA not only shows viscosity dependent optical properties but also exhibits slight solvatochromic nature. Fluorescence of MBCJA increases on increasing the glycerol in MeOH/ glycerol mixture. Clearly, the viscosity of glycerol is 1560 times higher than methanol (viscosity of glycerol, η= 945 mpa.s at 25 °C and viscosity of MeOH η=0.6 mpa.s)

Consequently, in viscous medium, the molecular rotation is hindered thus favouring the radiative decay of the LE state. A 12 nm shift in glycerol compared to MeOH is attributed to the difference in their dielectric constants (dielectric constant ε = 45.2 for glycerol, and ε = 32.7 for methanol) resulting in the solvent stabilization of the excited intramolecular-charge transfer (ICT) state. Notably, in glycerol, the molecular motion is not allowed easily, as a result, ICT plays the role. Accordingly, during photoexcitation, the dipole moment of the molecular rotor increases and some energy is transferred from excited state of the molecule to the solvent molecules resulting into the bathochromic shift. Therefore, MBCJA allows to measure the viscosity during the polarity changes.

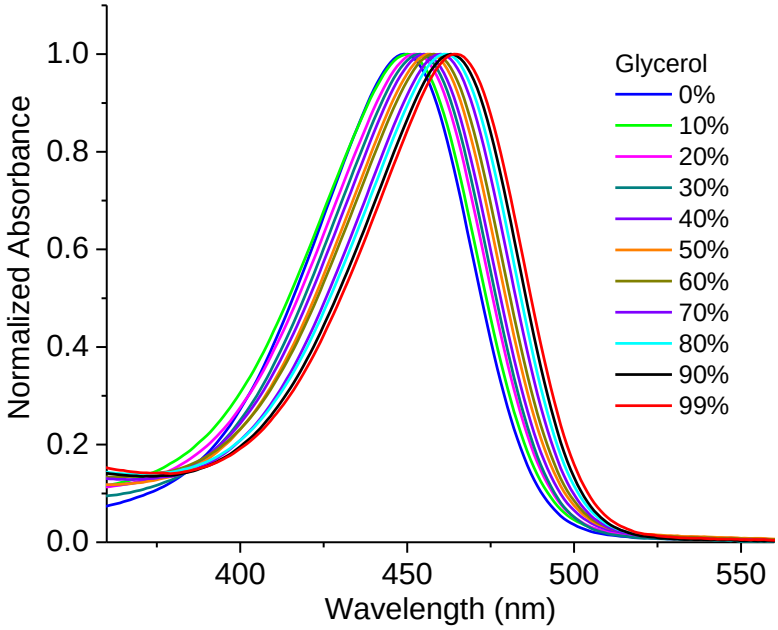

Figure 7 UV-Visible absorption spectra of 10^{-3} M solution of MBCJA in different composition of MeOH/Glycerol mixtures.

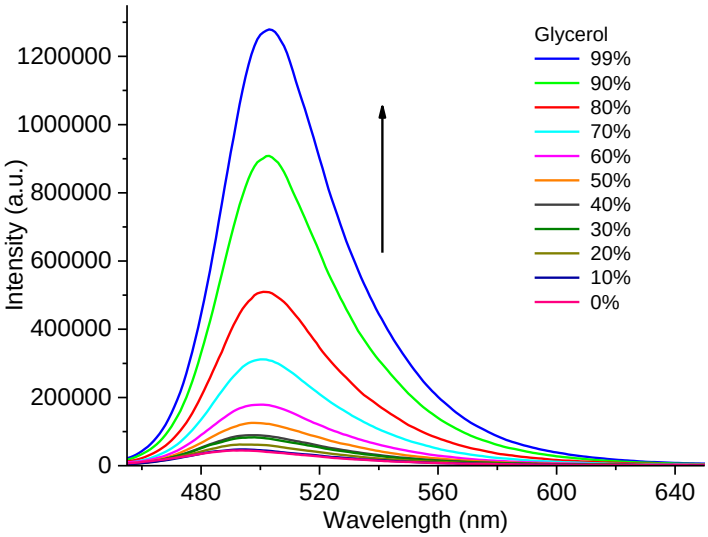

Figure 8 Emission spectra of 10^{-3} M solution of MBCJA in different composition of MeOH/Glycerol mixtures

The effect of aggregation on the optical properties of MBCJA was investigated using the dioxane/water mixtures, since dioxane is miscible in water. The aggregated form of MBCJA was obtained on increasing the water fraction in the mixture as the dye is insoluble in water. The absorption and emission spectra were recorded at different fractions of the solvent mixture. On increasing the water fraction in the mixture, a red shift of 28 nm was recorded in

the absorption spectra from 438 nm when only dioxane was used to 466 nm in presence of 80% of water in the mixture (Figure 9).

The emission spectra displayed an interesting phenomenon of the effect of dielectric constant of solvent on the non-radiative decay of MBCJA. It was expected that higher the water content in the mixture, higher will be the fluorescence due to aggregation effect. Contrary to it, a decrease in the emission spectra and red-shift was recorded on increasing the water fraction (Figure 10). Accordingly, the much large difference in the dielectric constant (2.25 for dioxane and 80 for water) resulted in the better stability of twisted intramolecular charge transfer (TICT) state and hence favouring non-radiative decay and shift.[59,68] Above the 90% of water content, a red-shifted band was recorded at around 582 nm with enhanced emission suggesting the formation of emissive aggregates.[231] In general, the role of aggregation overcomes the TICT effect.

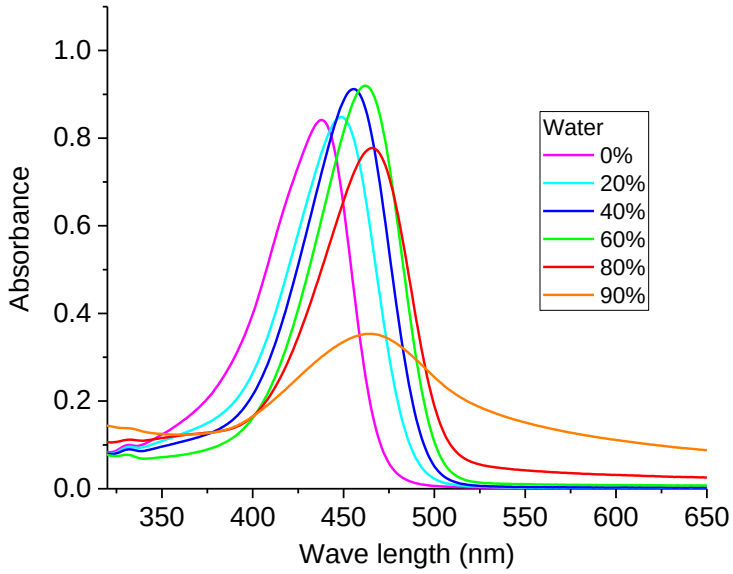

Figure 9 UV-Visible absorption spectrum of 10^{-5} M solution of JCVBM in different composition of Dioxane/Water mixtures.

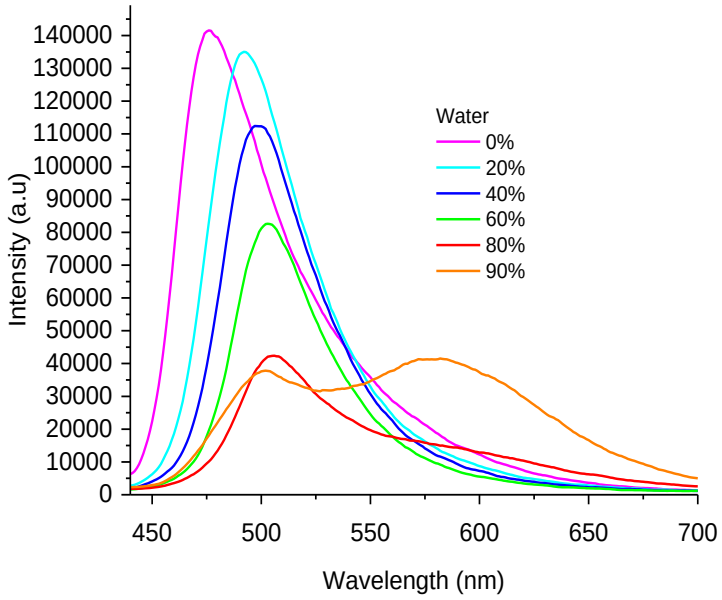

Figure 10 Fluorescence emission spectrum of 10^{-5}M solution of JCVBM in different dioxane/water composition of mixtures ($\lambda_{exc.}$= 430nm).

To further evaluate the spectroscopic properties of MBCJA in solvents of different dielectric constants, the emission spectra were recorded in different solvents including dioxane, chloroform, toluene, acetone and methanol (Figure 11). Clearly, fluorescence decreased in solvents of high dielectric constant (33 for methanol, 20.7 for acetone, 4.81 for chloroform and 2.25 for dioxane). This suggests that the emission intensity of MBCJA also depends on the polarity of the solvents since all these solvents have almost similar viscosities. Clearly, the role of polarity in stabilizing the TICT is displayed thus favouring the non-radiative decay in higher polar solvents.

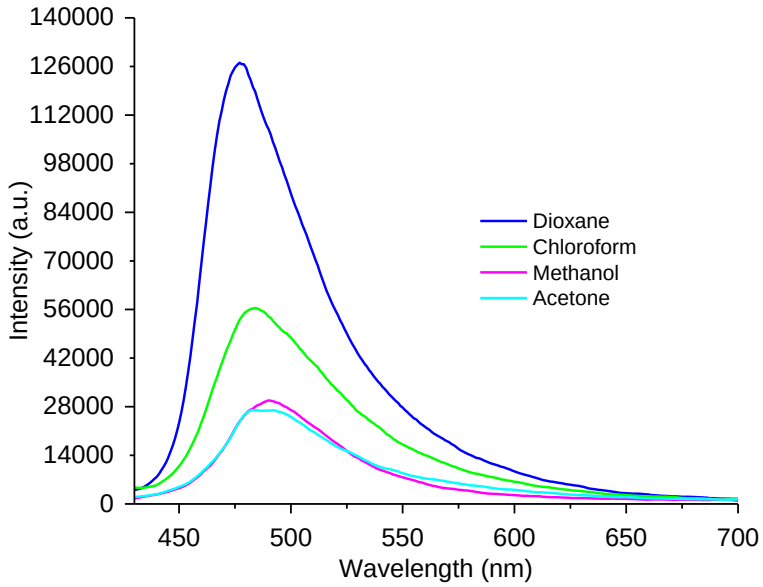

Figure 11 Fluorescence emission spectrum of 10^{-5}M solution of JCVBM in different solvents ($\lambda_{exc.}$= 420nm).

4.3.2. Spectroscopic characterization of polymer films

Both absorption and emission spectra of polymer blend/MBCJA films were recorded. The absorption spectra of MBCJA in pure PBMA and all blends were blue shifted to around 360 nm while PMMA/MBCJA film shows maximum absorption at 447 nm (Figure 12). The blue shift of the fluorophore in PBMA is caused by the lower polarity and T_g of polymer matrix, which in turn increases the interaction of a dye with a polymer.[232,233] The similar maximum absorption of blends and PBMA indicates that the interaction of dye with the polymer remains the same, since, only 0.1wt. % of dye is used.

Emission spectra of the MBCJA/polymer blend films also exhibited blue shift on going from PMMA to PBMA. A shift in maximum emission was recorded from 426 nm in MBCJA/ PBMA to 476 nm in MBCJA/PMMA film (Figure 13). Under the UV lamp, a clear blue emission in blends and PBMA contrary to the yellow emission in pure PBMA is easily visible to the naked eye (Figure 14). Clearly, the strength of blue colour increases on increasing the weight fraction of PBMA in the blends, thus suggesting solvatochromic behaviour in the solid state.

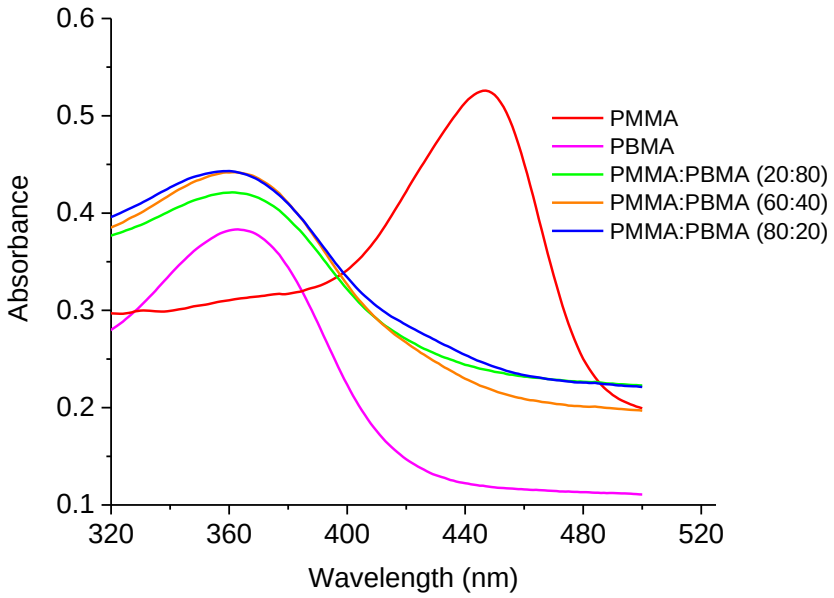

Figure 12 Normalized absorption spectra of 0.1 wt. % MBCJA/polymer films

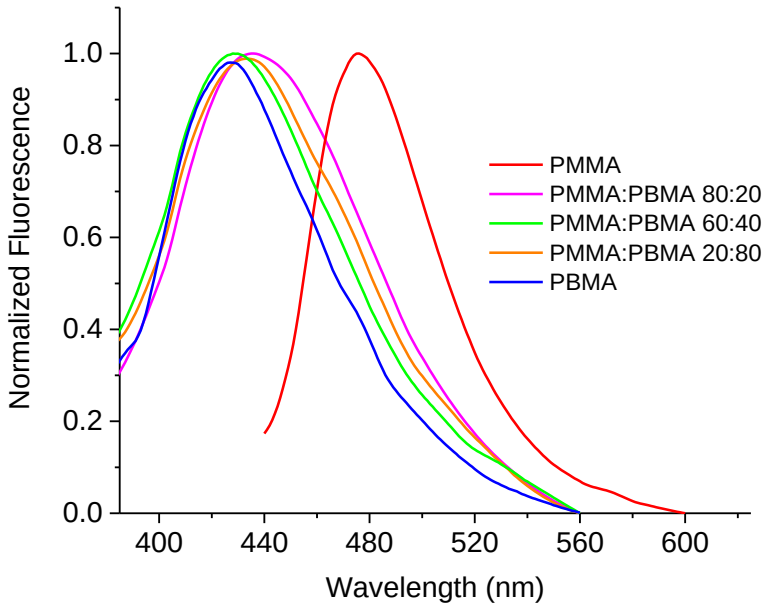

Figure 13 Normalized emission spectra of MBCJA/polymer films (λ_{exc}. for PMMA films = 420 nm and λ_{exc}. for PBMA films =350nm)

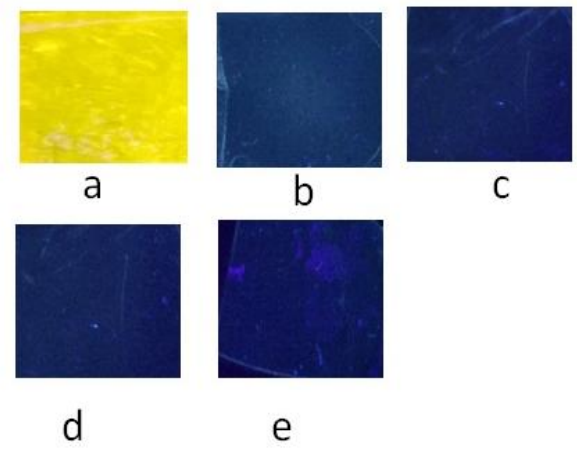

Figure 14 Images of MBCJA (0.1wt. %) in (a) PMMA, (b) PMMA:PBMA (0.2:0.8), (c) PMMA:PBMA (0.6:0.4) (d) PMMA:PBMA (0.8:0.2) and (e) PBMA under the UV lamp excitation at 366 nm

4.3.3. Glass transition temperature (T_g) of polymer films

To investigate the effect of T_g on the vapochromic behaviour, a series of polymer blends of PMMA and PBMA were prepared by altering the composition of the two polymers. The T_g of PMMA decreases while that of PBMA increases on addition of 0.1 wt.% of MBCJA. This behaviour suggests the molecular mixing of dyes resulting in plasticization of higher T_g polymer and inverse effect in lower T_g polymers.[234] These results also confirm slightly different interaction of dye with both polymers and are supported by the blue shift of the MBCJA in PBMA. Interestingly, the T_g of PMMA decrease from 105 °C in neat polymer to 88 °C in dye doped polymer, clearly supporting the plasticizing effect due to dye –polymer interactions. On the other hand, the T_g of PBMA increased slightly from 20 °C in neat polymer to 27 °C in dye mixed polymer. Polymer blends with dyes displayed slightly higher T_g than their corresponding neat blends. This behaviour suggests that the T_g of the dye must be above to that of the T_g of blends resulting in antiplasticization of the blends. The measurement of single T_g and the modification of the polymer blend T_g by the presence of dye suggests the molecular mixing of dye with the polymer.[234,235]Applying the well know Fox equation, the theoretical value of T_g of the blends were calculated.[234,236] The Fox equation (as shown below) assumes random mixing between the two polymers and allows to predict the properties of blend from the individual polymer properties.[237]

$$\frac{1}{T_g} = \frac{w_1}{T_{g1}} + \frac{w_2}{T_{g2}}$$

Where T_g is the glass transition of the blend and T_{g1} and T_{g2} represent the glass transition temperature and w_1 and w_2 are the weight fractions of individual polymers respectively.

As seen from the table 1, deviations recorded between the experimental and Fox equation are generally due to the intermolecular forces including hydrogen bonding, dipole-dipole interactions or acid-base interactions which are unaccounted in the Fox equation.[238,239]

Table 1 Glass transition temperature of the polymer films measured by DSC and calculated from Fox equation

Polymer	**[a]T_g (° C)**	**[b]T_g (° C)**
Pure PMMA (without dye)	105	
PMMA (with dye)	88	
PBMA (without dye)	20	
PBMA (with dye)	27	
PMMA:PBMA 0.8:0.2 (with dye)	90	
PMMA:PBMA 0.8:0.2 (without dye)	85	56
PMMA:PBMA 0.6:0.4 (with dye)	95	
PMMA:PBMA 0.6:0.4 (without dye)	83	39
PMMA:PBMA 0.2:0.8 (with dye)	24	
PMMA:PBMA 0.2:0.8 (without dye)	22	24

[a]T_g = Glass transition measured by DSC
[b]T_g= Glass transition of pure blends calculated from Fox equation

4.3.4. Effect of VOCs exposure on MBCJA/polymer films

The vapochromic properties of MBCJA/polymer films were explored on exposing the films to different VOCs. Lower concentration of the dye (0.1wt. %) was selected to ensure no quenching due to aggregation and other undesired effects. The solvents were chosen based on different polarity, vapour pressure, solubility parameter (δ) (Flory-Huggins interaction parameter (χ) is not available for the solvents used). Based on these parameters, the solvents interact differently with the polymer films and consequently the viscosity changes accordingly. The change in viscosity inside the polymer film is provided by the variations in the free volume of the matrix caused by the relaxation of the macromolecular chains which in

turn allows greater mobility and finally decrease in local viscosity.[107] The T_g of the polymer films was therefore expected to change the viscosity accordingly on exposure to the solvents.

Table 2 Vapour pressure, polarity index[240], and solubility parameter[241] for the solvents and polymers used as VOCs.

solvent	Polarity index	Vapour pressure (mmHg)	Dielectric constant ε	$\delta(cal\ ^{cm-3})^{1/2}$
Diethyl ether	2.8	440	4.33	7.74
Methanol	5.1	97.6	33.6	14.52
PMMA[242]			4.4	9.76
PBMA[242]			4.4	9.51

4.3.4.1. Effect of diethyl ether exposure on vapochromic behaviour of MBCJA/polymer films

Exposure of PMMA/MBCJA film to diethyl ether indicate a significant decrease in the emission intensity during the initial exposure (Fig. 15a). On the other hand slightly higher variation in fluorescence was recorded in PBMA/MBCJA film (Fig. 15e), suggesting that FMR experiences greater flexibility in PBMA than PMMA on solvent exposure. Considering that the δ for PMMA 9.76 $(cal\ cm^{-3})^{1/2}$ and PBMA 9.51 $(cal\ cm^{-3})^{1/2}$[2243] is very similar but different from the diethyl ether 7.2 $(cal\ cm^{-3})^{1/2}$, the slight interaction is favoured by the higher vapour pressure of diethyl ether. In solid PMMA film, the rotation of the MBCJA, is completely hindered due to lower flexibility of polymer chains. On exposing the PMMA film to diethyl ether, the viscosity decreases, allowing the FMR molecules to rotate freely resulting in TICT deactivation. A slight increase in intensity after the initial decrease in PMMA is assumed due to the accelerated film swallowing caused by the higher vapour pressure of diethyl ether. This result in increasing the internal pressure faster than the matrix can relax. Thereafter, the thermodynamic equilibrium is attained and no further expansion of film is allowed. Consequently, the rate of desorption of solvent becomes equal to that of adsorption and hence there is no more increase in viscosity of the matrix. The difference in emission spectra of both PMMA and PBMA films is most probably due to the different T_g of these polymers, since, all other parameters are very similar.

The different dye containing PMMA/PBMA blends with different T_g were also exposed to a saturated atmosphere of diethyl ether vapours. Accordingly, PMMA/PBMA (0.8/0.6) blend, having T_g of 94 °C, displayed no significant variation in the fluorescence. It seems that besides T_g, intermolecular interactions between two different polymers might have changed

the solubility parameter of the blend, so does the different fluorescence behaviour. Similar results were recorded for PMMA/PBMA (0.6/0.4), having similar T_g (95 °C), during solvent exposure. Contrary, to our assumption, the PMMA/PBMA (0.2/0.8) even with T_g of 22 °C only, exhibit not so significant variation in fluorescence. This behaviour is possibly ascribed to the stronger polymer-polymer interaction which changes the solubility parameter of the blend resulting in poor solvent interaction with the blend. Notably, strong variations only occurred for PMMA based films where strong variation of the intensity emission was caused by the prompt variation in polymer matrix viscosity as soon as diethyl ether vapours get in contact with it. In the case of PBMA films (Figure 15e), only a shift to lower emission intensities occurred, thus suggesting the effect of fluorophore dilution only, instead of an effect of its FMR features.

4.3.4.2. Effect of methanol exposure on vapochromic behaviour of MBCJA/polymer films

Both pure and blend polymer films were also exposed to a more polar protic solvent, methanol. Notably, the variation in the intensity in both PMMA and PBMA was poor when compared to that from diethyl ether exposure (Fig. 16a and 16e). Evidently, the lower vapour pressure and much different δ for methanol (14 cal cm^{-3})$^{1/2}$ [241] than both polymers hindered the polymer-solvent interaction. A small variation in the emission intensity is possibly based on the acid-base interactions between the polymer and solvent. PMMA and PBMA being polymers with Lewis basic character due to the presence of ester functional groups with the carbonyl oxygen atom, can donate electrons. Methanol on the other hand has some acidic character and may form acid-base complex with PMMA and PBMA, resulting in some plasticizing effect.[244] The slight red-shift in the fluorescence of the films is attributed to the higher polarity of methanol. The results suggest that better polymer solvent interaction is vital for the vapochromic response of the fluorescent polymer. The role of T_g only comes into play only if the solvent effectively interacts with the polymer. The exposure of blends evidently indicates that blend of PMMA:PBMA (0.2:0.8), i.e the film with lowest T_g, display slightly better variation in fluorescence than the other blends indicating the some role of T_g might be involved (Fig. 16 d). Also, the slight interaction with methanol for this blend than diethyl ether is probably favoured by the solubility parameter of the blend which might be close to former than the latter. The other two blends with identical T_g resulted with similar vapochromic response. (Fig. 16b and 16c)

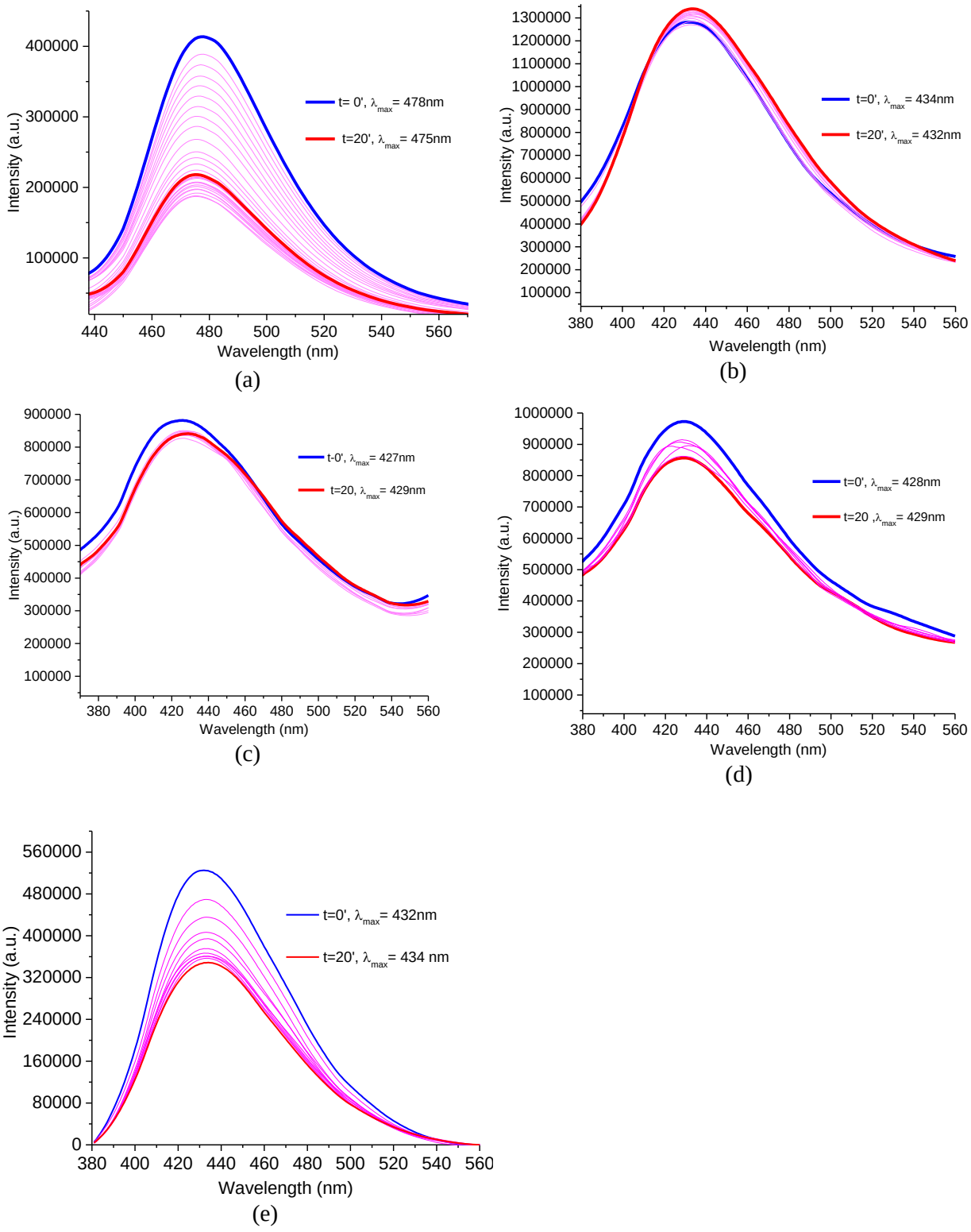

Figure 15 Fluorescence variation of 0.1 wt% MBCJA in (a) PMMA (b) PMMA:PBMA (0.8:0.2), (c) PMMA:PBMA (0.6:0.4), (d) PMMA:PBMA (0.2:0.8) (e) PBMA on exposure to diethyl ether vapours for 20 min ($\lambda_{exc.}$ for PMMA = 420 nm and $\lambda_{exc.}$ for PBMA and blends =350 nm)

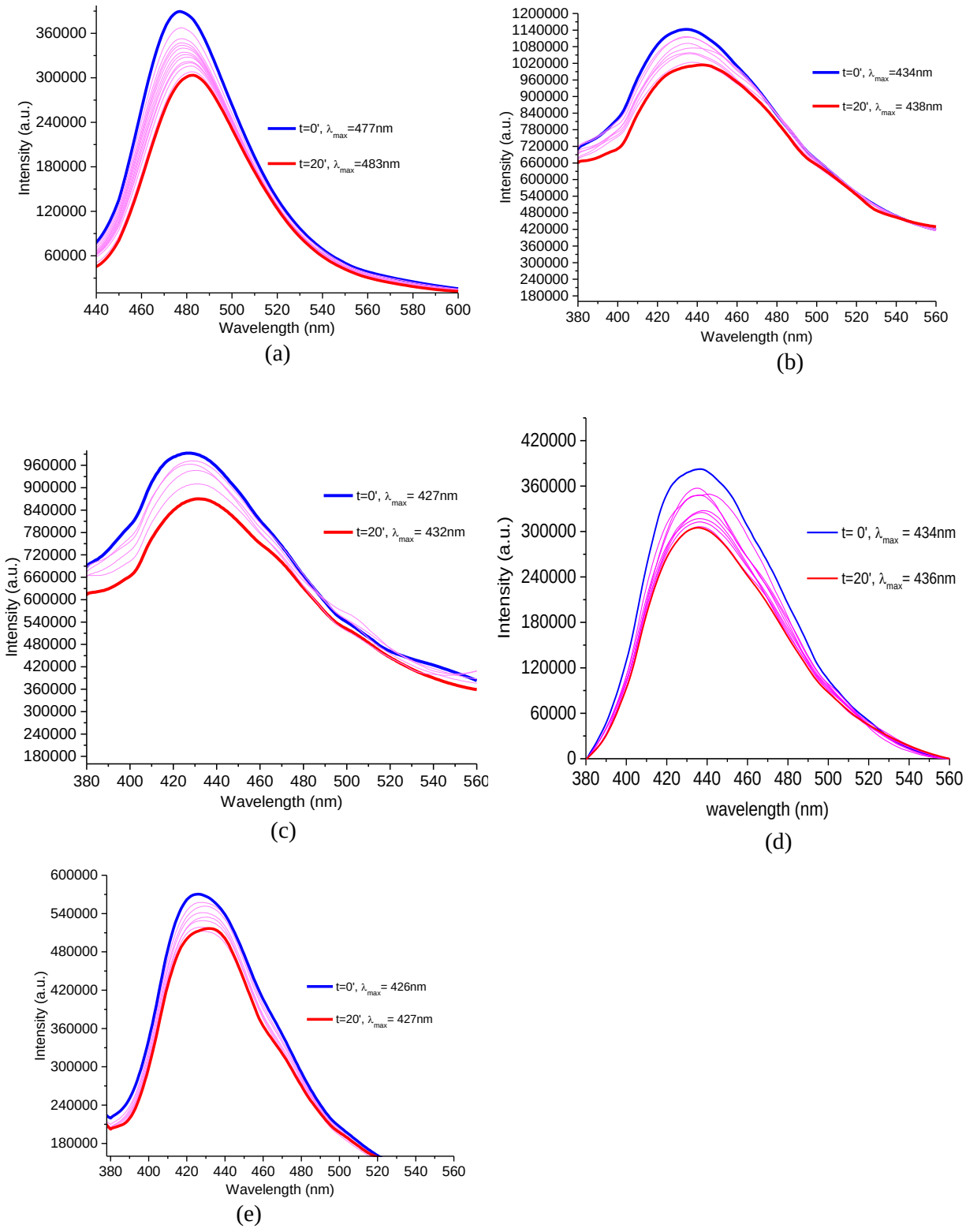

Figure 16 Fluorescence variation of 0.1wt% MBCJA in (a) PMMA (b) PMMA:PBMA (0.8:0.2), (c) PMMA:PBMA (0.6:0.4), (d) PMMA:PBMA (0.2:0.8) (e) PBMA on exposure to methanol vapours for 20 min ($\lambda_{exc.}$ for PMMA = 420nm and $\lambda_{exc.}$ for PBMA and blends =350nm)

4.4. Conclusions

The work investigated the effect of T_g on the vapochromic behaviour of a FMR in polymer matrix. Polymer T_g changed effectively on mixing with dye. Mixing of dye caused lowering the T_g of a polymer with higher T_g (PMMA) due to plasticization and vice versa. This is in accordance to the strong dye-polymer interactions even at the low dye content (0.1 wt. %). The T_g of blends does not change according to the variations in composition of the mixture suggesting strong intermolecular interactions within the blend components. The polymer films were exposed to VOCs including diethyl ether and methanol. The pure dye containing PMMA films on solvent exposure indicated a significant change in the emission intensity than the fluorescence recorded from the blends and from PBMA films. Based on the strong compatibility and single T_g of the blends, strong intermolecular interactions are supposed to occur in the blends. These interactions along with T_g must probably plays a role in the solvent interaction with blends and accordingly changed the fluorescence response of the fluorophore mixed in polymer matrices.

Chapter 5

5. General Conclusions and Perspectives

This work is concerned with the development and applications of FMRs and solvatochromic probes for the detection of Volatile Organic Compounds (VOCs) which are associated with harmful effects on the environment. The detection methods that have been already developed for the sensing VOCs still need to address many issues. On the other hand the fluorescence methods are reported to overcome many such limitations. Accordingly, we worked on the exploration of the significant photophysical features of special fluorescent molecules known as FMRs for the detection of VOCs. The application of FMRs for the measurement of microviscosity changes makes them promising candidates for the detection of VOCs. Such versatile photophysical features are exploited for the detection of VOCs using polymeric materials as supporting materials. Polymer matrices do enhance the sensitivity and selectivity of the fluorophores involved in the chemical sensing.

In the first part of my PhD work, the sensing ability of novel FMRs, including DPAP and TPAP, for the detection VOCs is demonstrated. Unlike most of the FMRs which are only sensitive to viscosity, both DPAP and TPAP are characterized by high sensitivity towards both solvent viscosity and polarity. Interestingly, both TICT and ICT states of these molecular probes play a role during the photoexcitation in the polar medium. The polymer films of PMMA and PC containing DPAP exhibited much interesting vapochromic response on exposure to different solvents when exposed to saturated atmosphere of polar solvents with higher interaction ability with polymer. Contrary, the results suggest that DPAP/polymer films on interaction with non-polar solvent displayed negligible vapochromic response. Notably, a decrease and red-shift in emission spectra was recorded on exposing DPAP/PMMA films to the polar and better polymer interacting solvents. On the other hand, DPAP/PC films displayed much interesting and significantly different response on exposure to highly interacting solvents. Initially, a decrease and the red-shift in the emission spectra similar to DPAP/PMMA films was recorded which was then followed by the increase in fluorescence. This effect was attributed to the solvent–induced crystallization of PC resulting in restriction of the molecular rotation of the dispersed FMR. Overall, the changes occuring within the polymer matrix on solvent exposure directly influence the photophysical features of the FMRs thus making the system suitable for the detection of VOCs. The different extent

of solvent interaction with polymer induces different changes in the viscosity and polarity of the polymer matrix. These changes directly influence the molecular motion of the FMRs which, in turn, define their photophysics. The reproducibility of the vapochromic behaviour of the DPAP/polymer films is also appreciable.

The second part of this work focused on the sensitivity of other FMR namely, TPAP, towards polarity, viscosity and particularly polymer thickness by dispersing the fluorophore in PC films of variable thickness. The results from the first part of the work already confirmed the the role of the polymer-solvent interaction, polarity and vapour pressure of the VOC on the vapochromic features of the FMR containing polymer film. Assuming that the thickness of the polymer film must influence the vapochromic response of **TPAP**/PC films, both the spectral signal features and the kinetics of its response were demonstrated. The change in the fluorescence behaviour during the initial 5 minutes on exposure of TPAP/ PC films to $CHCl_3$ was recorded. Notably, the higher fluorescence variation was recorded for the thinner films attributed to the higher solvent sorption in these films. The effect of crystallization in thicker TPAP/PC films resulted in different emission features.

The next part of the work focused on exploring the vapochromic features of a new solvatochromic probe with higher selectivity response. Considering that selectivity issue of the chemical sensors still acts as major restriction when it comes to their application, the demand for selective chemical probes is increasing. We have successfully demonstrated the significant selectivity of new chromophore namely NPEMI-E. The structural features of the chromophore induce strong ICT character in the chromophore as demonstrated experimentally and significantly supported by the computational results. The vapochromic features of NPEMI-E mixed in PC exhibited interesting sensing ability towards polar and strong interacting solvent like $CHCl_3$. The NPEMI-E/PC films undergo significant fluorescence changes even visible to the naked eye on exposure to $CHCl_3$ only. The other VOCs used were not found suitable for promoting effective solavtochromic response of the NPEMI-E/PC films thereby confirming the selectivity of the chromophore towards $CHCl_3$ The quantificantion by hue method of the present solvatochromic probe further supported NPEMI-E as a suitable selective solavtochromic probe.

The final part of the work demonstrated the analysis of the effect of polymer T_g on the vapochromic ability of the newly synthesized FMR namely 2-(methylbutyl)-2-cyano-3-Julolidine acrylate **(MBCJA)**. This is in accordance to the idea of exploring all the possible

factors that are most probably expected to effect the vapochromic response towards the development of the suitable vapochromic fluorescent polymer films. The segmental mobility of the polymer chains can determine the molecular motion of the FMR inside the matrix and is directly related to the T_g of the polymer. Accordingly, FMRs in polymers with different T_g could result in different vapochromic behaviour. The significant sensitivity of MBCJA towards the viscosity as revealed by the optical properties in solutions of different viscosity clearly suggested the primary role of TICT in the photophysics of this fluorophore. MBCJA when inserted in PMMA and PBMA in addition to their blends resulted in fluorescent polymer films with different T_g. The change in T_g of the pure polymers even on adding the very small concentration of the FMR is caused due to either plasticzation or antiplastication process. Clearly, the measurement of single T_g supported the strong compatibility of the polymers and the dye molecules. Maximum variation in fluorescence was recorded in PMMA than PBMA and blends on exposure to VOCs like diethyl ether. It is assumed that the much lower T_g of PBMA already facilitated the molecular motion of the FMR before solvent exposure and hence the emission change was not so signficant like the change recorded in PMMA containing dye. The slight fluorescence variation in blends on exposure to diethyl ether suggest strong intramolecular interactions in the blends. These interactions possibly decreased the interaction ability of the blend films towards the solvent. Interestingly, the the polymer-solvent interaction seems to play a significant role in altering the vapochromic features of the fluorescent polymer films. The role of T_g is only valid if the solvent-polymer interaction is sufficient to cause some viscosity changes. Alternatively, the exposure to more polar but poor interacting solvent like methanol hardly influenced the emission behaviour in blends and pure PMMA and PBMA dye containing films. These results suggested that polymer solvent interaction plays primarily role in determination of the vapochromic response of the dye/polymer films. The findings from our work consistently support the effective preparation and use of a new class of vapochromic plastic materials with tuneable properties. Also, this aims at the determination of the sensitivity, and the detection limit of the dye/polymer films. Further work needs to be focused on the validation of the proposed approach towards a more extended set of solvents and physical conditions. It is worth noting that the observed variable kinetics with film thickness might be exploited for the realization of functional materials with controllable spectroscopic response. The simple and low-cost approach for the vapochromic detection of $CHCl_3$ can be envisioned to exploit NPEMI-E/PC films as vapochromic films in the production of inexpensive chloroform optical sensors.

Further investigation is required for effectively exploring the effect of T_g on the vapochromic response of the dye/polymer films.

Chapter 6

6. Characterization techniques

6.1. Fluorescence spectroscopy

Fluorescence spectra of solutions were recorded on a Horiba Jobin-Yvon Fluorolog®-3 spectrofluorometer at room temperature equipped with 450W xenon arc lamp double-grating excitation and single-grating emission monochromoters. The emission spectra of solutions were measured by in quartz cuvettes with 10 mm optical path length. The emission spectra of films were analysed by using an F-3000 Fibre Optic Mount apparatus coupled with optical fibre bundles in dark at room temperature. Light generated from the excitation spectrometer is directly focused on the polymer film using an optical fibre bundles. Emission from the sample is then directed back through the bundle into the collection port of the sample compartment.

6.2. UV-Vis Spectroscopy

Absorption spectra were measured with Perkin-Elmer Lambda 650 spectrometer at room temperature. Solutions were analysed in quartz cuvettes with 10 mm optical path length.

6.3. Fourier-Transform-Infrared Spectroscopy

FT-IR spectra were recorded with Perkin Elmer spectrum GXFT-IR at room temperature on KBr pellets

6.4. Nuclear Magnetic Resonance

NMR spectra were recorded with Bruker Advance DRX 400 at room temperature at 400 MHz (^{1}H) and 100 MHz (^{13}C) in $CDCl_3$ solution. Chemical shifts are scaled in ppm relative to trimethylsilane (TMS) using a residual $CHCl_3$ peak in $CDCl_3$ solution as internal standard (7.26 and 77.0 ppm respectively relative to TMS)

6.5. Differential Scanning Calorimetry

DSC of TPAP/PC films was carried out under nitrogen atmosphere by using a Mettler DSC 30 instrument. Samples of 10–20 mg were heated from 40 to 300 °C at 10 °C/min. Melting enthalpies were evaluated from the integrated areas of melting peaks by using indium for calibration.

DSC measurements for the MBCVJ/Polymer films were done by using Mettler Toledo Stare system DSC 822e equipped with a cooling system under nitrogen atmosphere. The system was calibrated with two standards, indium with a fusion temperature 156.6°C, and zinc with a fusion temperature of 419.5 °C. The samples were heated from -10 to 150 °C at a rate of 10 °C min^{-1}.

6.6. Film Thickness

Film thickness was measured through a dial indicator Borletti CM1S with ruby movement bearing

6.7. Confocal Microscopy Imaging

Microscopy images and lifetime measurements were collected by using a Leica TCS SP5 SMD inverted confocal microscope (Leica Microsystems AG, Wetzlar, Germany) equipped with an external pulsed diode laser (PicoQuant GmbH, Berlin, Germany) for excitation at 405 nm. The laser repetition rate was set to be 40 MHz. Each of the image sizes were 512×512 pixels and acquired with a scan speed of 400 Hz (lines per second). The pinhole aperture was set at 1.00 Airy. Polymer films fixed on microscope glass slides were viewed with a 100 × 1.3 NA oil immersion objective (Leica Microsystems). The images were collected using low excitation power at the sample (10-20 μW). Emissions were monitored in the 430-490 nm range by acoustic-optical tuneable beam splitter (AOBS) based built in detectors. Acquisition lasted until about 100-200 photons per pixel were collected, at photon counting rates of 100-500 kHz. Emission lifetime images (FLIM) of the polymer films were elaborated using Picoquant Symphotime software for FLIM analysis.

6.8. Quantum mechanical calculations

Quantum mechanical (QM) calculations of optical absorptions and emission transitions were performed using hybrid DFT functionals (here, B3LYP) and their long-range corrected extensions (here, CAM-B3LYP), which are generally considered suitable for describing molecular systems displaying extended electronic delocalization and their corresponding electronic excitations. Solvent effects have been included implicitly by the polarisable continuum model (PCM). All QM calculations were performed using the Gaussian09 software package.

6.9. Hue method

The fluorescence colour changes of polymer films were investigated by means of the hue method. The hue method consists in converting RGB pictures of the fluorescent samples taken under UV irradiation (using a cheap conventional camera of any kind) to HSV stacks. HSV (Hue, Saturation and Value) is a colour format where the colour of each pixel is identified by the coordinates of its position in a cylindrical space The three different coordinates H, S and V can be determined as follows: H is the colour tone expressed as an angular value from 0° to 360°, that corresponds to the wavelength where the emitted light shows its maximum; S locates the point along the cylinder radius, accounting for colour purity; V is given by the maximum intensity of the signal produced by the pixel, locating the pixel itself along the cylinder axis. RGB images collected with any digital device can be easily converted in the relevant HSV stack by simple mathematical calculation; images can then be compared in terms of colour hue H without artefacts due to different illumination conditions, which would affect only the V and S parameters. Notably, the H, S and V parameters are intrinsically connected with the properties of the emitted light. Considering the light spectrum, H reflects the emission wavelength, S the bandwidth of the peak and V its height. Accordingly, hue values can be used to follow changes in the emission wavelength of a sample, without the need for optical discriminators such as filters or monochromators.

7. References

1 M. R. Ras, F. Borrull and R. M. Marcé, *TrAC - Trends Anal. Chem.*, 2009, **28**, 347–361.

2 S. Król, B. Zabiegała and J. Namieśnik, *TrAC - Trends Anal. Chem.*, 2010, **29**, 1092–1100.

3 K. R. Parker and J. A. Wiens, *Ecol. Appl.*, 2005, **15**, 2037–2051.

4 B. Huang, C. Lei, C. Wei and G. Zeng, *Environ. Int.*, 2014, 71, 118–138.

5 R. J. Delfino, *Environ. Health Perspect.*, 2002, 110 Suppl, 573–589.

6 H. Guo, S. C. Lee, L. Y. Chan and W. M. Li, *Environ. Res.*, 2004, **94**, 57–66.

7 S. Endo, B. I. Escher and K. U. Goss, *Environ. Sci. Technol.*, 2011, **45**, 5912–5921.

8 S. Manzetti, E. R. Van Der Spoel and D. Van Der Spoel, *Chem. Res. Toxicol.*, 2014, **27**, 713–737.

9 G. P. Pappas, R. J. Herbert, W. Henderson, J. Koenig, B. Stover and S. Barnhart, *Int. J. Occup. Environ. Health*, 2000, **6**, 1–8.

10 L. Molhave, *Indoor Air*, 1991, **1**, 357–376.

11 U. S. H. Kenneth Hudnell Ph.D., D. A. Otto, D. E. House and L. Mølhave, *Arch. Environ. Heal. An Int. J.*, 1992, **47**, 31–38.

12 H. Guo, S. C. Lee, L. Y. Chan and W. M. Li, *Env. Res*, 2004, **94**, 57–66.

13 K. Rumchev, J. Spickett, M. Bulsara and M. Phillips, *Thorax*, 2004, **59**, 746–751.

14 A. McCulloch, *Chemosphere*, 2003, **50**, 1291–1308.

15 T. Kasi, T. Nishiwaza H. Arito , K. Nagno, S. Yamamotoi T. Matsuhimai, *J. Occup. Health*, 2002, **44**, 193–202.

16 P. Wang and W. Zhao, *Atmos. Res.*, 2008, **89**, 289–297.

17 R. G. Derwent, *Volatile Org. Compd. Atmos.*, 1995, 1–15.

18 A. Kansal, *J. Hazard. Mater.*, 2009, 166, 17–26.

19 A. Guenther, C. N. Hewitt, D. Erickson, R. Fall, C. Geron, T. Graedel, P. Harley, L. Klinger, M. Lerdau, W. A. McKay, T. Pierce, B. Scholes, R. Steinbrecher, R. Tallamraju, J. Taylor and P. Zimmerman, *J. Geophys. Res.*, 1995, **100**, 8873.

20 F. Fehsenfeld, J. Calvert, R. Fall, P. Goldan, A. B. Guenther, C. N. Hewitt, B. Lamb, S. Liu, M. Trainer, H. Westberg and P. Zimmerman, *Global Biogeochem. Cycles*, 1992, **6**, 389–430.

21 P. Wolkoff, *Indoor Air*, 1995, **5**, 5–73.

22 J. Williams and R. Koppmann, in *Volatile Organic Compounds in the Atmosphere*, 2007, pp. 1–32.

23 S. Wang, H. M. Ang and M. O. Tade, *Environ. Int.*, 2007, 33, 694–705.

24 L. A. Wallace, E. Pellizzari, B. Leaderer, H. Zelon and L. Sheldon, *Atmos. Environ.*, 1987, **21**, 385–393.

25 C.-W. Lee, Y.-T. Dai, C.-H. Chien and D.-J. Hsu, *Environ. Res.*, 2006, **100**, 139–49.

26 A. B. Stefaniak, P. N. Breysse, M. P. M. Murray, B. C. Rooney and J. Schaefer, *Environ. Res.*, 2000, **83**, 162–173.

27 V. Lindfors and T. Laurila, *Boreal Environ. Res.*, 2000, **5**, 95–113.

28 A. Guenther, C. Geron, T. Pierce, B. Lamb, P. Harley and R. Fall, *Atmos. Environ.*, 2000, **34**, 2205–2230.

29 D. K. W. Wang and C. C. Austin, *Anal. Bioanal. Chem.*, 2006, **386**, 1089–1098.

30 Y. Wang, C. Liu, T. Wu, Z. Hao and Z. Wang, *Chinese J. Popul. Resour. Environ.*, 2016, **14**, 298–308.

31 H. L. Wang, L. Nie, J. Li, Y. F. Wang, G. Wang, J. H. Wang and Z. P. Hao, *Chinese Sci. Bull.*, 2013, **58**, 724–730.

32 A. Talapatra and A. Srivastava, *J. Environ. Prot. (Irvine,. Calif).*, 2011, **2**, 21–36.

33 W. Zeng, T. Liu and Z. Wang, *J. Mater. Chem.*, 2012, **22**, 3544.

34 W. Zeng, T. Liu and Z. Wang, *Phys. E Low-Dimensional Syst. Nanostructures*, 2010, **43**, 633–638.

35 R. C. Bailey and J. T. Hupp, *Anal. Chem.*, 2003, **75**, 2392–2398.

36 B. Li, G. Sauvé, M. C. Iovu, M. Jeffries-El, R. Zhang, J. Cooper, S. Santhanam, L. Schultz, J. C. Revelli, A. G. Kusne, T. Kowalewski, J. L. Snyder, L. E. Weiss, G. K. Redder, R. D. McCullough and D. N. Lambeth, *Nano Lett.*, 2006, **6**, 1598–1602.

37 Z. Li, Q. Zhao, W. Fan and J. Zhan, *Nanoscale*, 2011, **3**, 1646–1652.

38 M. Penza, G. Cassano, P. Aversa, F. Antolini, A. Cusano, M. Consales, M. Giordano and L. Nicolais, *Sensors Actuators, B Chem.*, 2005, **111**–**112**, 171–180.

39 H. Yamagiwa, S. Sato, T. Fukawa, T. Ikehara, R. Maeda, T. Mihara and M. Kimura, *Sci. Rep.*, 2014, **4**, 6247.

40 C. K. Ho, M. T. Itamura, M. Kelley and R. C. Hughes, *Sandia Rep.*, 2001, 2001, 34.

41 K. (et al. . Lee, in *Smart Sensors for Health and Environment Monitoring*, ed. Chong-Min Kyung, 2015, pp. 171–188.

42 A. Lobnik, M. Turel and Š. Urek, *Adv. Chem. Sensors*, 2012, 1–28.

43 M. Zheng, H. Tan, Z. Xie, L. Zhang, X. Jing and Z. Sun, *ACS Appl. Mater. Interfaces*, 2013, **5**, 1078–1083.

44 R. F. etal. Steiner, *Topics in Fluorescence Spectroscopy*, Springer US, 1991.

45 J. R. Lakowicz, *Topics in Fluorescence Spectroscopy V4*, 2002, vol. 5.

46 R. Y. Tsien, *Biochemistry*, 1980, **19**, 2396–2404.

47 G. Grynkiewicz, M. Poenie and R. Y. Tsien, *J. Biol. Chem.*, 1985, 260, 3440–3450.

48 H. Xu, R. Chen, Q. Sun, W. Lai, Q. Su, W. Huang and X. Liu, *Chem. Soc. Rev.*, 2014, **43**, 3259–3302.

49 J. R. Lakowicz, *Principles of fluorescence spectroscopy*, Springer-Verlag, US, 2006.

50 G. v. Bünau, *Berichte der Bunsengesellschaft für Phys. Chemie*, 1970, **74**, 1294–1295.

51 B. and B.-S. Valeur, *Molecular fluorescence: Principles and Applications*, 2012.

52 M. A. Haidekker A. Mark, M. Nipper , A. Mustafic , D. Lichlyter , M. Dakanali and E. A. Theodorakis, in *Advanced Fluorescence Reporters in Chemistry and Biology I: Fundamentals and Molecular Design*, ed. Demchenko A.P, Springer-Verlag, Berlin Heidelberg, 2010, 267–308.

53 G. Marowsky, E. P. Schäfer, J. W. Keto and F. K. Tittel, *Appl. Phys.*, 1976, **9**, 143–146.

54 S. Bi, C. Qiao, D. Song, Y. Tian, D. Gao, Y. Sun and H. Zhang, *Sensors Actuators, B Chem.*, 2006, **119**, 199–208.

55 U. Resch-Genger, *Standardization and Quality Assurance in Fluorescence Measurements I*, 2008, vol. 5.

56 Z. Q. Hu, Y. C. Feng, H. Q. Huang, L. Ding, X. M. Wang, C. S. Lin, M. Li and C. P. Ma, *Sensors Actuators, B Chem.*, 2011, **156**, 428–432.

57 A. N. Fletcher, *Photochem. Photobiol.*, 1969, **9**, 439–444.

58 P. C. Beaumont, D. G. Johnson and B. J. Parsons, *J. Chem. Soc. Faraday T.*, 1993, **89**, 4185–4191.

59 M. A. Haidekker and E. A. Theodorakis, *J. Biol. Eng.*, 2010, **4**, 11.

60 Z. R. Grabowski, K. Rotkiewicz and W. Rettig, *Chem. Rev.*, 2003, **103**, 3899.

61 W. Rettig, *J. Mol. Struct.*, 1982, **84**, 303–327.

62 B. D. Allen, A. C. Benniston, A. Harriman, S. a Rostron and C. Yu, *Phys. Chem. Chem. Phys.*, 2005, **7**, 3035–40.

63 K. Rotkiewicz, K. H. Grellmann and Z. R. Grabowski, *Chem. Phys. Lett.*, 1973, **19**, 315–318.

64 K. Y. Law, *Chem. Phys. Lett.*, 1980, **75**, 545–549.

65 W. Schuddeboom, S. A. Jonker, J. M. Warman, U. Leinhos, W. Kuehnle and K. A. Zachariasse, *J. Phys. Chem.*, 1992, **96**, 10809–10819.

66 S. Sasaki, G. P. C. Drummen and G. Konishi, *J. Mater. Chem. C*, 2016, **4**, 2731–2743.

67 M. A. Haidekker, W. Akers, D. Lichlyter, T. P. Brady and E. A. Theodorakis, *Sens. Lett.*, 2005, **3**, 42–48.

68 M. A. Haidekker, T. P. Brady, D. Lichlyter and E. A. Theodorakis, *Bioorg. Chem.*, 2005, **33**, 415–425.

69 M. A. Haidekker and E. A. Theodorakis, *Org. Biomol. Chem.*, 2007, **5**, 1669–78.

70 M. E. Nipper, S. Majd, M. Mayer, J. C. M. Lee, E. A. Theodorakis and M. A. Haidekker, *Biochim. Biophys. Acta - Biomembr.*, 2008, **1778**, 1148–1153.

71 M. A. Haidekker, T. P. Brady, S. H. Chalian, W. Akers, D. Lichlyter and E. A. Theodorakis, 2004, **32**, 274–289.

72 M. a Haidekker, T. Ling, M. Anglo, H. Y. Stevens, J. a Frangos and E. a Theodorakis, *Chem. Biol.*, 2001, **8**, 123–131.

73 M. Shinitzky and Y. Barenholz, *Biochim. Biophys. Acta - Rev. Biomembr.*, 1978, **515**, 367–394.

74 D. Axelrod, D. E. Koppel, J. Schlessinger, E. Elson and W. W. Webb, *Biophys. J.*, 1976, **16**, 1055–1069.

75 R. O. Loutfy and D. M. Teegarden, *Macromolecules*, 1983, **16**, 452–456.

76 M. A. Haidekker, D. Lichlyter, M. B. Johny and C. A. Grimes, *Sens. Lett.*, 2006, **4**, 257–261.

77 P. Bosch, F. Catalina, T. Corrales and C. Peinado, *Chem. - A Eur. J.*, 2005, **11**, 4314–4325.

78 F. Zhou, J. Shao, Y. Yang, J. Zhao, H. Guo, X. Li, S. Ji and Z. Zhang, *European J. Org. Chem.*, 2011, 4773–4787.

79 O. S. Wenger, *Chem. Rev.*, 2013, **113**, 3686–3733.

80 J. W. Grate, L. K. Moore, D. E. Janzen, D. J. Veltkamp, S. Kaganove, S. M. Drew and K. R. Mann, *Chem. Mater.*, 2002, **14**, 1058–1066.

81 W. Lu, M. C. W. Chan, N. Zhu, C. M. Che, Z. He and K. Y. Wong, *Chem. - A Eur. J.*, 2003, **9**, 6155–6166.

82 Z. M. Hudson, C. Sun, K. J. Harris, B. E. G. Lucier, R. W. Schurko and S. Wang, *Inorg. Chem.*, 2011, **50**, 3447–3457.

83 J. R. Kumpfer, S. D. Taylor, W. B. Connick and S. J. Rowan, *J. Mater. Chem.*, 2012, **22**, 14196–14204.

84 I. Platonova, A. Branchi, M. Lessi, G. Ruggeri, F. Bellina and A. Pucci, *Dye. Pigment.*, 2014, **110**, 249–255.

85 G. Martini, E. Martinelli, G. Ruggeri, G. Galli and A. Pucci, *Dye. Pigment.*, 2015, **113**, 47–54.

86 G. Iasilli, F. Martini, P. Minei, G. Ruggeri and A. Pucci, *Faraday Discuss.*, 2016, **196**, 113–129.

87 J. Mei, Y. Hong, J. W. Y. Lam, A. Qin, Y. Tang and B. Z. Tang, *Adv. Mater.*, 2014, 26, 5429–5479.

88 J. Luo, Z. Xie, J. W. Y. Lam, L. Cheng, B. Z. Tang, H. Chen, C. Qiu, H. S. Kwok, X. Zhan, Y. Liu, D. Zhu and B. Z. Tang, *Chem. Commun. (Camb).*, 2001, **381**, 1740–1741.

89 J. Luo, Z. Xie, J. W. Y. Lam, L. Cheng, H. Chen, C. Qiu, H. S. Kwok, X. Zhan, Y. Liu, D. Zhu and others, *Chem. Commun.*, 2001, **381**, 1740–1741.

90 J. Chen, C. C. W. Law, J. W. Y. Lam, Y. Dong, S. M. F. Lo, I. D. Williams, D. Zhu and B. Z. Tang, *Chem. Mater.*, 2003, **15**, 1535–1546.

91 X. Fan, J. Sun, F. Wang, Z. Chu, P. Wang, Y. Dong, R. Hu, B. Z. Tang and D. Zou, *Chem. Commun.*, 2008, 2989–2991.

92 S. Li, Q. Wang, Y. Qian, S. Wang, Y. Li and G. Yang, *J. Phys. Chem. A*, 2007, **111**, 11793–11800.

93 Y. Hong, J. W. Y. Lam and B. Z. Tang, *Chem. Soc. Rev.*, 2011, **40**, 5361.

94 G. Zhang, M. P. Aldred, W. Gong, C. Li and M. Zhu, 2012, 7711–7713.

95 J. Mei, N. L. C. Leung, R. T. K. Kwok, J. W. Y. Lam and B. Z. Tang, *Chem. Rev.*, 2015, **115**, 11718–11940.

96 a P. Alivisatos, W. Gu and C. Larabell, *Annu. Rev. Biomed. Eng.*, 2005, **7**, 55–76.

97 I. L. Medintz, H. T. Uyeda, E. R. Goldman and H. Mattoussi, *Nat. Mater.*, 2005, **4**, 435–446.

98 H. Tong, Y. Hong, Y. Dong, M. Häussler, Z. Li, J. W. Y. Lam, Y. Dong, H. H.-Y. Sung, I. D. Williams and B. Z. Tang, *J. Phys. Chem. B*, 2007, **111**, 11817–11823.

99 Y. Hong, S. Chen, C. W. T. Leung, J. W. Y. Lam and B. Z. Tang, *Chem. Asian J.*, 2013, **8**, 1806–12.

100 N. Zhao, M. Li, Y. Yan and J. W. Y. Lam, *J. Mater. Chem. C*, 2013, **1**, 4640.

101 D. Ding, C. C. Goh, G. Feng, Z. Zhao, J. Liu, R. Liu, N. Tomczak, J. Geng, B. Z. Tang, L. G. Ng and B. Liu, *Adv. Mater.*, 2013, **25**, 6083–6088.

102 Y. Guo, X. Feng, T. Han, S. Wang, Z. Lin, Y. Dong and B. Wang, *J. Am. Chem. Soc.*, 2014, 7–10.

103 J. Z. Liu, H. M. Su, L. M. Meng, Y. H. Zhao, C. M. Deng, J. C. Y. Ng, P. Lu, M. Faisal, J. W. Y. Lam, X. H. Huang, H. K. Wu, K. S. Wong and B. Z. Tang, *Chem. Sci.*, 2012, **3**, 2737–2747.

104 W. Z. Yuan, Y. Tan, Y. Gong, P. Lu, J. W. Y. Lam, X. Y. Shen, C. Feng, H. H. Y. Sung, Y. Lu, I. D. Williams, J. Z. Sun, Y. Zhang and B. Z. Tang, *Adv. Mater.*, 2013, **25**, 2837–2843.

105 N. Zhao, J. W. Y. Lam, H. H. Y. Sung, H. M. Su, I. D. Williams, K. S. Wong and B. Z. Tang, *Chem. - A Eur. J.*, 2014, **20**, 133–138.

106 Y. Hong, J. W. Y. Lam and B. Z. Tang, *Chem. Commun.*, 2009, 4332.

107 P. Minei and A. Pucci, *Polym. Int.*, 2016, **65**, 609–620.

108 R. Hu, J. W. Y. Lam, Y. Yu, H. H. Y. Sung, I. D. Williams, M. M. F. Yuen and B. Z. Tang, *Polym. Chem.*, 2012, 95–105.

109 A. B. Hantzsch, *Dtsch. Chem. Ges.*, 1922, **55**, 953–979.

110 C. Reichardt, *Chem. Rev.*, 1994, **94**, 2319–2358.

111 Y. Li, M. Zhou, Y. Niu, Q. Guo and A. Xia, *J. Chem. Phys.*, 2015, **143**.

112 B. Valeur and M. N. Berberan-Santos, *Molecular Fluorescence: Principles and Applications*, Wiley-VCH, Weinheim, 2012.

113 A. K. Singh and M. Darshi, *Biochim. Biophys. Acta - Biomembr.*, 2002, **1563**, 35–44.

114 D. M. Shin and D. G. Whitten, *J. Phys. Chem.*, 1988, **92**, 2945–2956.

115 A. S. Klymchenko, *Acc. Chem. Res.*, 2017, DOI: 10.1021/acs.accounts.6b00517.

116 V. Montana, D. L. Farkas and L. M. Loew, *Biochemistry*, 1989, **28**, 4536–4539.

117 A. S. Klymchenko and Y. Mely, *Prog. Mol. Biol. Transl. Sci.*, 2013, **113**, 35–58.

118 O. A. Kucherak, P. Didier, M. Yves and A. S. Klymchenko, 2010, 616–620.

119 F. L. Dickert, U. Geiger, P. Lieberzeit and U. Reutner, *Sensors Actuators, B Chem.*, 2000, **70**, 263–269.

120 W. Luo, D. Neiner, A. Karkamkar, K. Parab, E. B. Garner III, D. A. Dixon, D. Matson, T. Autrey and S.-Y. Liu, *Dalt. Trans.*, 2013, **42**, 611–614.

121 R. F. Landis, M. Yazdani, B. Creran, X. Yu, V. Nandwana, G. Cooke and V. M. Rotello, *Chem. Commun. (Camb).*, 2014, **50**, 4579–81.

122 J. M. Rankin, Q. Zhang, M. K. LaGasse, Y. Zhang, J. R. Askim and K. S. Suslick, *Analyst*, 2015, **140**, 2613–2617.

123 C. Zhang and K. S. Suslick, *J. Am. Chem. Soc.*, 2005, **127**, 11548–11549.

124 J. H. Krech and S. L. Rose-Pehrsson, *Anal. Chim. Acta*, 1997, **341**, 53–62.

125 M.-C. Tu, J. A. Cheema, U. H. Yildiz, A. Palaniappan and B. Liedberg, *J. Mater. Chem. C*, 2017, **5**, 1803–1809.

126 J. M. Rankin, Q. Zhang, M. K. LaGasse, Y. Zhang, J. R. Askim and K. S. Suslick, *Analyst*, 2015, **140**, 2613–2617.

127 F. Ciardelli, G. Ruggeri and A. Pucci, *Chem. Soc. Rev.*, 2013, **42**, 857–70.

128 J. Kunzelman, B. R. Crenshaw, M. Kinami and C. Weder, *Macromol. Rapid Commun.*, 2006, **27**, 1981–1987.

129 R. Meallet-Renault, R. Pansu, S. Amigoni-Gerbier and C. Larpent, *Chem. Commun.*, 2004, 2344–2345.

130 M. P. Robin and R. K. O'Reilly, *Polym. Int.*, 2015, **64**, 174–182.

131 B. Frank, A. P. Gast, T. P. Russell, H. R. Brown and C. Hawker, *Macromolecules*, 1996, **29**, 6531–6534.

132 Y. Wang, *Chem. Phys. Lett.*, 1986, **126**, 209–214.

133 C. T. Chen, *Chem. Mater.*, 2004, **16**, 4389–4400.

134 M. Shimizu, K. Mochida, M. Katoh and T. Hiyama, *J. Phys. Chem. C*, 2010, **114**, 10004–10014.

135 S. Feng, Q.-S. Li, L.-N. Yang, Z.-Z. Sun, T. A. Niehaus and Z.-S. Li, *J. Power Sources*, 2015, **273**, 282–289.

136 E. L. Terry L. Richardson, *Industrial Plastics: Theory and Applications*, 2004.

137 L. Basabe-Desmonts, D. N. Reinhoudt and M. Crego-Calama, *Chem. Soc. Rev.*, 2007, **36**, 993–1017.

138 A. Reisch and A. S. Klymchenko, *Small*, 2016, **12**, 1968–1992.

139 B. A. Miller-Chou and J. L. Koenig, *Prog. Polym. Sci.*, 2003, 28, 1223–1270.

140 S. P. Chen and J. A. D. Edin, *Polym. Eng. Sci.*, 1980, **20**, 40–50.

141 P. M. Budd, N. B. McKeown and D. Fritsch, *J. Mater. Chem.*, 2005, **15**, 1977–1986.

142 H. L. Frisch, *J. Appl. Polym. Sci.*, 1970, **14**, 1657–1657.

143 J. E. Mark, *Physical Properties of Polymers Handbook*, springer science + Business Media, LLC, New york, 2nd edn., 2007.

144 R. W. Rousseau, *Handbook of Separation Process Technology*, Wiley, 1987.

145 W. J. Koros, I. Polymer Chemistry and A. C. S. Meeting, *Barrier polymers and*

structures, American Chemical Society, 1990.

146 J. Crank and G. S. Park, *Diffusion in Polymers*, Academic Press, 1968.

147 A. R. Berens and H. B. Hopfenberg, *J. Memb. Sci.*, 1982, **10**, 283–303.

148 S. Kanehashi and K. Nagai, *J. Memb. Sci.*, 2005, **253**, 117–138.

149 S. A. Stern, S.-M. Fang and H. L. Frisch, *J. Polym. Sci. Part A-2 Polym. Phys.*, 1972, **10**, 201–219.

150 P. OTY and A. E. Mishuck, *J. Am. Chem. Soc.*, 1947, **69**, 1631.

151 P. J. Flory, *J. Chem. Phys.*, **10**, 1942.

152 M. L. Huggins, *J. Chem. Phys.*, 1941, **9**, 440.

153 T. H. Russell, B. J. Edwards and B. Khomami, *EPL (Europhysics Lett.*, 2014, **108**, 66003.

154 J. E. Mark, *Physical Properties of Polymers Handbook*, springer science + Business Media, 2nd editio., 2007.

155 A. F. M. Barton, *CRC Handbook of Polymer-Liquid Interaction Parameters and Solubility Parameters*, 1990.

156 J. . V. and J.L.Duda, *Encycl. Polym. Sci. Eng.*, 1986, **5**, 36–68.

157 J. S. Vrentas and J. L. Duda, *J. Polym. Sci. Polym. Phys. Ed.*, 1977, **15**, 403–416.

158 P. Neogi and G. Zahedi, *Ind. Eng. Chem. Res.*, 2014, **53**, 672–677.

159 R. A. Ware, S. Tirtowidjojo and C. Cohen, *J. Appl. Polym. Sci.*, 1981, **26**, 2975–2988.

160 F. L. B. Omena De Oliveira, M. C. A. Moreira, L. L. O. Couto and T. R. Correia, *Polym. Bull.*, 2011, **67**, 1045–1057.

161 C. Li, Q. Kong, Q. Fan and Y. Xia, *Mater. Lett.*, 2005, **59**, 773.

162 A. Siegmann and P. H. Geil, *J. Macromol. Sci. Part B*, 1970, **4**, 239.

163 W. V. Titow, M. Braden, B. R. Currell and R. J. Loneragan, *J. Appl. Polym. Sci.*, 1974, **18**, 867–886.

164 R. P. Kambour, F. E. Karasz and J. H. Daane, *J. Polym. Sci. Part A-2 Polym. Phys.*, 1966, **4**, 327–347.

165 V. Vittoria, F. de Candia, P. Iannelli and A. Immirzi, *Die Makromol. Chemie, Rapid Commun.*, 1988, **9**, 765–769.

166 A. Yoshioka and K. Tashiro, *Macromolecules*, 2004, **37**, 467–472.

167 A. Perevedentsev, P. N. Stavrinou, P. Smith and D. D. C. Bradley, *J. Polym. Sci. Part B Polym. Phys.*, 2015, **53**, 1492–1506.

168 J. S. Papanu, D. S. Soane (Soong), A. T. Bell and D. W. Hess, *J. Appl. Polym. Sci.*, 1989, **38**, 859–885.

169 X. Zhang, B. Li, Z.-H. Chen and Z.-N. Chen, *J. Mater. Chem.*, 2012, **22**, 11427–11441.

170 G. Iasilli, A. Battisti, F. Tantussi, F. Fuso, M. Allegrini, G. Ruggeri and A. Pucci, *Macromol. Chem. Phys.*, 2014, **215**, 499–506.

171 L. Liu, Y. Shao, J. Peng, C. Huang, H. Liu and L. Zhang, *Anal. Chem.*, 2014, **86**, 1622–1631.

172 A. Qin, J. W. Y. Lam and B. Z. Tang, *Prog. Polym. Sci.*, 2012, **37**, 182–209.

173 J. Wu, W. Liu, J. Ge, H. Zhang and P. Wang, *Chem. Soc. Rev.*, 2011, **40**, 3483–3495.

174 L. L. Zhu, X. Li, F. Y. Ji, M. Xiang, Q. C. Wang and H. Tian, *Langmuir*, 2009, **25**, 3482–3486.

175 L. L. Zhu, D. H. Qu, D. Zhang, Z. F. Chen, Q. C. Wang and H. Tian, *Tetrahedron*, 2010, **66**, 1254–1260.

176 H. Li, Z. Chi, B. Xu, X. Zhang, Z. Yang, X. Li, S. Liu, Y. Zhang and J. Xu, *J. Mater. Chem.*, 2010, **20**, 6103.

177 X. Zhang, Z. Chi, H. Li, B. Xu, X. Li, W. Zhou, S. Liu, Y. Zhang and J. Xu, *Chem. - An Asian J.*, 2011, **6**, 808–811.

178 X. Zhang, Z. Chi, Y. Zhang, S. Liu and J. Xu, *J. Mater. Chem. C*, 2013, **1**, 3376.

179 M. Koenig, G. Bottari, G. Brancato, V. Barone, D. M. Guldi and T. Torres, *Chem. Sci.*, 2013, **4**, 2502.

180 M. Koenig, T. Torres, V. Barone, G. Brancato, D. M. Guldi and G. Bottari, *Chem. Commun.*, 2014, **50**, 12955–12958.

181 F. Donati, A. Pucci, C. Cappelli, B. Mennucci and G. Ruggeri, *J. Phys. Chem. B*, 2008, **112**, 3668–3679.

182 A. Pucci, S. Nannizzi, G. Pescitelli, L. Di Bari and G. Ruggeri, *Macromol. Chem. Phys.*, 2004, **205**, 786–794.

183 N. De Mitri, G. Prampolini, S. Monti and V. Barone, *Phys. Chem. Chem. Phys.*, 2014, **16**, 16573.

184 A. Pucci, G. Ruggeri, S. Bronco, F. Signori, F. Donati, M. Bernabò and F. Ciardelli, *Prog. Org. Coatings*, 2011, **72**, 21–25.

185 P. Minei, A. Battisti, S. Barondi, M. Lessi, F. Bellina, G. Ruggeri and A. Pucci, *ACS Macro Lett.*, 2013, **2**, 317–321.

186 A. Shundo, Y. Okada, F. Ito and K. Tanaka, *Macromolecules*, 2012, **45**, 329–335.

187 M. Koenig, B. Storti, R. Bizzarri, D. M. Guldi, G. Brancato and G. Bottari, *J. Mater. Chem. C*, 2016, **4**, 3018–3027.

188 L. Giribabu, V. K. Singh, C. V. Kumar, Y. Soujanya, P. Y. Reddy and M. L. Kantam, *Sol. Energy*, 2011, **85**, 1204–1212.

189 D.R.Lide, *CRC Handbook of Chemistry and Physics, 76th edition*, Taylor and Francis Boca Raton FL, 88th, edn., 1996, vol. 53.

190 R. C. W. (ed), *Handbook of Chemistry and Physics*, Boca Raton, 1978.

191 J. Brandrup, E. Immergut and E. A. Grulke, *Polymer handbook*, John Wiley & Sons, Inc., New York, 1990.

192 Z. Fan, C. Shu, Y. Yu, V. Zaporojtchenko and F. Faupel, *Polym. Eng. Sci.*, 2006, **46**, 729–734.

193 J. P. Mercier, G. Groeninckx and M. Lesne, *J. Polym. Sci. Part C Polym. Symp.*, 1967,

16, 2059–2067.

194 P. Minei, M. Koenig, A. Battisti, M. Ahmad, V. Barone, T. Torres, D. M. Guldi, G. Brancato, G. Bottari and A. Pucci, *J. Mater. Chem. C*, 2014, **2**, 9224–9232.

195 S. Raut, J. Kimball, R. Fudala, H. Doan, B. Maliwal, N. Sabnis, A. Lacko, I. Gryczynski, S. V Dzyuba and Z. Gryczynski, *Phys. Chem. Chem. Phys.*, 2014, **16**, 27037–42.

196 B. Liu and B. Z. Tang, *Macromol. Rapid Commun.*, 2013, **34**, 704.

197 A. P. Silva, H. Q. N. Gunaratne, T. Gunnlaugsson, A. J. M. Huxley, C. P. McCoy, J. T. Rademacher and T. E. Rice, *Chem. Rev.*, 1997, **97**, 1515–1566.

198 M. C. Janzen, J. B. Ponder, D. P. Bailey, C. K. Ingison and K. S. Suslick, *Anal. Chem.*, 2006, **78**, 3591–3600.

199 R. Angelone, F. Ciardelli, A. Colligiani, F. Greco, P. Masi, A. Romano, G. Ruggeri and J. L. Stehlé, in *IOP Conference Series: Materials Science and Engineering*, Strasbourg, France, 2009.

200 R. Angelone, F. Ciardelli, A. Colligiani, F. Greco, P. Masi, A. Romano, G. Ruggeri and J.-L. Stehlé, *Appl. Opt.*, 2008, **47**, 6680–6691.

201 A. A. Colligiani, F. Brustolin, V. Castelvetro, F. Ciardelli and G. Ruggeri, in *Proc. SPIE 4104, Organic Photorefractives, Photoreceptors, and Nanocomposites*, San Diego, CA, USA, 2000.

202 A. T. R. Williams, S. A. Winfield and J. N. Miller, *Analyst*, 1983, **108**, 1067–1071.

203 H. J. Yvon, *A guide to recording Fluorescence Quantum Yields*, Horiba Jobin Yvon, 2012.

204 P. Minei, M. Ahmad, V. Barone, G. Brancato, E. Passaglia, G. Bottari and A. Pucci, *Polym. Adv. Technol.*, 2016, **27**, 429–435.

205 K. Cantrell, M. M. Erenas, I. De Orbe-Payá and L. F. Capitán-Vallvey, *Anal. Chem.*, 2010, **82**, 531–542.

206 A. Hakonen, J. E. Beves and N. Strömberg, *Analyst*, 2014, **139**, 3524–7.

207 B. R. Battisti Antonella, Minei Pierpaolo, Pucci Andrea, *Chem. Commun.*, 2016, **53**, 248–251.

208 A. R. Smith, *ACM SIGGRAPH Comput. Graph.*, 1978, **12**, 12–19.

209 F. J. Devlin, J. W. Finley, P. J. Stephens and M. J. Frisch, *J. Phys. Chem.*, 1995, **99**, 16883–16902.

210 D. Jacquemin, E. A. Perpete, I. Ciofini and C. Adamo, *Acc. Chem. Res.*, 2009, **42**, 326–334.

211 T. Yanai, D. P. Tew and N. C. Handy, *Chem. Phys. Lett.*, 2004, **393**, 51–57.

212 G. Brancato, G. Signore, P. Neyroz, D. Polli, G. Cerullo, G. Abbandonato, L. Nucara, V. Barone, F. Beltram and R. Bizzarri, *J. Phys. Chem. B*, 2015, **119**, 6144–6154.

213 V. Barone and M. Cossi, *J. Phys. Chem. A*, 1998, **102**, 1995–2001.

214 M. Cossi, N. Rega, G. Scalmani and V. Barone, *J. Comput. Chem.*, 2003, **24**, 669–681.

215 G. M. J. Frisch, W. Trucks and E. Schlegel, *Gaussian 09, Revision A. 1; Gaussian*, Wallingford CT, 2009.

216 B. Mysliwa-Kurdziel, K. Solymosi, J. Kruk, B. Boddi and K. Strzalka, *Eur. Biophys. J.*, 2008, **37**, 1185–1193.

217 H. Singh, J. Sindhu and J. M. Khurana, *Sensors Actuators, B Chem.*, 2014, **192**, 536–542.

218 A. E. Da Hora Machado, J. A. De Miranda, S. Guilardi, D. E. Nicodem and D. Severino, *Spectrochim. Acta - Part A Mol. Biomol. Spectrosc.*, 2003, **59**, 345–355.

219 A. Matwijczuk, D. Kluczyk, A. Gorecki, A. Niewiadomy and M. Gagos, *J. Phys. Chem. B*, 2016, **120**, 7958–7969.

220 Z. Diwu, Y. Lu, C. Zhang, D. H. Klaubert and R. P. Haugland, *Photochem. Photobiol.*, 1997, **66**, 424–431.

221 R. W. Sinkeldam and Y. Tor, *Org. Biomol. Chem.*, 2007, **5**, 2523–2528.

222 A. Hawe, M. Sutter and W. Jiskoot, *Pharm. Res.*, 2008, 25, 1487–1499.

223 C. Reichardt, *Solvents and Solvent Effects in Organic Chemistry*, Wiley-VCH Verlag GmbH & Co., KGaA, Weinheim, 2011.

224 C. Reichardt, *Pure Appl. Chem.*, 2008, **80**, 1415–1432.

225 N. Tirelli, S. Amabile, C. Cellai, A. Pucci, L. Regoli, G. Ruggeri and F. Ciardelli, *Macromolecules*, 2001, **34**, 2129–2137.

226 A. Pucci, N. Tirelli, G. Ruggeri and F. Ciardelli, *Macromol. Chem. Phys.*, 2005, **206**, 102–111.

227 S. P. Avraam I. Isayev, Ed., *Encyclopedia of Polymer Blends, Volume 2: Processing*, Wiley-VCH Verlag GmbH & Co., 2011.

228 B. R. Crenshaw, J. Kunzelman, C. E. Sing, C. Ander and C. Weder, *Macromol. Chem. Phys.*, 2007, **208**, 572–580.

229 A. Mustafic, H. M. Huang, E. A. Theodorakis and M. A. Haidekker, *J. Fluoresc.*, 2010, **20**, 1087–1098.

230 E. M. Marian Kryszewski, Andrzej Galeski, *Polymer Blends: Volume 2: Processing, Morphology, and Properties*, Springer US, New York, USA.

231 Q. Dai, W. Liu, L. Zeng, C.-S. Lee, J. Wu and P. Wang, *CrystEngComm*, 2011, **13**, 4617–4624.

232 J. S. Lin, *Eur. Polym. J.*, 2003, **39**, 1693–1700.

233 Marek W. Urban, *Handbook of Stimuli-Responsive Materials*, Wiley-VCH Verlag GmbH & Co.

234 A. Slark, *Polymer-London-*, 1997, **38**, 2407–2414.

235 I. M. Kalogeras and W. Brostow, *J. Polym. Sci. Part B Polym. Phys.*, 2009, **47**, 80–95.

236 T. G. Fox, *Bull. Am. Phys. Soc.*, 1956, **1**, 123–35.

237 Y. Huang and D. R. Paul, *J. Polym. Sci. Part B Polym. Phys.*, 2007, **45**, 1390–1398.

238 X. Lu and A. Weiss, *Macromolecules*, 1992, **25**, 3242–3246.

239 J. M. Rodriguez-Parada, J. M. Rodriguez-Parada, V. Percec and V. Percec,

Macromolecules, 1986, **19**, 55–64.

240 D. R. Lide, *CRC handbook of chemistry and physics: a ready-reference book of chemical and physical data*, 2004, vol. 89th.

241 Allan F.M. Barton, *Handbook of Poylmer-Liquid Interaction Parameters and Solubility Parameters*, 1990.

242 L. de BROUCKERE and G. OFFERGELD, *J. Polym. Sci.*, 1958, 105–118.

243 E. M. Marian Kryszewski, Andrzej Galeski, *Polymer blends: volume 2: processing, morphology and properties*, Springer US.

244 K.L.Mittal and H.R Andreson Jr, *Acid-base Interaction: Relevance to Adhesion Science and Technology*, .

List of Publications:

1. P. Minei, M. Koenig, A. Battisti, M. Ahmad, V. Barone, T. Torres, D. M. Guldi, G. Brancato, G. Bottari and A. Pucci, *J. Mater. Chem. C*, **2014**, **2**, 9224–9232.

2. P. Minei, M. Ahmad, V. Barone, G. Brancato, E. Passaglia, G. Bottari and A. Pucci, *Polym. Adv. Technol.*, **2016**, **27**, 429–435.

3. M. Ahmad, I. Platonova, A. Battisti, P. Minei, G. Brancato and A. Pucci *J. Polym. Sci.B Polym. Phys.*, **2017** in press, DOI: 10.1002/polb.24367

International Conferences: Schools and Training

1. Attended one day workshop "Nanostructured Metal Optics, From Theory to Enhanced Spectroscopies, Sensing, Imaging" at Scuola Normale Superiore, Pisa, Italy, April, 2016.

2. Attended XIX International Summer School "Aggregation-Induced Emission (AIE): Phenomenon, Principle and Application" at Krutyn, Poland, May 15-21, 2016.

3. Attended Laboratory Safety courses at NEST Scuola Normale Superiore, Pisa, Italy.

4. Attended one day workshop on "Researching in Europe. Research Policy of the European Union and the Funding Programs" at SNS, Pisa, Italy, June 2016